Modeling Development and Disease In Human Engineered Cardiac Tissue

by

Cassady E. Rupert

B.A. Physics, Cornell University, Ithaca, NY 2013

Submitted in partial fulfillment of the requirements for the degree of Doctor of Philosophy in Biomedical Engineering, a joint program in the Division of Biology and Medicine and the School of Engineering at Brown University

Center for Biomedical Engineering

and

School of Engineering

PROVIDENCE, RHODE ISLAND

October 2019

This dissertation by Cassady E Rupert is accepted in its present form by the School of Engineering, Center for Biomedical Engineering as satisfying the dissertation requirement for the degree of Doctor of Philosophy.

Date_____ _____

Kareen LK Coulombe, Advisor

Recommended to the Graduate Council

Date_____ _____

Lauren Black III, Reader

Date_____ _____

Vicki Colvin, Reader

Date_____ _____

Robert Hurt, Reader

Date_____ _____

Edith Mathiowitz, Reader

Date_____ _____

Ulrike Mende, Reader

Approved by the Graduate Council

Date_____ _____

Andrew Campbell, Dean of the Graduate School

Curriculum Vitae

Cassady E. Rupert

Brown University

School of Engineering

184 Hope Street, Box D

Providence, RI 02912

Cassady_Rupert@brown.edu

EDUCATION

2019 Ph.D., Biomedical Engineering

Brown University, Providence, RI. 2013-2019

2013 B.A. Physics

Cornell University, Ithaca, NY. 2009-2013

GRADUATE-LEVEL RESEARCH EXPERIENCE

Doctoral Research

Brown University, School of Engineering, Center for Biomedical Engineering

Mentor: Kareen L. K. Coulombe, Ph.D.

Project: Development and disease in human pluripotent stem cell-derived cardiomyocytes

Rhode Island Hospital, Providence, RI

Cardiovascular Research Center, September – December 2013

Mentor: Ulrike Mende, M.D.

Project: Implementation of an automated image analysis method

Bioengineering Internship

University of Washington, Department of Pathology, Summer 2013

Mentors: Charles E. Murry, M.D., Ph.D., Kareen L. K. Coulombe, Ph.D.

Project: Hypertrophic stimulation of engineered cardiac tissue

TEACHING EXPERIENCE

Sheridan Center Teaching Certificate I

Brown University Sheridan Center for Teaching & Learning, Fall 2016

Teaching Assistant

Cardiovascular Engineering (ENGN 1520) Brown University, Dr. Kareen Coulombe, Fall 2016

Teaching Fellow

Cardiovascular Engineering (ENGN 1520) Brown University, Dr. Kareen Coulombe, Fall 2015

Undergraduate Mentor

- Jasmine Gabor, ScB student in Biomedical Engineering, May 2018 – Present. Project: Determining gender-specific cardiotoxic effects of estrogen-mimicking compounds in hiPSC-derived cardiomyocytes.
- Gian Ignacio, ScB student in Biomedical Engineering, May 2017 – May 2018. Project: Increasing electrical and mechanical maturity in cardiac tissue through carbon nanotube hybrid scaffolding.
- Maria Paredes, ScB student in Biomedical Engineering, September 2016 – May 2017. Project: Single-cell patterning of hiPSC-derived cardiomyocytes.
- Jason Thomas, ScB student in Biology, June 2016 – May 2017. Project: Biophysical characterization of contraction in hiPSC-derived cardiac tissue
- Dalia Ruiz, ScB student in Biomedical Engineering, January 2016-May 2016. Project: Mechanical creep for maturation of engineered cardiac tissues.

- Heidi Chang, ScB student in ChemE, June2014 – May 2016. Project: 3D volume analysis of human induced pluripotent stem cell-derived cardiomyocytes.
- Carlota Pereda Serras. ScB student in Biology, June 2014 – May 2015. Project: Characterization of diseased human neonatal cardiac fibroblasts.

HONORS & AWARDS

- GAANN Fellow, Institute for Molecular and Nanoscale Innovation, Brown University, 2016-2018
- 2015-2016 Brown University School of Engineering Outstanding Teaching Assistant Award
- 2015-2016 Presidential Award for Excellence in Teaching
- 2014 BMES Outstanding Contribution, Cardiovascular Engineering track. 2014
- Eccleston Fellow, Brown University, 2012-2013

PEER-REVIEWED PUBLICATIONS

Rupert CE, Kim TY, Choi B-R, Coulombe, KLK. Human cardiac fibroblasts uniquely modulate electromechanical function of hiPSC-cardiomyocytes in engineered myocardium. *Stem Cell Reports*. Submitted 2019-06-04

Liu M, Shi G, Zhou A, **Rupert CE**, Coulombe KLK, Dudley SC Jr (2018). Activation of the unfolded protein response downregulates cardiac ion channels in human induced pluripotent stem cell-derived cardiomyocytes. *Journal of Molecular and Cellular Cardiology*. 2018 Apr;117:62-71.

Rupert CE, Coulombe KLK (2017). IGF1 and NRG1 Enhance Proliferation, Metabolic Maturity, and the Force-Frequency Response in hESC-Derived Engineered Cardiac Tissues. *Stem Cells Int*. 2017;2017:1-13.

Rupert CE, Chang HH, Coulombe KLK (2017). Hypertrophy Changes 3D Shape of hiPSC-Cardiomyocytes: Implications for Cellular Maturation in Regenerative Medicine. *Cell Mol Bioeng*. 2017;10(1):54-62.

Rupert CE, Coulombe KLK. (2015). The Roles of Neuregulin-1 in Cardiac Development, Homeostasis, and Disease. *Biomarker Insights*, 2015;10(Suppl. 1), 1–9.

INVITED ORAL PRESENTATIONS

Rupert CE, Coulombe KLK (2019). Modulation of Adult Cardiac Fibroblasts for Engineering Healthy and Vulnerable Human Cardiac Tissue. *Regenerative Medicine Workshop.* Charleston, SC.

Rupert CE, Kim TY, Choi BR, Coulombe KLK (2018). Development of engineered human cardiac tissues of improved or pathological phenotypes by modulating cardiac fibroblast content and passage. *BMES*. Atlanta, GA.

Rupert CE, Regnier M, Murry CE, Coulombe KLK (2014). Engineering Mature Cardiac Tissue In Vitro: Biomechanical and Biochemical Stimulation of Physiological Hypertrophy. *BMES*. San Antonio, TX.

SELECTED ABSTRACT PUBLICATIONS & POSTERS

Rupert CE, Kim TY, Choi BR, Coulombe KLK (2018). Cardiac fibroblasts in engineered human heart tissues: Cellular engineers of the cardiomyocyte extracellular environment. *Gordon Research Conference: Signal Transduction by Engineered Extracellular Matrices*. Andover, NH. Poster.

Rupert CE, Kim TY, Choi BR, Coulombe KLK (2017). Genetically engineered cardiac fibroblasts for electrical maturation of hiPSC-cardiomyocytes. International Society for Stem Cell Research Annual Meeting. Boston, MA. Poster.

Rupert CE, Kim TY, Choi BR, Coulombe KLK (2017). Carbon nanomaterials for engineering conduction into human cardiac tissues. *Conference for Cellular and Molecular Bioengineering*. Kona, HI. Poster.

Rupert CE, Chang H, Coulombe KLK (2016). High throughput image analysis reveals three dimensional morphological changes in hypertrophically stimulated human induced pluripotent stem cell-derived cardiomyocytes. BMES Annual Conference. Minneapolis, MN. Poster.

Rupert CE, and Coulombe KLK (2015). Neuregulin-1 Influences Differentiation Efficiency and Specificity of Human Induced Pluripotent Stem Cells to Cardiomyocytes. *International Society for Stem Cell Research 2015 Annual Meeting.* Stockholm, Sweden. Poster.

Rupert CE and Coulombe KLK (2014). Engineering the Contractile Maturation of hESC-derived Cardiomyocytes in 3D Tissues. *Signal Transduction in Engineered Extracellular Matrices, Gordon Research Conference.* Waltham, MA. Poster.

FELLOWSHIP APPLICATIONS

SERVICE

- 2017 – Organizer for Brown University's 2017 Young Scholars Conference
- 2017 – Brown University Graduate Women in Science and Engineering Regional Coordinator
- 2016 – Organizer for Brown University's 2016 Young Scholars Conference
- 2015 – Tissue Engineering and Regenerative Medicine World Congress – Student Co-chair, "The hype and hope of cardiovascular tissue engineering strategies"
- 2014-2015 - Brown University Graduate Biomedical Engineering Society Vice President

Professional Development

- CU Boulder College of Engineering and Applied Science ACTIVE Faculty Development and Leadership Intensive. Participant: 11/01/2018 – 11/03/2018
- NIH Career Development Award, Grant Writers' Seminars and Workshops, LLC. Attendee: 2/29/2016
- Effective Performance Workshop, Brown University Graduate School & Trinity Repertory Theater. Selected participant: 11/01/2015 – 11/30/2015
- Young Scholars Conference, Brown University. Attendee: 9/25/2015 – 9/26/2015
- Write Winning Grants, Grant Writers' Seminars and Workshops, LLC. Attendee: 2/25/2015

Preface and Acknowledgements

I gratefully acknowledge the support of my thesis advisor, Dr. Kareen Coulombe; committee members, Drs. Lauren Black, Vicki Colvin, Robert Hurt, Edith Mathiowitz, and Ulrike Mende; and past and current Coulombe Lab members, in particular, Dr. Fabiola Munarin, Dr. Nicholas Kaiser, Rajeev Kant, Travis Wallace, Alicia Minor, Heidi Chang, Carlotta Pereda Serras, Jason Thomas, Gian Christian Ignacio, and Chinedu Irofuala. I thank my loved ones, without whom this endeavor would not have been possible.

Table of Contents

Abstract

Cardiovascular engineering using human pluripotent stem cell (hPSC)-derived cardiomyocytes holds incredible potential for disease modeling, therapeutic development and testing, and cardiac regeneration. The heterogeneity and plasticity of hPSCs and hPSC-cardiomyocytes can be both assets and obstacles to the generation and advancement of new technologies, and a deeper understanding of how to manipulate these cells is needed. The research pursued in this dissertation explores novel means to engineer healthy and diseased states in hPSC-cardiomyocytes from the single-cell to tissue level. Studies were performed using a broad scale of metrics including cell and tissue structure, gene expression, bioenergetic phenotype, and electromechanical function in order to obtain a fuller picture of hPSC-cardiomyocyte response to mechanical, biochemical, and cellular stimuli. Important and novel findings show that (1) confocal microscopy imaging of single cells reveals hPSC-cardiomyocyte contractile lattice and cytosolic volume respond independently to hypertrophic stimulation; (2) developmental growth factors stimulate proliferation and metabolic maturation of hPSC-cardiomyocytes in engineered tissues; (3) adult human cardiac fibroblasts can be manipulated to produce physiological and pathophysiological phenotypes in engineered tissues; and (4) metabolic selection to purify hPSC-cardiomyocyte populations changes bioenergetic phenotype. Taken together, these results stress the importance of considering hPSC-cardiomyocyte immaturity and plasticity in engineered cardiac tissues, and that, because of these features, hPSC-cardiomyocytes provide unexpected avenues for engineering development and disease in the dish.

Chapter 1: Introduction

Cardiovascular engineering is an exciting field that is progressing toward the clinic, where stem cell and tissue engineering in vitro models and clinical therapies can tackle the leading global cause of death – heart disease. The field faces a number of obstacles before these translational goals can be fully realized. Obstacles addressed in this dissertation are broadly (1) the need for widely adaptable, careful characterization and analysis of input cell populations and (2) the challenges of engineering tissues with physiological phenotypes to accurately and meaningfully recapitulate human myocardium in the dish.

The research described in this dissertation was undertaken to develop and implement tools to mature and manipulate stem cell-derived cardiomyocytes and engineered cardiac tissue made from them. Chapters 2 through 6 are the manuscripts produced in these efforts, and their individual introductory sections provide motivation specific to each chapter. The present chapter provides the reader with an introduction to cardiomyocyte differentiation from human pluripotent stem cells, their purification and inclusion in engineered cardiac tissues, as well as many approaches employed to increase structural and functional development and maturation of engineered myocardium.

Stem cells and cardiomyocyte differentiation

Translational opportunities in cardiac tissue engineering have been made possible due to advances in stem cell and developmental biology, making feasible the widespread use of human pluripotent stem cells (hPSCs) and directed differentiation of cardiomyocytes. Early work was performed with embryonic stem cells (ESCs) cultured as embryoid bodies (EBs) from which serum-induced differentiated ESC-derived cardiomyocytes (ESC-cardiomyocytes) were harvested, first described using mouse ESCs.[1] This approach lacked clinical applicability because of the allogeneic nature of ESCs, the limit to scaling up and enhancing spontaneous differentiation, and the ethical and regulatory questions surrounding the cell type. In 2007, two

groups showed the transduction of human somatic cells with either four[2] or six[3] transcription factors resulted in human induced pluripotent stem cells (hiPSCs), a biomedical tool to personalize treatment and model disease phenotypes. Simultaneous advances in differentiation of cardiomyocytes from pluripotent stem cells made hiPSCs a valuable tool in cardiac tissue engineering. First developed in hESCs[4] but shown to be similarly effective in hiPSCs,[5] directed differentiation of cardiomyocytes via modulation of Activin/Nodal and BMP signaling, key pathways in mesoderm and cardiac commitment *in utero*, provided a method to produce large numbers of hPSC-cardiomyocytes, at a high efficiency.

More recent advances in cardiomyocyte differentiation and maintenance have been developed and chemically defined culture conditions to make translational applications feasible. The now standard differentiation protocol replaces the human recombinant proteins used in the aforementioned differentiation method with small molecule modulators of Wnt signaling, Chiron and Inhibitors of Wnt Protein (IWPs), to obtain ~85% enriched iPSC-cardiomyocyte populations.[6] This protocol was further defined with the development of a refined cardiomyocyte differentiation and maintenance media which replaced the widely used B27 supplement of 21 components with just two supplemental components, L-Ascorbic Acid and human serum albumin.[7] The use of small molecules and chemically defined media eliminates batch-to-batch variability, unavoidable with other protocols, and simplifies *in vitro* differentiation conditions, which is critical for both basic science discoveries and translational research.

Purifying cardiomyocyte populations

Though advances in cardiomyocyte differentiation protocols have reduced cost and variability, the process still yields heterogenous cell populations of fibroblast-like non-cardiomyocytes and cardiomyocytes.[9,8] To reduce this heterogeneity, several methods have been developed to enrich for cardiomyocytes upon differentiation. The first, lactate purification, takes advantage of immature cardiomyocyte's unique ability to use lactate instead of glucose as a precursor in

oxidative phosphorylation.[10] By culturing differentiated cardiomyocytes in glucose-depleted, lactate-enriched media, non-cardiomyocytes die of nutrient deficiency while cardiomyocytes survive.[11] Though used widely in the field, there remains little known about how this process changes the bioenergetic phenotype of surviving hPSC-cardiomyocytes.

Antibiotic selection is also used to purify hPSC-cardiomyocyte populations. This process involves genetically engineering stem-cell lines with a cardiac-specific promotor, such as α-myosin heavy chain, to drive antibiotic resistance.[12] After differentiation, cells are treated with the antibiotic, and only those expressing the cardiac marker survive selection. Unlike lactate purification, the selection process is based on a global cardiomyocyte marker, eliminating the possibility of selecting for specific hPSC-cardiomyocyte phenotypes. Though efficient in purifying populations, the process of engineering these lines is costly and time intensive, which limits the widespread adaption across research groups.

Lastly, cell-sorting has been used to enrich differentiated populations from cardiomyocytes. Signal-regulatory protein alpha (SIRPA) has been identified as a cardiac-specific cell surface marker, and has been used to label and enrich hPSC-cardiomyocyte populations using flow assisted cell sorting (FACS) and magnet assisted cell sorting (MACS).[13] Antibody-based sorting methods are particularly unattractive for broad use. Antibodies are costly, and the singularization of cells required for efficient sorting results in a significant loss of hPSC-cardiomyocytes. Metabolic, antibiotic, and antibody selection are all effective but inefficient means of purifying hPSC-cardiomyocyte populations to the recommended >80% cardiomyocyte purity.[14] For these methods to be adopted for high throughput production of hPSC-cardiomyocytes, the effect on cell phenotype must be investigated, and the cost – both monetary and in cell loss – must be reduced.

Cardiac tissue engineering

Scaffold-Free

HPSC-cardiomyocytes, derived from all three of the differentiation techniques described above, have been incorporated successfully into engineered tissue. The extracellular environment that individual hPSC-cardiomyocytes encounter affects how the tissue construct performs as a functional unit, and a range of systems have been employed to manipulate this extracellular space. Scaffold-free systems, such as cell-aggregating patches or cell sheets, rely on the input cell populations to produce and remodel their own ECM. Orbital shaking has been used to facilitate aggregation of hESC-cardiomyocytes in patches that show electrical syncytium and engraftment capability on rodent hearts.[17,16,15] Scaffold-free cell sheets using 3-4 cell thick hiPSC-cardiomyocyte monolayers as patches have also shown neovascularization and improved heart function when implanted in a rodent myocardial infarct (MI) model.[18] These studies demonstrate the ability of hPSC-cardiomyocytes to produce and remodel ECM, however, they are significantly limited by the minimalist approach. The ECM composition and mechanical properties cannot be directly manipulated, hindering the ability to elicit structural and functional maturation.

Native mammalian polymeric scaffolds

Native polymeric scaffolds of varying complexity have gained significant standing in the cardiovascular engineering field due to their cyto- and immuno-compatibility. Collagens are the most abundant of the fibrillar proteins in native myocardium[19] and are thus a commonly used scaffold component in engineered tissues.[20,21,22] Fibrin, another fibrillar protein which makes up >15% of the cardiac ECM[19] is also frequently used in native polymeric scaffolds either alone[23,24] or in combination with collagen.[25] Not surprisingly, both primary and hPSC-derived cardiomyocytes are able to survive in and remodel matrices made from these native polymers to

form synchronously beating engineered tissues. These scaffolds, however, lack the structural hierarchy and complexity of native myocardium and are reliant on the ability of input cell populations to efficiently organize their surrounding ECM. In order to recapitulate the physiological environment of a cardiomyocyte with increased fidelity, decellularized, processed cardiac ECM has been used as a matrix component.[26] Although decellularized ECM is an ideal candidate for biomimicry, it introduces unpredictable heterogeneity into engineered tissues that will vary based on ECM source and batch-to-batch variability.

Non-mammalian natural scaffolds

Although native mammalian polymeric scaffolds possess the most physiologically relevant composition for clinical application in humans, other natural scaffolds have been explored to circumvent the sourcing problems involved in obtaining mammalian scaffolds. Biological alternatives have been investigated as a means to introduce more control over scaffold sourcing, structure and mechanical properties. Alginate and chitosan have both gained popularity as natural, tunable scaffold components.[27] Cardiomyocytes have been successfully incorporated into pristine alginate scaffolds,[28] and modification of alginate with peptides improves engineered tissue formation and performance.[30,29] Similarly, chitosan has been shown to support cardiomyocyte survival *in vitro* in its pristine,[31] and to a greater extent, chemically modified[32] form.

Synthetic scaffolds

Synthetic scaffolds have also shown promise in cardiac tissue engineering due to their easily tunable properties and resulting versatility. Polymers that are popular in cardiac tissue engineering are easy to handle, easily modifiable, often conductive, and include Poly(glycerol sebacate) (PGS),[33] polyglycolic acid (PGA),[34] and 50%/50% polylactic acid (PLLA)/polylactic glycolic acid (PLGA).[35] In order to improve the biocompatibility of these synthetic polymers,

many groups have engineered hybrid scaffolds of synthetic and natural polymers, including PLACL/collagen,[36] PGA/fibrin,[37] and graphene/chitosan.[38] All of the described scaffolds face similar challenges and must be biocompatible, functional, and versatile. They must also attain FDA approval, which makes scaffolds composed of already-approved materials particularly attractive. It is likely that no one scaffold formulation will prevail and that many scaffolds, each suited for certain applications, will reach translation via unique paths.

Maturation state of stem cell-derived cardiomyocytes & engineered tissues

Due to the immaturity of PSC-cardiomyocytes at early stages after terminal differentiation, engineered tissues made from these cells lack the full functionality of adult myocardium. One of the most widely researched areas of cardiovascular engineering is developing methods to facilitate maturation of engineered muscle. A benchmark of functional maturity for clinical application has yet to be determined and is debated in the field, and methods of obtaining more highly performing tissues continue to be developed. These methods fall broadly into three categories: biochemical, electrical, and mechanical stimulation and are often used in combination.

Biochemical

The use of biochemical factors has been effective for improving function of hPSC-cardiomyocytes and tissues made from them. Growth factors insulin-like growth factor 1 (IGF1) and neuregulin-1 (NRG1) have been used individually to promote PSC-cardiomyocyte proliferation[39] and electrical maturation,[40] respectively, The biochemical approach to stimulate maturation has gone beyond growth factors to include growth hormones and steroids. Tri-iodo-l-thyronine (T3), a growth hormone, has recently gained popularity in the field for its positive effect on hPSC-cardiomyocyte bioenergetic maturation.[41] The glucocorticoid dexamethasone has been shown to increase contractility and structural maturity in fetal murine CMs, and when

administered in combination with T3[42] or T3 and IGF1,[43] improves hPSC-cardiomyocyte bioenergetic and contractile maturation. A pro-survival cocktail of biochemical factors has been shown to aid graft survival on post-MI rodent hearts.[4] These studies give a glimpse at the incredible potential of biochemical manipulation of engineered cardiac tissues,

Electrical

Electrical stimulation has been widely used as a biomimetic means to stimulate maturity in engineered cardiac tissue.[44] This method has been shown to induce maturation at a morphological level by increasing structural organization to resemble that of native myocardium.[45] Electrical stimulation has also been shown to enhance the electrical properties of engineered cardiac tissues. The excitation threshold (the electrical impulse necessary to elicit synchronous cardiomyocyte contraction) is lowered from 5 V/cm in unstimulated to 2 V/cm in stimulated tissues,[46] and the maximum capture rate (the fastest rate of stimulation a tissue can follow) is increased from 3 Hz in unstimulated to 4.5 Hz in stimulated tissues.[47] At the cellular level, expression of Connexin 43 (Cx43, a gap-junction protein involved in the propagation of action potentials between cardiomyocytes) is upregulated.[46] Recently, ramping up of pacing frequency during culture to supraphysiological levels was shown to improve tissue force-frequency response with the underlying hypothesis that this culture regimen exercises the tissues as they form and mature.[48] Overall, electrical stimulation is a bioinspired means of improving cell and tissue electrical function, however, the extent to which this tool can be used to precondition hPSC-cardiomyocytes for electromechanical coupling with adult cardiomyocytes has not been demonstrated.

Mechanical

Human hearts contract upward of two billion times in a lifetime, so it is unsurprising that mechanical preconditioning of engineered tissues has most successful in improving functional

maturity. Culture conditions inspired by the heart's mechanical environment during development and adulthood have proven effective. As well as developing in a specific biochemical and electrical context, the fetal heart beats *in utero* throughout gestation and thus maturing cardiomyocytes are subjected to cyclic stress from beating, sheer stress from blood flow, and static stress from fetal heart growth.[49] All of these biomechanical forces have been recapitulated *in vitro* to facilitate physiological maturation of engineered cardiac tissues. Adult biomechanics are most commonly employed during engineered cardiac tissue culture.

Cyclic stretching has been shown to increase cardiomyocyte alignment,[50] protein production,[51] and force generation.[52] Similar increases in force production have been reported with the use of static stretch,[20,52, 53] however, contradictory reports of alignment and protein expression are present across studies. Pulsatile flow at varying shear stresses has been demonstrated to be differentially beneficial in engineered tissues, increasing contractile myofilament protein expression, structural organization, and force production.[54,55] Biochemical, electrical, and mechanical methods for stimulating maturation in engineered cardiac tissues have all shown efficacy to some extent and are valuable techniques, but they still leave engineered cardiac tissues functionally performing below native myocardium, often by one or two orders of magnitude. Combinations of the conditioning regimens may improve function, but recently the field has looked beyond hPSC-cardiomyocytes for cellular contributors to engineered tissue maturity.

Support cells

Ventricular composition

A method that has been used to form more mature, organized cardiac tissue is co-culturing cardiomyocytes with other relevant cardiac cell populations, which modulate the biochemical, electrical, and mechanical environment of the tissue. In native human myocardium,

cardiomyocytes compose up to 90% of volume in the left ventricle[56] but account for only 30% of cells in the human heart.[57] This cellular heterogeneity is reflected in engineered cardiac tissues, where peak contractile performance is achieved at roughly 50% to 75% hPSC-cardiomyocytes (by number).[58] Because of this need for a non-cardiomyocyte population in engineered tissues, many groups have begun to identify and optimize potential support cell types in their systems.

Non-cardiac cells

Several cell types not found in the native ventricle have been successfully leveraged to promote engineered cardiac tissue function. A range of support cells including mesenchymal stromal cells (MSCs), umbilical vein endothelial cells (HUVECs),[59,61,60] brain pericytes,[62] and neonatal dermal fibroblasts[63,58] have been reported to improve engineered cardiac tissue formation and function. These non-cardiac cells provide support related to their native functions; however, the mechanistic details of these benefits are often only partially understood. Effects of MSCs and HUVECs are generally attributed to paracrine signaling,[65,64] while pericytes and dermal fibroblasts provide structural and mechanical support.[66,67] Though moderate improvements have been attained with the use of non-cardiac support cells, native support cells remain an attractive option, to elicit more dramatic changes in engineered cardiac tissues.

Cardiac fibroblasts

Cardiac fibroblasts (CFs) are the cell type responsible for structural integrity via matrix deposition and remodeling and are found regularly integrated among cardiomyocytes. In order to impart these structural cues *in vitro*, several groups have used fibroblasts as a supportive cell type in engineered cardiac tissue. It has been shown in two dimensions that NIH-3T3 fibroblasts can elicit and propagate action potentials when co-cultured with cardiomyocytes.[68] In three dimensions, 3T3-J2,[31] mouse embryonic,[69] and cardiac fibroblasts[70] have been co-cultured with cardiomyocytes, resulting in increased beating frequency and Cx43 expression, a more mature

cardiomyocyte morphology, and greater force and protein production, respectively. Cardiac fibroblasts act as both paracrine signalers and matrix remodelers. Cardiac fibroblasts secrete factors including IL-1ß, to improve infarct healing after acute injury, and TGF-ß, to increase ventricular remodeling during heart failure.[71] Additionally, cardiac fibroblasts are the main producers and maintainers of the heart's ECM, controlling the mechanical environment cardiomyocytes experience during development, homeostasis, and disease. Cardiac fibroblasts act as sources of both biochemical and mechanical stimulation of cardiac tissue maturity and are therefore a support cell source with great potential in cardiac tissue engineering.

Modeling development and disease in engineered human cardiac tissue

The tools to differentiate cardiomyocytes, engineer cardiac tissue, and modulate tissue behavior are numerous, often drawn from multiple points in development and adulthood, and provide countless opportunities to advance cardiovascular engineering. Through the research described in the subsequent chapters, I develop and demonstrate means to model and study cardiac development and disease in an in vitro engineered human cardiac tissue platform. I show that from the single- to multi-cellular scales and in the differentiation to engineered tissue culture time windows, hiPSC-cardiomyocytes possess unique and exciting characteristics. I demonstrate that previous assumptions surrounding three-dimensional cell volume, lactate purification, growth factor administration, and cardiac fibroblast electromechanical participation must be carefully examined due to the phenotypic plasticity of hiPSC-cardiomyocytes along the development-to-disease spectrum. I show (1) that hiPSC-cardiomyocyte myofibril and cytosolic volume measures are not surrogates, (2) that developmental growth factors elicit specific and novel responses in 3D hESC-cardiomyocytes engineered tissues, and (3) that human cardiac fibroblasts uniquely modulate the electromechanical state of hiPSC-cardiomyocyte engineered tissues. In light of this work, the field of cardiac tissue engineering should carefully consider the

metrics we use to evaluate 3D tissues and the physiological state of the cell populations which we incorporate in them.

Chapter 2: The Roles of Neuregulin 1 in Cardiac Development, Homeostasis, and Disease

Publication Reference: Rupert CE, Coulombe KL. The roles of neuregulin-1 in cardiac development, homeostasis, and disease. Biomarker Insights. 2015;10(Suppl 1):1-9. doi:10.4137/BMI.S20061

Key words: Neuregulin-1, ErbB receptors, cardiomyocyte, therapeutic, cardiac regeneration, stem cells

Abstract

Neuregulin-1 (NRG-1) and its signaling receptors, erythroblastic leukemia viral oncogene homolog (ErbB) 2, 3, and 4, have been implicated in both cardiomyocyte development and disease as well as homeostatic cardiac function. NRG-1/ErbB signaling is involved in a multitude of cardiac processes ranging from myocardial and cardiac conduction system development to angiogenic support of cardiomyocytes and to cardioprotective effects upon injury. Numerous studies of NRG-1 employ a variety of platforms, including *in vitro* assays, animal models, and human clinical trials, with equally varying and sometimes contradictory outcomes. NRG-1 has potential as a therapeutic tool for stem cell therapies, tissue engineering applications, and clinical diagnostics and treatment. This review presents a concise summary of the growing body of literature in order to highlight the temporally persistent significance of NRG-1/ErbB signaling throughout development, homeostasis, and disease in the heart and specifically in cardiomyocytes.

Introduction

Neuregulin-1 (NRG-1), a member of the neuregulin growth factor family, has been implicated in a number of cellular processes via paracrine and juxtacrine signaling through receptor tyrosine

kinases, ErbBs, in the family of epidermal growth factor receptors (EGFRs).[72] The discovery of neuregulins was made in the context of cancer and neural research, unrelated to the cardiovascular system.[76,73,77,74,75] However, in the late 1990s, several groups performing studies to disrupt NRG/ErbB signaling discovered its crucial role in cardiac development.[78–80] NRG remained for the most part in the realm of neurological research, but in recent years, it resurfaced in the cardiovascular field due to adverse side effects of chemotherapeutics that target this signaling pathway.[81,82]

Numerous studies of NRG-1/ErbB signaling in the heart have been carried out since discoveries of its critical roles in both cardiac development and disease. Results have indicated its ubiquitous importance in the heart from womb to tomb (Figure 1), however the specifics of developmental, homeostatic, and cardioprotective mechanisms are broadly scattered and sometimes contradictory. This review aims to weave together many threads of information that have been gained about NRG/ErbB signaling during different spatial and temporal contexts into a cohesive and coherent timeline. This is done to emphasize the potential of NRG-1 as a therapeutic throughout this time course: from a biostimulant in stem cell therapy, to a possible biomarker or drug during cardiac disease. Because this review will follow NRG-1 through development, homeostasis, and disease with a focus on cardiomyocyte biology, readers are directed to other reviews for additional details and a broader perspective of NRG/ErbB signaling.[85,84,83]

NRG-1 Structure and Signaling

NRG-1 is a member of the neuregulin family of signaling proteins that act on NRG-responsive cells by binding to the extracellular domain of ErbB receptor tyrosine kinases and was discovered in 1992 during the search for ligands for ErbB2 in mammary tumor cells.[72,74] Fifteen isoforms of NRG have been subsequently identified[86], indicative of the host of biological targets of the protein *in vivo*. Importantly, these isoforms are distinguished by their N-terminal sequence

(I, II, or III), EFG-like domain (α or β, resulting from alternative splicing at the C-terminal which determines receptor affinity), and synthesis location (transmembranous or nonmembranous).[72] Type I NRG-1 is transmembranous and requires proteolytic cleavage by three transmembrane proteases (meltrin[87], memapsin[88], and tumor necrosis factor-α-converting enzyme[89]) to be active and secreted, with the EFG-domain available for ErbB binding.[90] This type of neuregulin is endogenous in the heart at high levels and will be the focus of this review. Type II NRG-1 expresses an N-terminal secretory signal peptide and is thus an active ligand upon secretion; it is not present at significant levels in the heart, and type II-specific research is mostly focused on the role in psychological disorders.[92,91] Type III NRG-1 is, for the most part, expressed in neuronal cells and will not be discussed further. Henceforth, in this review, NRG-1 will refer to only type I NRG-1.

NRG-1 acts by means of paracrine signaling through ErbB2, 3, and 4.[93] NRG-1 binds to the extracellular ligand-binding domain of ErbB3 and ErbB4 (but not ErbB2), which induces a conformational change in ErbB3 and 4 and subsequent dimerization with either ErbB2 or activated ErbB3 or ErbB4. The many splice variants of NRG-1 are a source of possible redundancy in ErbB signaling, with the NRG-1α isoform displaying 100-fold weaker binding affinity than NRG-1β.[94] Genetic variants in NRG-1 and ErbB4 have been associated with sudden cardiac death and congenital left ventricular outflow tract defects, respectively.[95,96] Upon NRG-1 binding and dimerization, ErbB2, 3, and 4 receptors' intracellular kinase domains phosphorylate their dimerization partner's C-terminus. This initiates a host of downstream signaling pathways, leading to, among other phenomena, migration, growth, adhesion, and differentiation in a context-dependent manner. Investigation of these downstream effects has led not only to important discoveries in the cardiovascular realm but also to insights into cancer

pathology.[97] Moving forward, the spatial context examined will be within the heart, and the temporal context will span development to heart failure.

NRG-1/ErbB Signaling in Development

Cardiac Muscle Development

The first associations made between NRG-1/ErbB signaling and the heart implicated it in cardiac muscle development *in vivo*. When ErbB4[78] or ErbB2[79] were deleted in mice, a significant deficit in ventricular trabeculation and endo-cardial cushion formation (from which the atrioventricular valves develop) was observed, and mice died mid-embryogenesis. Similar results were seen upon deletion of NRG-1 in mice, who also died during embryogenesis.[80] A less severe phenotype was observed in zebrafish, where *erbb2*$^{-/-}$ cardiomyocytes exhibited irregular myofibril organization, deviating from the spatiotemporal organization of wild-type cardiomyocytes.[98] Significant trabeculation did not occur in *erbb2*$^{-/-}$ zebrafish, and by 4.5 days post-fertilization, myofibrils were more dense at the base and less dense at the apex of the heart versus wild type controls, accompanied by suppressed whole heart function as measured by fractional shortening (%FS). Although mutant zebrafish survived through early stages of development, defects resulting from ErbB2 removal caused early death. Further into cardiac development, NRG-1, synergistically with insulin-like growth factor 1 (IGF-1), was shown to be necessary for compact zone expansion in mouse embryos, in addition to previously described effects.[99] *In vitro*, treatment of neonatal rat ventricular myocytes (NRVMs) with NRG-1 resulted in increased protein production (indicated by >2-fold increase in S6 kinase peptide phosphorylation), F-actin organization, and subsequent hypertrophy (both assessed qualitatively through phalloidin staining).[100] Rapamycin inhibited these effects, indicating PI-3-kinase/p70^{S6K} activation is necessary for NRG-1-induced protein synthesis and myofibrillogenesis. Taken together, this evidence demonstrates that NRG-1/ErbB signaling is crucial for proper heart

formation, a process that must be at least partially recapitulated in stem cell therapies aimed to regenerate the heart.

Cardiac Conduction System Development

In vivo experiments have demonstrated the importance of NRG-1 in the development of the cardiac conduction system (CCS). Injection of mouse embryos with NRG-1 induced ectopic CCS development in a dose-dependent manner (with no increased response above 2.5 pM) and increased both the number of pacemaker cells as well as the conduction velocity.[101] Because trabeculation, endo-cardial cushion formation, compact zone expansion, and CCS development occur sequentially during development, these studies, when examined as a whole, demonstrate the temporal importance of NRG-1/ErbB signaling and the multitude of downstream effectors of ErbB activation. When the nuances of these sequential effects are fully elucidated, NRG-1 has the potential to become a tool with multiple specific uses in cardiac stem cell therapy. Administered at the appropriate time, it could direct cardiomyocyte sub-populations into desired phenotypes during cardiac development.

Cardiomyocyte Differentiation from Pluripotent Stem Cells

Some progress has been made to untangle NRG-1/ErbB signaling effects in the stem cell environment. Importantly, NRG-1 also exhibits developmental effects in pluripotent stem cell (PSC)-derived cardiomyocytes *in vitro*; however, treatment results vary and can be contradictory. By examining the context and time dependence of NRG-1/ErbB signaling, seemingly disparate effects of NRG-1 administration *in vitro* instead become a roadmap of NRG-1's diverse effects on cardiomyocyte development. Initial reports suggested NRG-1 globally increased cardiomyocyte differentiation from mouse embryonic stem cells (mESCs).[102] More specifically, NRG-1 was shown to increase cardiomyogenesis, and in particular "working-type" atrial and ventricular cardiomyocytes, via ErbB signaling in mESCs when administered

days 5 through 9 of differentiation.[103] When treated with NRG-1 days 1 through 3 of differentiation, mESCs were reported to preferentially differentiate into “nodal-type” pacemaker cardiomyocytes.[104] During development *in vivo*, the CCS develops after heart trabeculation and compaction, which contradicts the aforementioned preferential differentiation of nodal-type cardiomyocytes (found almost exclusively in the CCS) with early NRG-1 treatment. Because differentiation methods vary between studies and the uniformity and time-course of differentiation varies depending upon the differentiation method used, it is difficult to make comparisons of the timing of NRG-1 treatments, and comprehensive time-course studies are necessary. The *in vitro* platform will clearly not perfectly mimic *in vivo* processes, and the mechanisms of this preferential differentiation may lead to further understanding of NRG-1’s uses in stem cell therapy (Table 1).

To reconcile sometimes contradictory results, differential receptor activation has been examined in mESCs treated with NRG-1. ErbB4 receptors were implicated in increased cardiomyocyte differentiation (>20% increase in beating embryoid bodies (EBs) over controls) in mESCs treated days 5 through 7 of differentiation via the hanging drop method. NRG-1 treatment also increased EB mRNA expression levels of cardiomyocyte contractile components cardiac troponin T (cTNT) and myosin light chain 2a (MLC2a), as well as protein expression levels of cTNT, Nkx2.5 (an important cardiac lineage transcription factor), and connexin 40 (a major component of gap junctions in the CCS).[105] However, the ErbB3/ErbB2 receptors were shown to be necessary for cardiac induction of mESCs when treated with NRG-1 during days 1 through 3 of differentiation.[106] Interestingly, in rat cardiac myocytes, ErbB2 and ErbB4 expression has been shown to persist into adulthood while ErbB3 expression ceases.[107] These studies help reconcile the different effects of and cardiomyocyte subtypes produced by NRG-1 treatment during cardiomyocyte differentiation and help to illustrate the importance of the time dependence of NRG-1’s effects, particularly with respect to their receptor binding to ErbB3 or

ErbB4. The differential downstream effects of specific ErbB receptor binding by NRG-1 need further investigation.

The use of mESCs to study NRG-1 in the context of differentiation and development has led to important insights into timing and means of signaling, and yet it is important to utilize human cell platforms in order to orient the capabilities of NRG-1 towards tissue engineering and therapeutic applications in the clinical setting. When human embryonic stem cell-derived cardiomyocytes (hESC-CMs) were treated with NRG-1 on day 10 of differentiation, an increase in the proportion of working-type cardiomyocytes was reported by patch clamp measurements of action potential, and when NRG-1/ErbB signaling was inhibited in these hESC-CMs, an increase in nodal-type cardiomyocytes was observed.[40] Interestingly, the time dependence of these results does not always coincide with the timeline of cardiac development *in vivo* as mentioned above, demonstrating the need for a more robust study of temporal NRG-1/ErbB signaling in human cardiomyocytes.

NRG-1/ErbB Signaling in Homeostasis

Cardiomyocyte Metabolic Activity

Although the levels of NRG-1 decrease in the heart after development, it is still present and plays an important role in many homeostatic processes. NRG-1/ErbB signaling has been implicated in mitochondrial activity in several contexts. The cardioprotective actions NRG-1/ErbB signaling have been studied in part because of cardiotoxic side-effects of chemotherapeutics.[108] Anthracyclines are some of the most effective anticancer drugs that have been developed, but cardiac complications began to be reported within 1 to 3 years of their introduction.[109,110] Anthracycline-induced cardiotoxicity, which at the molecular level increases oxidative stress in the heart, manifests clinically with a variety of symptoms ranging from arrhythmias and sudden cardiac death to left ventricular dysfunction and congestive heart

failure.[108] ErbB4 expression and its heterodimerization with ErbB2 were found to be down-regulated in neonatal rat cardiomyocytes treated with the anthracycline doxorubicin.[111] In rat cardiomyocytes, NRG-1/ErbB signaling was able to attenuate myocardial damage, resulting from anthracycline-associated oxidative stress.[109,112]

The mechanisms of the cardioprotective effects of NRG-1/ErbB signaling have been further investigated and found in adult rat cardiomyocytes to be at least in part due to increased voltage-gated ion channel expression, mitochondrial turnover, and fatty acid transporter mRNA suppression.[113] Similar results have been observed in rats *in vivo*, where administration of NRG-1 has rescued mitochondrial function, reduced oxidative stress, and inhibited cytochrome *c* release in coronary ligation-induced heart failure.[114] Conversely, when a Cre-*loxP* system was implemented in mice to delete ErbB2 in cardiomyocytes, attenuating NRG-1/ErbB signaling, the number and disorganization of mitochondria increased.[115] A second mechanism of NRG-1's cardioprotective effect is the downstream activation of Src/Focal Adhesion Kinase (FAK). NRG-1β-specific Src and FAK phosphorylation in cardiomyocytes resulted in increased sarcomere organization (via p130CAS and CRB adaptor proteins), myosin light chain activation (via Erk1/2), cell survival, and cell-cell junction formation at intercalated disks.[117,116]

Studies of NRG/ErbB signaling in both cardiac and non-cardiac cells have shed light on its role in metabolic activity. Glucose uptake was stimulated by NRG-1 treatment in neonatal rat ventricular myocytes.[118] The same phenomena was observed in L6E9 rat skeletal muscle cells, where chronic NRG-1 treatment enhanced oxidative metabolism and mitochondrial activity by stimulating the expression of PGC-1α and PPARδ.[119] In ErbB4 expressing PC12 cells, NRG-1 treatment was found to regulate ROS elevation from H_2O_2 induced oxidative stress via the PI3K-PKB/Akt pathway.[120] ErbB2 signaling was found to regulate mitochondrial activity in a temporal manner via the mitochondrial inner membrane protein UCP2. Upon constitutive overexpression of ErbB2 in MCF7 cells, UCP2 levels were increased, which contributes to mitochondrial

uncoupling and has been shown to increase cardiomyocyte viability during oxidative stress.[121] Taken together, evidence from studies covering a wide scope of contexts clearly implicates NRG/ErbB signaling as a crucial player in regulating metabolic activity through multiple pathways.

Maintaining Cardiac Homeostasis

NRG-1/ErbB signaling is critical for cardiomyocyte response to physiological stress. During exercise-induced physiological hypertrophy in rats, NRG-1 was upregulated at both the mRNA and protein expression level in ventricular cardiomyocytes in conjunction with hypertrophy (assessed by heart weight and cardiomyocyte diameter) and proliferation (by an increase in mononucleated BrdU positive cardiomyocytes, indicating a true increase in new, rather than multinucleated cells). In the same study, isolated c-kit positive embryonic cardiac stem cells showed greater than 3-fold incorporation of BrdU over control.[122] These results are supported by a similar study in which NRG-1 treatment increased hypertrophy in both neonatal and adult rat ventricular myocytes and increased proliferation in only neonatal ventricular cardiomyocytes, with emphasis here on the temporal context dependence of signaling.[107] As cardiomyocyte proliferation peaks during development *in utero* and declines drastically to negligible levels in adulthood, the ability to stimulate cardiomyocyte proliferation in NRVMs over ARVMs may be a result of developmental biology of the cells themselves.[123] During pregnancy-induced physiological hypertrophy in mice and rats, NRG-1 and ErbB2 and 4 phosphorylation levels increased in the mom, and partial inhibition of NRG/ErbB signaling reduced left ventricular fractional shortening and enhanced pregnancy-induced left ventricular dilation.[124] *In vivo*, and to some extent *in vitro*, models clearly demonstrate the NRG/ErbB signaling responds to physiological changes during homeostasis and impacts cardiomyocyte physiology.

NRG-1 has also been implicated in regulating cardiac response to β-adrenergic activity. When myocytes isolated from heterozygous NRG-1 knockout mice underwent β-adrenergic stimulation to increase contractility, presence of a muscarinic agonist was unable to decrease contractility, indicating that NRG-1 plays an important role in modulating β-adrenergic stimulation via inhibitory parasympathetic activity.[125] In isolated rabbit papillary muscle, NRG-1 treatment decreased sensitivity to the β-adrenergic agonist isoproterenol, presenting a negative inotropic effect (evidenced by a decreased peak twitch active tension response to isoproterenol of papillary muscles simultaneously treated with NRG-1). This response was attenuated by a NOS inhibitor, suggesting that NO, to some extent, mediates the negative inotropic effect of NRG-1.[126] When stimulated with β-adrenergic agonist norepinephrine, adult rat ventricular myocytes were protected from apoptosis by NRG-1 treatment only when simultaneously undergoing electrical stimulation.[127] NRG-1/ErbB signaling responds to both physiological and pathological stress via multiple, non-redundant pathways and permeates heart function throughout adulthood.

Heterotypic Interactions with Endothelial Cells

Cardiac vascular endothelium is a critical component of cardiac maintenance, is physically and biochemically communicating with cardiomyocytes, and is also susceptible to the effects of NRG/ErbB signaling. Endothelial cells are themselves the major producers of NRG-1, and interrupting this signaling in mouse endothelium has led to capillary loss, increased expression of hypoxia-inducible transcription factor, and decreased cardiac function.[129,128] Isolated cardiac microvascular endothelial cells have been reported to release NRG-1 in a dose dependent response to oxidative stress by H_2O_2 treatment, and this activity was shown to subsequently decrease H_2O_2-induced apoptosis in adult rat ventricular myocytes.[130] The protective effects of cardiac microvascular endothelium (CMVE) against cardiomyocyte apoptosis were diminished when ErbB2 signaling was blocked in a similar study, indicating, once again, a receptor

dependence of the protective action of NRG-1 signaling.[131] Endothelial cells can themselves employ autocrine NRG/ErbB signaling to induce angiogenesis in a metalloproteinase-dependent manner.[132] *In vitro* and *in vivo* endothelial cell platforms have also indicated that hypoxia-induced endothelial NRG-1 expression increases angiogenesis via paracrine upregulation of VEGF.[133] The importance of NRG-1 in CMVE provides yet another avenue whose exploration could reveal therapeutic applications of NRG-1 not limited just to cardiomyocytes, but to their support system as well.

NRG-1/ErbB Signaling in Heart Disease

Acute Heart Failure

NRG-1/ErbB signaling is ubiquitous throughout cardiac development and homeostasis, but its role in heart disease (both acute and chronic heart failure) has been the focus of a majority of NRG-1-related research. An indication of the role of NRG-1 in acute heart failure is the decrease in ErbB2 and NRG-1 expression associated with the need for inotropic support and decreased ejection fraction (EF), respectively, in clinical data.[134] In acute heart failure models, NRG-1 can often exert a cardioprotective effect by means of pathways discussed above. NRG-1 and phosphorylated ErbB4 levels have been reported to increase directly after ischemic/reperfusion injury in rats, and preconditioning with NRG-1 intravenously, 20 minutes before injury reduces the resulting infarct in a PI3K/Akt-dependent manner.[135] Endothelial cell-derived NRG-1 has been implicated in this cardioprotective mechanism; when NRG-1 was selectively deleted in ECs in an ischemic mouse model, systolic function was significantly impaired.[136] In a rat myocardial infarct (MI) model, intravenous NRG-1 administration 4 weeks after injury reduced mitochondrial dysfunction and myocyte apoptosis, thus reducing left ventricular remodeling after injury.[114] When human NRG-1 was introduced in a similar rat MI

model using lentiviral gene transduction at the infarcted border zone also 4 weeks after injury, an increase in microvasculature was observed in the infarcted myocardium, accompanied by an upregulation of VEGF.[137] When NRG-1 was administered 4-days post-MI for sustained periods using microparticle delivery (shown to stably release growth factors for 4 weeks *in vitro*) in rats, overall cardiac function was improved, indicated by increased left ventricular ejection fraction (EF) and mass, and end-systolic and end-diastolic diameters and volumes (LVESD, LVEDD, LVESV, and LVEDV, respectively).[138] More specifically, cardiomyocyte proliferation increased as demonstrated by and increased number of Ki67-positive cells in the infarcted and peri-infarcted zones, and apoptosis and fibrotic remodeling decreased. Clearly, the beneficial effects of NRG-1 treatment and the detrimental effects of its removal in acute heart failure models provides solid evidence of its importance in the heart's response to injury.

Several mechanisms have been proposed to further elucidate the beneficial effects of NRG-1 during acute heart failure. Some studies have suggested that positive effects of NRG-1 treatment after MI may be due to increased cardiomyocyte proliferation[139,138,], however, definitive evidence of this phenomena has yet to be presented. Another study sought to explain NRG-1's mechanism of action using a rat MI model and found that NRG-1 treatment significantly upregulated cardiac myosin light chain kinases (cMLCKs) and phosphorylation of ventricular myosin light chain 2 (MLC-2v) which accompanied an increase in cardiac function (characterized by increased EF, %FS, LVEDD, and LVESD).[140] NRG-1 may also exert beneficial effects by downregulating genes involved in fibrosis (e.g. matricellular proteins, collagens, and basal lamina components).[141] These studies are all accompanied by an increase in cardiac function, and it is clear that NRG-1 acts through a multitude of pathways to protect and help restore heart function during the remodeling process that follows ischemic injury.

As has been a common thread in the discussion of NRG-1/ErbB signaling thus far, the timing of NRG-1 administration in acute heart failure appears to be important. Temporal dependence of

treatment was investigated in a rat MI model when NRG-1 was injected via the tail vein 1 or 8 weeks after injury. A decreased sensitivity to NRG-1 was observed with increasing time post-MI for NRG-1 administration, which may be caused by a temporary increase in ErbB2 expression immediately after injury. In addition to improving heart function, NRG-1 was reported to 'normalize' expression of genes related to metabolic function back to those of uninjured animals.[142] In a similar model of rat MI, intravenous NRG-1 treatment either 1 or 8 weeks post-MI improved hemodynamic function (increased mean arterial pressure, left ventricular pressure, and rate of contraction and relaxation over untreated) and showed an additive effect when administered with an angiotensin-converting enzyme inhibitor.[143] Both studies suggest that activation of NRG-1/ErbB signaling at various time points after acute MI can attenuate adverse remodeling and improve heart function, implying temporally broad therapeutic benefits of NRG-1 administration.

Chronic Heart Failure

NRG-1/ErbB signaling is not only limited to acute injury in the heart but also has been implicated during chronic heart failure (CHF). Although there are fewer studies in this context, NRG-1 continues to exhibit cardioprotective effects in CHF as previously described for acute heart failure. In a study examining 899 systolic heart failure patients, serum NRG-1 levels were found to be independently associated with the severity of heart failure.[144] Circulating NRG-1 may be a biomarker for heart failure as increased levels indicate increased compensatory efforts of the cardiovascular system. Increased circulating NRG-1, however, is accompanied with decreased expression of ErbB2 and ErbB4 receptors in failing human myocardium.[145] Expression levels can be rescued upon implantation of ventricular assist devices, indicating that ErbB levels are modulated by the degree of overload in chronic heart failure.[146] This phenomena has been reported by the same group in an aortic stenosis rat model, where ErbB2 and 4 levels were stable after 6 weeks of stenosis but significantly decreased 22 weeks after stenosis.[147] Because

chronic heart failure is associated with depressed ErbB receptor levels, administration of NRG-1 alone may no longer be sufficient to improve cardiac function in the long term. These studies emphasize the importance of uncovering the mechanisms of NRG-1 action over the course of disease progression in order to harness its benefits most effectively.

Therapeutic administration of NRG-1 has been shown to improve cardiac function in a variety of *in vivo* models of CHF. NRG-1 improved heart function and survival in a mouse myocarditis model.[143] Similar beneficial effects were observed in a canine chronic pacing model, where NRG-1 injections for 5 days improved left ventricular end diastolic and systolic pressure, cardiac contractility, and relaxation only in chronically paced animals and not in the control group, indicating that elevated levels of NRG-1 alone are not sufficient to elicit such responses.[143] In a study examining diabetic cardiomyopathy in rats, NRG-1 had similar beneficial effects which were attributed to attenuation of myocardial interstitial fibrosis.[148] Although much work has yet to be done to untangle the mechanisms of NRG-1 action in clinical and pre-clinical models of CHF, existing studies suggest that NRG-1 imparts benefits on heart function across a broad spectrum of disease pathologies.

NRG-1 in Clinical Trials

Because of the cardioprotective role of NRG-1/ErbB signaling and the dire consequences when this signaling is inhibited, recombinant human NRG-1 (rhNRG-1) has been used in two clinical trials with reported results and several other clinical trials are ongoing.[149–152] A phase II, randomized, double-blind trial enrolled 44 chronic heart failure (CHF) patients, characterized by a LVEF ≤40%. CHF patients received rhNRG-1 intravenously, 8 hours a day for 10 days and LVEF improved 31.99% in treated patients over a 15.05% increase with placebo 90 days after treatment, indicating that short-term administration can have long-term effects on the inhibition of adverse remodeling.[153] In a single-center, prospective, non-randomized, open-label study, rhNRG-1 was administered intravenously to 15 CHF patients (LVEF ≤40%) 6 hours a day for 11

days, and both acute and sustained hemodynamic responses were measured by Swan-Ganz catheterization.[154] Significant changes in cardiac function were observed within 8 hours of rhNRG-1 treatment, including increased cardiac output, stroke volume, and mean arterial pressure, however, the latter was the only hemodynamic parameter to display a significant change at 84 days post-treatment. The promising results of these two trials suggest that therapeutic use of rhNRG-1 will continue to be investigated in the CHF patient population. As scientific research continues to unravel the specific mechanisms of NRG-1/ErbB cardioprotection and improvement of contractile and hemodynamic function, the specificity of NRG-1/ErbB therapeutic treatment can be applied to an increasing diversity of developmental and disease conditions.

Conclusion

Because of the large number of time and context-dependent effects of which NRG-1/ErbB signaling is capable, NRG-1 will continue to be studied as a tool for both tissue engineering and therapeutic purposes. Human pluripotent stem cells (hPSCs) have provided a platform for tissue engineering with clinical applications, and the advent of cardiomyocyte differentiation from hPSCs in fully defined conditions[7,6] has set the stage for engineering functional cardiac tissue. HPSC-derived cardiomyocytes and thus the tissues made from them display an immature phenotype[155], and NRG-1, whose signaling has been implicated in cardiac development, is a prime candidate for increasing maturation of engineered myocardium. By obtaining a fuller understanding of when and how NRG-1/ErbB signaling directs cardiac development, we can harness this pathway for stem cell therapies targeting the heart.

NRG-1/ErbB signaling also plays an important role in angiogenesis and cardiac homeostasis, as well as having cardioprotective and therapeutic effects pre- and post-myocardial injury. At least 5 clinical trials are currently underway in which recombinant human NRG-1 is administered to chronic heart failure patients.[156] The effects of NRG-1 in the clinical setting have yet to be fully

uncovered, and the mechanisms of the observed homeostatic and cardioprotective functions must be untangled in order to fully utilize and tailor NRG-1/ErbB therapy. However, the ubiquity of NRG-1/ErbB signaling throughout life is an undeniably encouraging discovery with respect to NRG-1's possible therapeutic targets. The vast therapeutic applications of NRG-1 in cardiac development and disease are an incredible motivation to more fully understand the context-dependence of NRG-1/ErbB signaling.

Figures & Tables

Figure 1

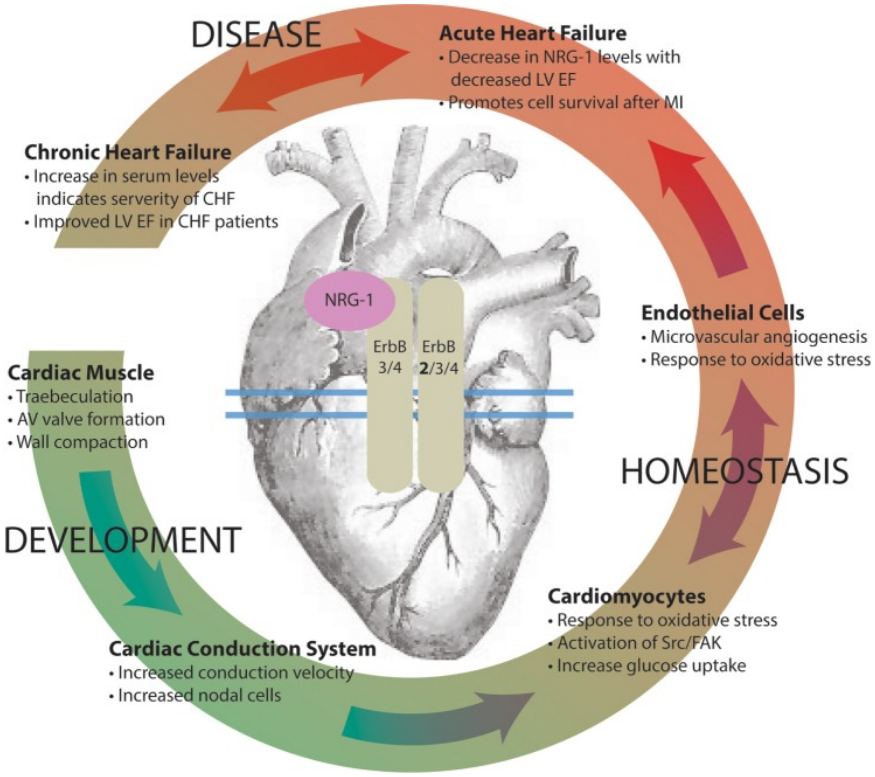

Figure 1. Developmental, homeostatic, and disease related effects of NRG-1/ErbB signaling in the heart. Upon binding of NRG-1 to an ErbB3 or 4 receptor, dimerization with another ErbB2 (preferred), 3, or 4 receptor initiates a cascade of downstream signals in the heart. Signaling plays an important role in development of cardiomyocytes and the cardiac system, homeostatic function of the heart via cardiomyocyte adaptability to stress and microvascular support, and the transition to disease in both acute and chronic heart failure (HF).

Table 1. Studies conducted on NRG-1/ErbB signaling during cardiac development. Studies include *in vivo* and *in vitro* platforms in mice, zebrafish, and mouse embryos, and rat, mouse, and human cell lines, respectively. Different experimental results are observed depending on platform, timing, and duration of treatment.

Model	Animal	Treatment	Results
In Vivo	Mouse	ErbB 4 deleted[78]	Death *in utero*, decreased trabeculation and AV cushion formation
		ErbB 2 deleted[79]	Death *in utero*, decreased trabeculation and AV cushion formation
		NRG-1 deleted[80]	Death *in utero*, decreased trabeculation and AV cushion formation
	Zebrafish	NRG-1 deleted[98]	Myofibrillar disorganization
	Mouse Embryo	NRG-1 & IGF-1 injected E11.5-E12.5[99]	GFs necessary for compact zone expansion and AV cushion formation
		NRG-1 9.5-11.5 dpc[101]	NRG-1 necessary for full CCS development

Model	Animal	Treatment	Results
In Vitro	NRVMs	NRG-1, 24 hours[100]	Increased F-actin organization and hypertrophy
	mESCs	NRG-1 d1-d3 of differentiation[104]	Preferential differentiation to nodal-type cardiomyocytes
		NRG-1 d1-d3 of differentiation[106]	Increased cardiac induction via ErbB3/ErbB2 signaling
		NRG-1 d3-d7 of differentiation[102]	Global increase in cardiogenesis
		NRG-1 d5-d7 of differentiation[105]	Increased cardiogenesis via ErbB4 signaling, increased contractile components
		NRG-1 d5-d9 of differentiation[103]	ErbB signaling increases working type cardiogenesis
	hESCs	NRG-1 Agonist d5-d12 of differentiation[40]	Increased proportion of working type cardiomyocytes

Chapter 3: Hypertrophy changes 3D shape of hiPSC-cardiomyocytes: Implications for cellular maturation in regenerative medicine

Publication reference: Rupert CE, Chang HH, Coulombe KLK. Hypertrophy Changes 3D Shape of hiPSC-Cardiomyocytes: Implications for Cellular Maturation in Regenerative Medicine. Cell Mol Bioengineering. August 2016:1-9. doi:10.1007/s12195-016-0462-7

Abstract

Advances in the use of human induced pluripotent stem cell (hiPSC)-derived cardiomyocytes for heart regeneration and in vitro disease models demands a greater understanding of how these cells grow and mature in 3-dimensional space. In this study, we developed an analysis methodology of single cardiomyocytes plated on 2D surfaces to assess their 3D myofilament volume and its z-height distribution, or shape, upon hypertrophic stimulation via phenylephrine (PE) treatment or long-term culture ("aging"). Cardiomyocytes were fixed and labeled with α-actinin for confocal microscopy imaging to obtain z-stacks for 3D myofilament volume analysis. In primary neonatal rat ventricular myocytes (NRVMs), area increased 72% with PE, while volume increased 31%. In hiPSC-cardiomyocytes, area increased 70% with PE and 4-fold with aging; however, volume increased significantly only with aging by 2.3-fold. Analysis of z-height myofilament volume distribution in hiPSC-cardiomyocytes revealed a shift from a fairly uniform distribution in control to a basally located volume in a flatter and spread morphology with PE and even more so with aging, a shape that was akin to all NRVMs analyzed. These results suggest that 2D area is not a sufficient measure of hiPSC-cardiomyocyte growth and maturation, and that changes in 3D volume and its distribution are essential for understanding hiPSC-cardiomyocyte biology for disease modeling and regenerative medicine applications.

Keywords

Confocal microscopy, image analysis, phenylephrine, aging, myofilament volume

Introduction

Heart disease is the leading global cause of death and is frequently due, at least in part, to native cardiomyocytes' extremely limited capacity for proliferation.[157,158] Fortunately, many advances in the generation and use of human induced pluripotent stem cell (hiPSC)-derived cardiomyocytes for myocardial regeneration have been made[7,159,160], and implanting engineered cardiac tissue to improve heart function is becoming a possibility[62,161]. However, a more complete understanding of how hiPSC-cardiomyocytes, the building blocks of these tissues, grow and mature is necessary to optimize their performance in engineered tissues and other regenerative therapies to increase efficacy in pre-clinical and clinical applications.

To date, most studies characterize the morphology of hiPSC-cardiomyocytes and other primary cardiomyocytes from two dimensional (2D) images, analyzing parameters including area, elongation, and perimeter.[162,165,164,163] However, cells are inherently 3-dimensional, even when plated on 2D substrates. We hypothesize that this height or z-component changes with cellular phenotype, affects total cell volume, and is therefore a critical component to assess in hiPSC-cardiomyocytes as we study their maturation. Several methods of measuring cell volume have been reported, including the use of suspended microchannel resonators, non-interferometric quantitative phase microscopy, and magnetic resonance imaging of cardiac tissue. [166,167,168] However, these techniques can be prohibitively complex, preventing their adoption beyond the labs in which they were produced. Developing a robust and widely accessible tool to analyze single cells in 3D is crucial to fully understanding how hiPSC-cardiomyocytes grow, mature, and respond to stimuli.

In this study, we develop a semi-automated, increased throughput image analysis protocol to quantify cell volume and shape using confocal microscopy z-stack imaging, CellProfiler[169], and MATLAB®. We successfully measure the myofilament volume of monodispered neonatal rat ventricular myocytes (NRVMs) plated on glass in order to validate our protocol and

subsequently demonstrate the sensitivity of the analysis by quantifying hypertrophy of NRVMs and hiPSC-cardiomyocytes in response to adrenergic stimulation by phenylephrine (PE) or hypertrophic stimulation by aging. Our results indicate that in hiPSC-cardiomyocytes 2D area is not an accurate predictor of 3D myofilament volume and that the z-height distribution of myofilament volume is sensitive to hypertrophic stimulation. Specifically, control (unstimulated) hiPSC-cardiomyocytes (~3 weeks old) were tall and round, and PE stimulation or aging induced a flatter 3D shape that resembles the shape of both control and stimulated NRVMs. Because these differences in hiPSC-cardiomyocyte morphology were only detected with careful analysis of 3D shape, it is critical to adopt robust volume analysis techniques in order to accurately describe cellular morphological behavior.

Methods

Cell Culture and Hypertrophic Stimulation

All hiPSC-cardiomyocytes were derived from the Gibco® Human Episomal iPSC Line (Life Technologies, Carlsbad, CA), following a previously reported protocol.[7] HiPSCs were maintained in chemically defined conditions on plates coated with truncated human vitronectin (VTN-N) in Essential 8™ medium (Life Technologies). For differentiation, hiPSCs were plated as colonies at a low density on truncated VTN-N-coated 6-well plates in Essential 8™ Medium. HiPSCs were grown to 80% confluency at which point chemically defined directed differentiation was performed in RPMI 1640 medium supplemented with 213 μg/mL L-Ascorbic Acid (Sigma-Aldrich, St. Louis, MO) and 500 μg/mL human serum albumin (ScienCell, Carlsbad, CA) (CDM3)[7] with the sequential application of CHIR 99021 (6 μM, d0-d1) followed by inhibitor of Wnt protein 2 (IWP2, 5 μM, d3-d5; Thermo Fisher Scientific, Waltham, MA, USA). After two to three weeks of differentiation, hiPSC-CMs were harvested using 0.25% Trypsin (Life Technologies) and dispersed into single cells via trituration. HiPSC-cardiomyocytes were replated on Matrigel-coated, #1.5 glass coverslips at approximately 26,000 cells/cm^2. Aged

hiPSC-cardiomyocytes were cultured for 12 months before being trypsinized and replated. Aged cells were cultured for 6 days before staining and imaging to correspond with replating time of PE-treated cells.

Neonatal rat ventricular myocytes (NRVMs) were a generous gift from Dr. Ulrike Mende (Cardiovascular Research Center, Rhode Island Hospital) and were harvested in accordance with all institutional and national guidelines for the care and use of laboratory animals as approved by the Institutional Animal Care and Use Committee. NRVMs and hiPSC-cardiomyocytes were given 72 hours to adhere and recover after replating and before beginning stimulation by phenylephrine (PE). Cells received either PE (2 μM) with Timolol (to ensure α-adrenergic stimulation, 0.2 μM)[170] or media alone for 72 hours. For cytosolic volume experiments, hiPSC-cardiomyocytes were incubated with Alexa Fluor® conjugated wheat germ agglutinin (WGA, 10 μg/mL, Thermo Fisher Scientific) for 10 minutes prior to fixation. All cells were then rinsed with KCl (100 mM) to induce diastole and fixed in 4% paraformaldehyde for 10 minutes at 4°C. Cells were stored in DPBS at 4°C until stained.

Immunocytochemistry and Imaging

Cells were blocked in 1.5% normal goat serum (NGS; Jackson ImmunoResearch Laboratories, Inc., West Grove, PA) and stained for α-actinin (Mouse monoclonal α-actinin, 1:800 dilution, Sigma-Aldrich) in 1.5% NGS overnight followed by 1 hour incubation at room temperature with Alexa Fluor® 594 Goat anti-Mouse as the secondary antibody (Life Technologies). Nuclei were labeled with DAPI, and the coverslips were inverted onto slides using VectaShield (Vector Laboratories, Burlingame, CA). Confocal microscopy (Zeiss 510 Meta Confocal Laser Scanning Microscope) was performed using a 63.3x oil immersion objective and z-stacks (0.43 μm thick optical sections) of single cells from each experimental condition ($n \geq 53$) were obtained.

Image Analysis

Collected images were processed in ImageJ[171] and analyzed with a custom pipeline in CellProfiler.[162] In brief, cell nuclei were identified from the compressed z-stack image of the channel recording DAPI (Fig. 1a). The cell body was identified in each slice of the z-stack using a combination of propagation from the identified nucleus and fluorescence intensity of the stained myofibrils (Figs. 1b, 1c). Measurements of cell body area were made in CellProfiler. Two-dimensional area for each cell was defined as the largest slice of its z-stack, as this value was not significantly different from compressed z-stack area and more closely represents cellular cross-sectional area. The maximum cross-sectional area was used to quantify 2D effects of hypertrophic stimulation (Fig. 2) and for normalization of volume distribution by slice area in individual cells (Figs. 4c-4f). Binning of volume distribution was performed by dividing the number of slices within a stack by 5 and averaging the parameter of interest within each section from z=0, defined as the cell-substrate interface, to z=1, defined as the top of the cell (Fig. 4b).

Because the thickness (z_{height}) between each z-stack slice was more than 10-fold less than the height of the cell, the volume was calculated as a trapezoidal prism, where N is the number of slices in the z-stack (Eqn. 1).

$$Volume = \sum_{\iota=1}^{N} \frac{area_{\iota} + area_{\iota-1}}{2} (z_{height})$$

A MATLAB® (MathWorks, Natick, MA, USA) code was implemented to calculate cell volume from the output CellProfiler area (Fig. 1d). Total cell height was calculated as the distance between the first slice with α-actinin or DAPI labeling at the cell-substrate interface and the last slice with α-actinin or DAPI labeling at the top of the cell (Fig. 4a). CellProfiler and MATLAB

codes are available for free download from the Brown Digital Repository, doi:10.7301/Z0WS8R5F.

Statistical Analysis

Each hypertrophy stimulation experiment was performed in triplicate with cells from independent cell isolations (NRVMs) or differentiation runs (hiPSC-cardiomyocytes). Data are presented as the average across all cell isolations or differentiation runs, and error bars represent the standard error of the mean (SEM). Intra- and inter-species comparisons were made with ANOVA followed by Tukey's multiple comparison test, and the volume-area relationship was characterized with linear regression. Comparison of myofilament and cytosolic volume measurements was made with paired Student's *t*-test. Significance for all analyses was determined as $P < 0.05$. All data analysis was performed in GraphPad Prism version 6.00 for Windows (GraphPad Software, La Jolla, CA).

Results

Hypertrophic Stimulation Increases Cardiomyocyte Area

To begin morphological assessment of cardiomyocytes, we characterized the hypertrophic response of monodisperse, plated neonatal rat ventricular myocytes (NRVMs) and hiPSC-cardiomyocytes to adrenergic stimulation with phenylephrine (PE) using two-dimensional area measurements. PE stimulates hypertrophy in rodent cardiomyocytes[172] and hESC-cardiomyocytes,[173,174] thus we hypothesized that cell area would increase in both PE-stimulated NRVMs and hiPSC-cardiomyocytes. To test this, cardiomyocytes were treated for 72 hours with PE and continued to beat spontaneously.

In addition to undergoing hypertrophy with PE stimulation, cardiomyocytes hypertrophy during development.[175] In order to assess if cardiomyocyte growth occurred during *in vitro* long-term

culture, hiPSC-cardiomyocytes were cultured for 12 months, during which time they maintained their automaticity, and were then replated for single-cell analysis. Aged cardiomyocytes had morphological signs of hypertrophy with a 4.5-fold increase in area, a 3.0-fold increase in perimeter, a 33 ± 14% increase in nuclear area (potentially due to increased nuclear ploidy[176]), and a 21 ± 5% increase in sarcomere length ($P < 0.05$, n=20 cells per group). This morphological hypertrophy with aging has been reported to coincide with more mature electromechanical properties of human pluripotent stem cell-derived cardiomyocytes.[164]

Cardiomyocytes stained for α-actinin, a protein of the myofibril z-disks, showed striations throughout the cell in both hiPSC-cardiomyocytes (Fig. 2a-c) and NRVMs (Fig. 2d-e). PE treatment significantly increased area in NRVMs by 72% from 2,492 ± 228 μm^2 to 4,299 ± 455 μm^2 and in hiPSC-cardiomyocytes by 70% from 1,148 ± 149 μm^2 to 1,950 ± 802 μm^2 (Fig. 2f; n=53 per group, $P < 0.05$). Aged hiPSC-cardiomyocytes showed a 3.5-fold increase in area over control with an area of 5,139 ± 421 μm^2 (n=53, $P < 0.01$). NRVMs had a significantly greater area than hiPSC-cardiomyocytes of the corresponding treatment group ($P < 0.05$). Area determined by membrane labeling in hiPSC-cardiomyocytes yielded similar results, where PE stimulation induced a 2-fold increase in area (n=27 cells per group, $P < 0.01$). These results confirmed that PE elicited a hypertrophic response in 2D area for both NRVMs and hiPSC-cardiomyocytes and that aged hiPSC-cardiomyocytes underwent hypertrophy during 12 months of culture.

Myofilament Volume Increases in Aged hiPSC-Cardiomyocytes

We next sought to determine if PE stimulation significantly increased cardiomyocyte volume. To accomplish this, a custom CellProfiler pipeline and MATLAB® code were written which reconstructed cardiomyocytes from confocal z-stacks to determine volume (Fig 3a). NRVM volume increased significantly with PE stimulation by 31% from 17,892 ± 1,752 μm^3 to 28,446 ±

3,274 μm^3 (n = 53 cells per group; $P < 0.01$). HiPSC-cardiomyocyte volume, however, increased only slightly from 5,673 ± 651 μm^3 to 6,583 ± 555 μm^3 and did not reach significance (n=53 cells per group, $P = 0.3$). Analysis of biological replicates revealed no significant difference in volume with PE stimulation among single differentiation runs. Hypertrophy of aged cardiomyocytes, however, resulted in a significant volume increase of 2.3-fold over control to 12,962 ± 1,050 μm^3 (n = 53 cells, $P < 0.01$). These results suggest that cell area does not accurately predict cell volume of hiPSC-cardiomyocytes.

Correlation of cell volume to cell area was performed in order to quantify the predictive value of area. Control and PE-stimulated NRVMs and aged hiPSC-cardiomyocytes were strongly correlated ($R^2 = 0.35$-0.83, Fig 3b) compared to control and PE-stimulated hiPSC-cardiomyocytes ($R^2 = 0.01$-0.02) (Fig 3c). Cardiomyocyte cytosolic volume was analyzed for control and PE-stimulated hiPSC-cardiomyocytes using the membrane marker wheat germ agglutinin (WGA; Fig 4a). Cytosolic volume was significantly greater than myofilament volume for both control and PE-stimulated cells (n = 27 cells per group, $P < 0.01$), and only cytosolic, not myofilament volume, increased significantly with PE treatment ($P < 0.01$; Fig 4b). Additionally, the relationship between area and volume determined by WGA labeling was strongly correlated ($R^2 = 0.88$-0.89; Fig 4c). These results suggest that cytosolic volume changes independently of myofilament volume during PE stimulation. Because we are interested in using this cell type in a regenerative context as a contractile cell, myofibril volume (the amount of contractile lattice per cell) is the functionally relevant morphological metric of interest. Additionally, myofilament markers are widely used in the literature to quantify cardiomyocyte morphology.[162,178,177] Thus, further studies of cardiomyocyte morphology were explored with myofilament quantification where we investigated morphological reasons why a significant increase in myofilament area was not accompanied by an increase in myofilament volume with PE stimulation.

Hypertrophic Stimulation Changes hiPSC-Cardiomyocyte 3D Shape

Because 3D myofilament volume and 2D area were not correlated for control and PE-treated hiPSC-cardiomyocytes (unlike NRVMs), we hypothesized that the 3D morphology of hiPSC-cardiomyocytes differed with and without PE stimulation. Cell height was first examined to determine how cells changed total height in the z-direction with hypertrophic stimulation (Fig 5b). No significant difference was observed in control and PE-treated NRVMs (8.23 ± 0.22 μm and 8.58 ± 0.19 μm, respectively), however, hypertrophic stimulation in hiPSC-cardiomyocytes with PE (9.49 ± 0.42 μm) or aging (6.35 ± 0.26 μm) led to a significantly decreased cell height compared to control (11.41 ± 0.45 μm, $P<0.01$).

To further investigate how cell shape changed in three dimensions, we analyzed the volume distribution in ten representative cells of each group. For each image slice of the z-stack (with z=0 corresponding to the cell-substrate interface and z=1 to the top of the cell, Fig 5c), cell area was normalized to the average maximum area of the control group of the same cell type and areas were binned by z-height for graphical representation. In NRVMs, distribution of cellular volume was similar in control and PE-stimulated cells, with significantly smaller areas in the top half of the cell compared to the bottom in both groups ($P<0.05$, Fig. 5d). The ~50% increase in area at z=0 and 0.25 height with PE treatment reflects our 2D area measurements and is not present at $z\geq0.5$. This significant increase in area for $z<0.5$ with PE treatment indicates that the volume increase measured with PE treatment is occurring in the bottom half of the cells. In hiPSC-cardiomyocytes, only PE-treated and aged groups showed significantly decreased area in the top half of the cells ($P<0.05$, Fig 5e), demonstrating a more uniform distribution of cell volume throughout the height of the cell in control hiPSC-cardiomyocytes.

These data suggest that hypertrophic stimulation via PE and aging causes a significant shift in hiPSC-cardiomyocyte myofilament volume distribution, concentrating it in the bottom half of the

cell. In contrast, PE treatment in NRVMs causes only slight redistribution of myofilament volume since volume is already concentrated in the bottom half of control NRVMs. Additionally, whereas PE treatment led to a significant increase in area in the bottom half of the cell ($z<0.5$) over control in NRVMs (*a, P*<0.05 versus control at same z-height, Fig 5d), PE treatment in hiPSC-cardiomyocytes did not significantly increase area at $z<0.5$ contrary to 2D area measurements (Fig 5e). This discrepancy may be due to the use of binning for analysis of 3D volume distribution and the fact that maximum slice area (used for normalization) was not always at $z=0$ (shown as a slightly less than 1.0 value for control hiPSC-cardiomyocyte area at $z=0$). This data analysis underscores the need for carefully defined metrics in 2D and 3D and suggests that a more complete picture of cellular morphology can be obtained with both area and volumetric analysis. Interestingly, aged hiPSC-cardiomyocytes displayed a significant increase in area at $z<0.5$ versus control (*b, P*<0.05 versus control, Fig 5e), showing a >3-fold increase in area at $z=0$. Further, aged hiPSC-cardiomyocyte area was significantly reduced and not different from control at $z\geq0.5$ (Fig 5e), similar to control NRVMs. However, all hiPSC-cardiomyocytes maintained ~10% area at $z>0.5$ suggesting a fundamental difference versus NRVMs. Taken together, these data suggest that while PE treatment leads to an increase in myofilament volume in NRVMs, it leads only to a redistribution of myofilament volume in hiPSC-cardiomyocytes and that hypertrophy (defined as an increase in cell volume) can be achieved with aging hiPSC-cardiomyocytes in culture.

Discussion

In this study, a new image analysis protocol was developed to analyze 3D morphology of neonatal rat ventricular myocytes (NRVMs) and hiPSC-cardiomyocytes. The protocol was then used to examine the effects of hypertrophic stimulation on cardiomyocyte shape in 3D. We demonstrate that (1) aging increases 2D area in hiPSC-cardiomyocytes and phenylephrine (PE) stimulation increases 2D area in both NRVMs and hiPSC-cardiomyocytes, (2) our image

analysis protocol can be successfully implemented to quantify 3D morphology of single cells from confocal z-stack images, (3) PE stimulation increases myofilament volume in NRVMs but not hiPSC-cardiomyocytes while aging increases myofilament volume in hiPSC-cardiomyocytes, and (4) the discrepancy in area versus volume quantification with PE stimulation in hiPSC-cardiomyocytes can be explained by differences in 3D morphology.

Our results provide a novel explanation for differing reports of hypertrophic response to phenylephrine stimulation in the literature. NRVMs are consistently observed to hypertrophy with phenylephrine stimulation, however, contradictory results have been reported for hiPSC-cardiomyocytes.[178,177] Using the image analysis method described in this study, we characterized three-dimensional volume and its distribution (or shape) and demonstrated an important difference between single NRVM and hiPSC-cardiomyocyte shape under control growth conditions. While untreated NRVMs are spread and undergo more spreading during phenylephrine stimulation, untreated hiPSC-cardiomyocytes present a taller, more variable, and rounded morphology and become flatter and more spread upon phenylephrine stimulation. This change in overall hiPSC-cardiomyocyte shape may account for why a significant increase in area is not accompanied by a corresponding increase in myofilament volume during PE stimulation in our study. Implementing this rigorous three-dimensional characterization in other systems may elucidate changes in cell shape which could underlie apparently conflicting responses of cells to growth stimuli.

This data also describes for the first time how hiPSC-cardiomyocyte shape changes with hypertrophic stimulation via aging. Metabolic[179] and functional[6,7] maturation have been demonstrated in aged pluripotent stem cell-derived cardiomyocytes, however, a change in three-dimensional shape has not been described. Cardiomyocytes increase in volume during fetal development,[180] and this study demonstrates that the same phenomena occurs in long-term *in vitro* culture of hiPSC-cardiomyocytes, with volume increasing more than 2-fold in aged

12-month-old cardiomyocytes versus 2-week-old control cells. It should be noted that while differences in hiPSC-cardiomyocyte volume and shape were observed with pathological (phenylephrine) and physiological (aging) hypertrophy, this protocol is a means to characterize those differences rather than a tool to identify pathological versus physiological mechanisms of hypertrophy. The findings presented here, where hiPSC-cardiomyocyte volume increased from 5,673 μm^3 at 2 weeks old to 12,962 μm^3 over one year of culture, is consistent with the limited data available for primary human cardiomyocytes, where volume was reported to be 5,835 μm^3 at birth.[181]

PE-stimulated growth of hiPSC-cardiomyocytes differs markedly from aging in long-term culture in our study, suggesting mechanistic differences in these two stimuli. With PE stimulation, we observed a redistribution of myofilaments, localizing at the cell-substrate interface and resulting in increased cell area without a corresponding increase in myofilament volume. This could be explained via PE-mediated changes in focal adhesion expression[182] that may initiate myofibril localization to the sub-sarcolemma compartment through changes in the cytoskeleton as shown in development.[183] The short duration of PE stimulation and culture may preclude new myofibril formation in young hiPSC-cardiomyocytes, even though we observed an increase in cell volume using a membrane label (Fig. 4). A similar increase in cardiomyocyte size (measured by surface area) without accompanying change in myofibril content has been observed in NRVMs stimulated for just 36 hours.[184] Taken together, these data suggest that acute (72-hour) PE stimulation of hiPSC-cardiomyocytes may progress through the same phases with slower kinetics, resulting in an increased cytosolic volume, focal adhesion mediated redistribution of myofilaments, and no increase in myofilament volume. In contrast, we observed both increased area and volume in aged hiPSC-cardiomyocytes, which may be attributed to alternative mechanisms of growth. Aged hiPSC-cardiomyocytes likely have more focal adhesions, similar to the approximately 3-fold increase in vinculin protein expression in 24-month-old vs 6-month-

old rat ventricles.[185] Further, in aged hiPSC-cardiomyocytes, myofibril formation likely occurs during long-term culture, reflected in a 2.3-fold increase in myofilament volume, a phenomenon well documented in cardiomyocytes undergoing early development where human cardiomyocyte volume increases approximately 4-fold in the first three months after birth.[181] Thus, additional study of the stimulation dependence and kinetics of myofibril assembly, re-organization, and relationship to transmembrane adhesions and the sarcolemma in hiPSC-cardiomyocytes will be a valuable area to pursue.

The analysis protocol described here has valuable uses for characterizing changes in cell shape over time, beyond models of hypertrophic stimulation. Cells are known to respond to and remodel the environment with which they are presented, and their three-dimensional shape may change due to this process. Further development of this image analysis protocol could elucidate how single cardiomyocytes interact with matrices in three dimensions, and future work will seek to adapt this protocol to more complex three-dimensional environments such as those found in engineered tissues.

In summary, we have developed a sensitive image acquisition and analysis protocol to characterize three-dimensional size and shape of single cells and demonstrated its ability to detect hypertrophy of hiPSC-cardiomyocytes. This protocol is easily adaptable across cell types and laboratories. As tissue engineering continues to develop in three-dimensional space, analysis methods must be created and adopted to mirror this, and the protocol reported here takes an important first step in providing higher throughput 3D analysis for single cells. It will be necessary to continue to push these analyses protocols toward characterizing dense, cellular 3D tissues in order to accurately understand these complex environments and cellular responses to them.

Acknowledgments

We gratefully acknowledge Celinda Kofron, Ph.D. for sharing NRVMs for this study and funding from NIH R00 HL115123 (to K.L.K.C.), the Brown University Eccleston Fellowship (C.E.R.), and a Brown University Karen T. Romer Undergraduate Teaching and Research Award (H.H.C.).

Conflict of Interest

Authors Rupert, Chang, and Coulombe declare that they have no conflict of interest.

Statements of Human and Animal Rights and Informed Consent

All studies on neonatal rat ventricular myocytes were performed with cells provided by Dr. Ulrike Mende's laboratory at the Rhode Island Hospital Cardiovascular Research Center, in accordance with all institutional and national guidelines for the care and use of laboratory animals as approved by the Institutional Animal Care and Use Committee.

Tables & Figures

Figure 1

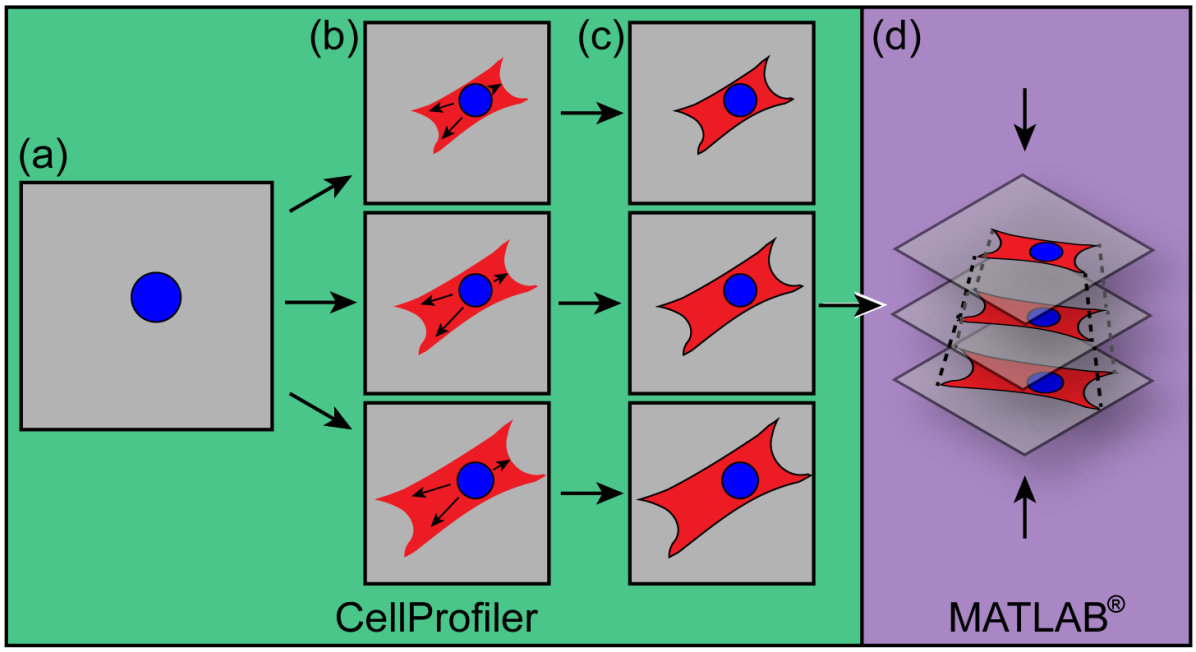

Figure 1. Automated image analysis compiles z-stack images to calculate cardiomyocyte volume. (a) The nucleus is identified from a compressed z-stack. (b) The nucleus mask is imposed on each slice of the α-actinin stained cell's z-stack images, and the *propagation* function is used to couple cell area within each slice with the nucleus. (c) Cell borders are drawn for cardiomyocyte area in each slice and measurements of the identified cell area is made for each slice in CellProfiler. (d) Measurement data is exported to MATLAB® where z-stack slices are reconstructed into 3D cardiomyocytes. See Methods for details.

Figure 2

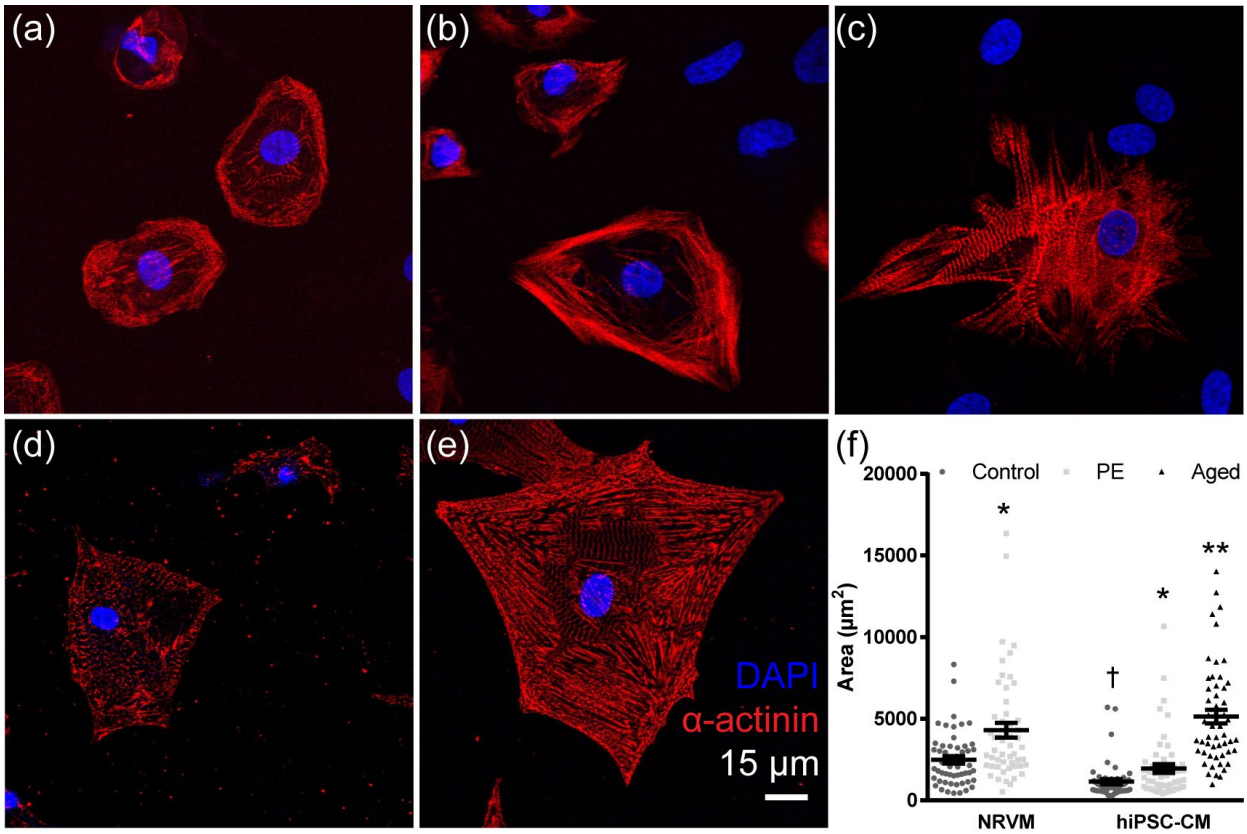

Figure 2. Cardiomyocyte 2D phenotype and area changes in hypertrophic stimulation. Single hiPSC-derived cardiomyocytes (hiPSC-CMs) were seeded in control conditions (a) stimulated with phenylephrine (PE; b) and aged for 12 months (c). Neonatal rat ventricular myocytes (NRVMs) were seeded in control conditions (d) and stimulated with PE (e) Cardiomyocytes were stained for α-Actinin (red) and nuclei (blue). Scale bar: 15 μm. (f) Cell area was calculated for NRVM control and PE and hiPSC-CM control , PE, and aged groups (n=53 per group); bars represent mean ± SEM. *P<0.05 versus control; **P<0.01 versus control; †P<0.05 versus NRVM control.

Figure 3

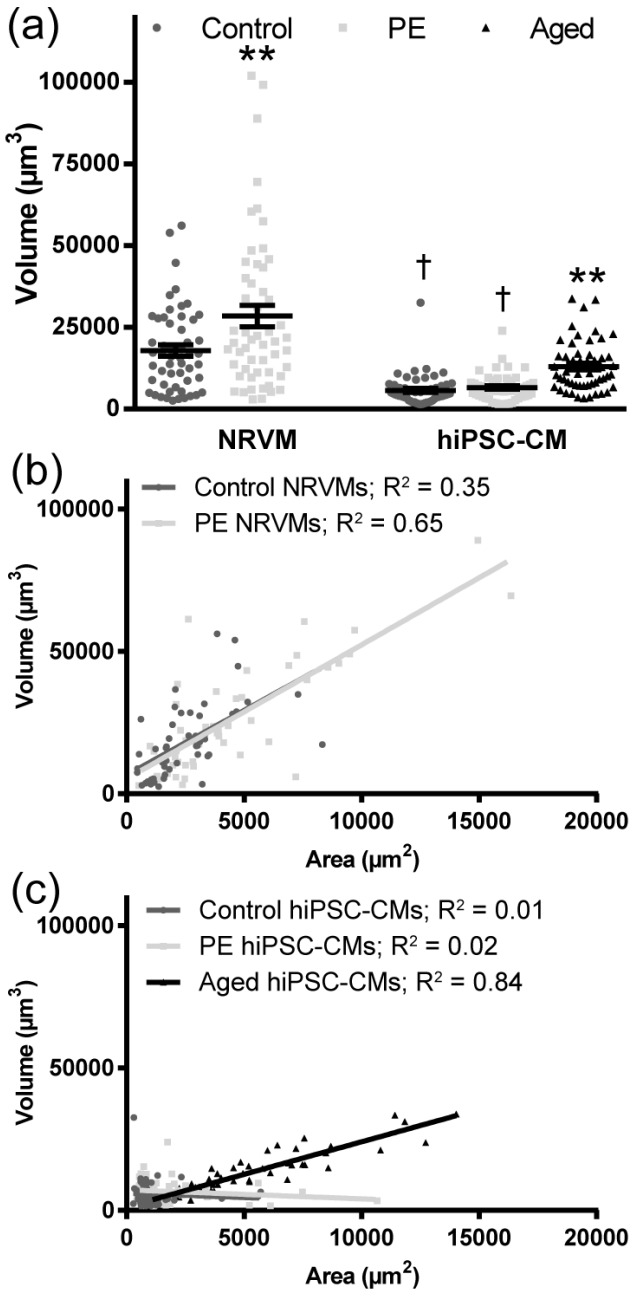

Figure 3. Volume correlates differentially with cardiomyocyte source and hypertrophic stimulation. (a) Neonatal rat ventricular myocyte (NRVM) and hiPSC-cardiomyocyte (hiPSC-CM) volume was determined under phenylephrine stimulation (PE) and aging (Aged). Bars represent mean ± SEM. **P*<0.05 vs. control of same species; ***P*<0.01 vs. control of same species; †*P*<0.05 vs. NRVM control. (b,c) The correlation between area and volume was plotted for NRVMs (b) and hiPSC-CMs (c) with R^2 values displayed next to each group.

Figure 4

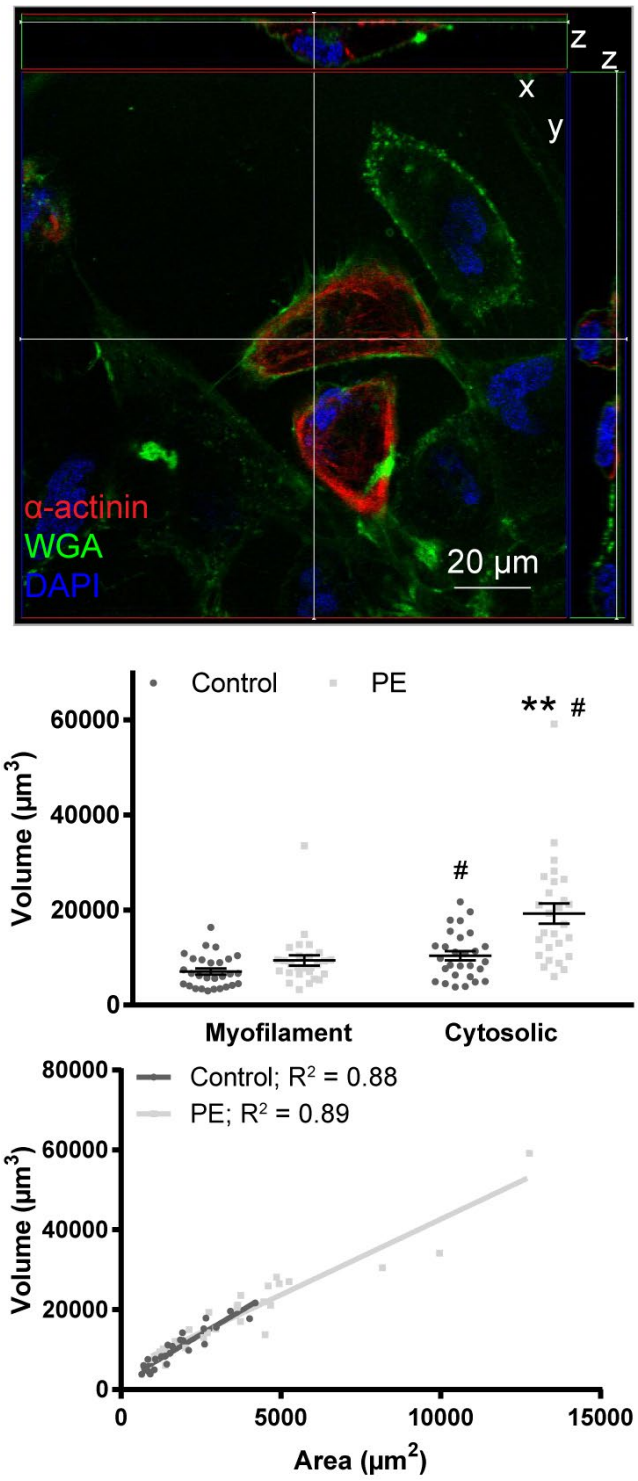

Figure 4. Cytosolic volume responds to hypertrophic stimulation in hiPSC-cardiomyocytes. (a) HiPSC-cardiomyocytes stained for α-actinin (red), wheat germ agglutinin (WGA, green), and nuclei (DAPI, blue) in orthoslice view. (b) HiPSC-cardiomyocyte myofilament and cytosolic volume determined by α-actinin and WGA staining, respectively for control and PE-stimulated conditions. Bars represent mean ± SEM. $^{**}P<0.01$ vs. control of same volume type; $^{\#}P < 0.01$ vs. myofilament volume of same treatment. (c) The correlation between area and cytosolic volume was plotted for hiPSC-cardiomyocytes with R^2 values displayed next to treatment group.

Figure 5

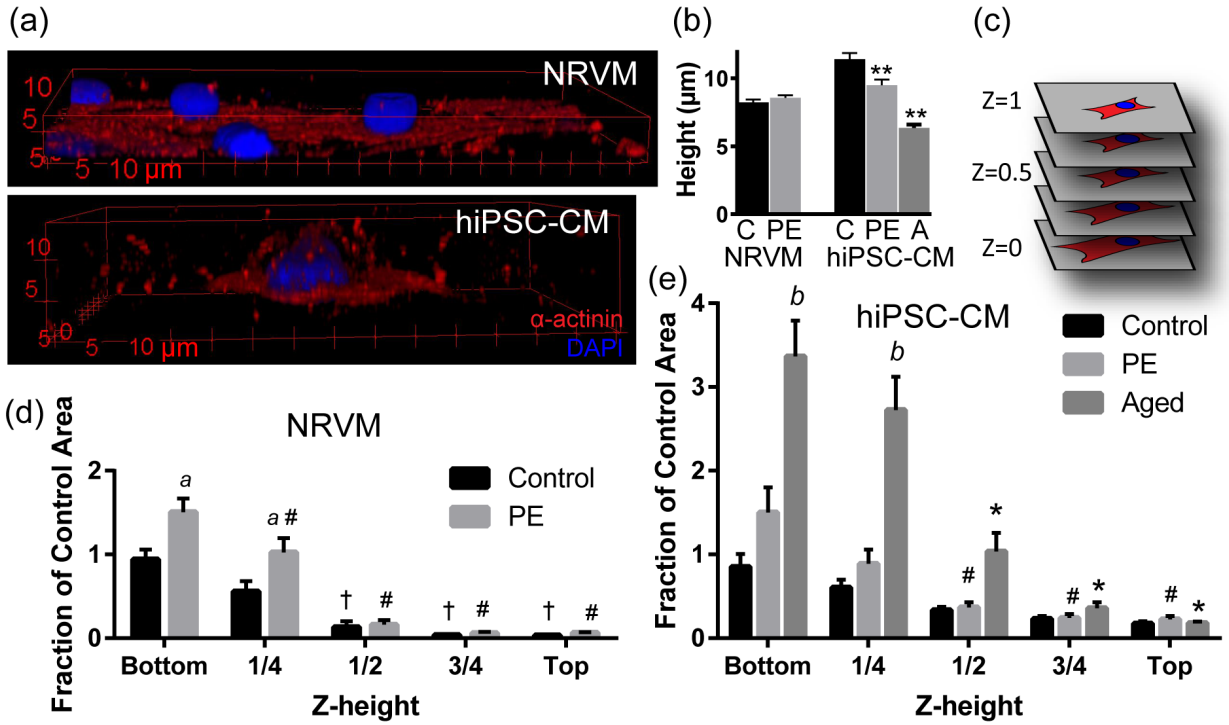

Figure 5. Volume and z-height distribution in hypertrophically stimulated cardiomyocytes. (a) Representative 3D renderings of control neonatal rat ventricular myocytes (NRVMs, top) and hiPSC-cardiomyocytes (hiPSC-CM, bottom) stained for α-actinin (red) and nuclei (blue). (b) Average height of NRVMs and hiPSC-cardiomyocytes under control (C), phenylephrine stimulation (PE) and aging (A) conditions. $^{**}P<0.01$ vs. control of same species. (c) Schematic for z-height convention. (d,e) Fraction of control maximum area as a function of z-height in NRVMs (d) and hiPSC-CMs (e). Note that the y-axis has the same linear scale (unit/inch) for direct comparison. $^{\dagger}P<0.05$ vs. z=0 within control; $^{\#}P<0.05$ vs. z=0 within PE; $^{*}P<0.05$ vs. z=0 within Aged; $^{a}P<0.05$ for PE vs. control at same z-height; $^{b}P<0.05$ for Aged vs. control at same z-height. Bars represent mean ± SEM.

Chapter 4: IGF-1 and NRG-1β Enhance Proliferation, Metabolic Maturity, and the Force-Frequency Response in hESC-derived Engineered Cardiac Tissues

Publication Reference: Rupert CE, Coulombe KLK. IGF1 and NRG1 Enhance Proliferation, Metabolic Maturity, and the Force-Frequency Response in hESC-Derived Engineered Cardiac Tissues. Stem Cells Int. 2017;2017:7648409. doi:10.1155/2017/7648409

Abstract

Insulin-like growth factor 1 (IGF1) and neuregulin-1β (NRG1) play important roles during cardiac development both individually and synergistically. In this study, we analyze how 3D cardiac tissue engineered from human embryonic stem cell (hESC)-derived cardiomyocytes and 2D plated hESC-cardiomyocytes respond to developmentally relevant growth factors both to stimulate maturity and to characterize the therapeutic potential of IGF1 and NRG1. When administered to engineered cardiac tissues, a significant decrease in active force production of ~65% was measured in all treatment groups, likely due to changes in cellular physiology. Developmentally-related processes were identified in engineered tissues as IGF1 increased hESC-cardiomyocyte proliferation 3-fold over untreated controls and NRG1 stimulated oxidative phosphorylation and promoted a positive force-frequency relationship in tissues up to 3 Hz. HESC-cardiomyocyte area increased significantly with NRG1 and IGF1+NRG1 treatment in 2D culture and gene expression data suggested increased cardiac contractile components in engineered tissues, indicating the need for functional analysis in a 3D platform to accurately characterize engineered cardiac tissue response to biochemical stimulation. This study demonstrates the therapeutic potential of IGF1 for boosting proliferation and NRG1 for promoting metabolic and contractile maturation in engineered human cardiac tissue.

Introduction

The development of defined methods to derive cardiomyocytes from human pluripotent stem cells (hPSCs) has provided a valuable platform to develop regenerative medicine technologies. Cardiomyocytes derived from human embryonic stem cells (hESC-cardiomyocytes) and tissues constructed from them have been shown to exhibit a cardiac phenotype characterized by gene expression patterns, electrophysiological behavior, and mechanical function. Previous research describes the response of engineered cardiac tissues (ECTs) to common drugs, however, little is known about how ECTs develop under *in utero*-like biochemical conditions. Just as embryonic development has informed directed differentiation of hESCs to the cardiac lineage, we hypothesize that fetal development can inform how ECTs grow and mature. In order for ECTs to advance towards the clinical realm as both a translational therapy and an *in vitro* model, a more thorough understanding of how to manipulate hESC-cardiomyocyte maturation in 3D tissues via developmental cues is required.

Two growth factors crucial to cardiac development *in vivo* are insulin-like growth factor 1 (IGF1) and neuregulin-1β (NRG1). IGF1 has been implicated in physiological growth of the heart, and studies performed to downregulate[186] and upregulate[187] its receptor in mouse models show dilated cardiomyopathy and cardiomyocyte physiological hypertrophy, respectively. At the cellular level, IGF1 has been shown to increase proliferation in hESC-cardiomyocytes via the PI 3-kinase/Akt pathway *in vitro.*[39] Thus, carefully regulated IGF1 signaling is required for proper development and maturation of the heart in order to achieve both cardiomyocyte proliferation and growth, yet the timing of IGF1 stimulation likely alters this response. Similarly, a critical need for appropriate NRG1 signaling during development has been demonstrated. When NRG1[80] or its receptors ErbB2[79] and ErbB4[78] are deleted in mice, ventricular trabeculation and endocardial cushion formation are depressed, and mice die mid-embryogenesis. When mice embryos are cultured *ex vivo*, NRG1 is required for complete cardiac conduction system

development[101]. A synergistic effect of IGF1 and NRG1 has also been reported in mice *in utero* where their combined presence is necessary for ventricular wall expansion and atrioventricular cushion formation.[99] We hypothesized that we could improve functional maturation of engineered cardiac tissue formed from hESC-cardiomyocytes by extending the developmental period beyond the stereotypical two-week differentiation time point via application of developmental growth factors IGF1 and NRG1 independently or in combination after formation of 3D hESC-derived engineered cardiac tissues.

In the current study, we demonstrate that our ECTs are sensitive to biochemical stimulation with IGF1 and NRG1 and that hESC-cardiomyocytes in 3D tissues respond in unique patterns to these growth factors that is not predicted from previous studies. We show that force production declines by 60-70% in ECTs with IGF1 and/or NRG1 stimulation. However, we discovered that our ECTs respond sensitively to IGF1 and NRG1 stimulation in proliferative activity and metabolic capacity, respectively and that the force-frequency relationship is preserved or improved with NRG1 or NRG1+IGF1, respectively. We show that hESC-cardiomyocytes exhibit increased area when plated in 2D and treated with NRG1 or IGF1+NRG1 and that this 2D "hypertrophy" does not correlate with increased force in 3D tissues. These data suggest that 2D and transgenic mouse models are not sufficient to fully predict the effects of biochemical stimulation on 3D hESC-derived engineered cardiac tissues and that our platform for forming and characterizing ECTs uniquely possesses the sensitivity to describe tissue response to physiologically relevant growth factors for regenerative medicine applications.

Materials & Methods

2.1 Cell culture and differentiation

Undifferentiated RUES2 human embryonic stem cells (hESCs) from Rockefeller University were maintained in mouse embryonic-fibroblast conditioned media, supplemented with basic

fibroblast growth factor (R&D Systems). HESCs were differentiated into cardiomyocytes with a previously described directed differentiation protocol (Figure 1A).[188] Briefly, CHIR99021 (Cayman Chemical), Activin A, bone morphogenetic protein 4 (BMP4; R&D Systems), and Tankyrase inhibitor XAV 939 (Tocris Bioscience) were applied sequentially in defined, monolayer culture conditions on Matrigel™ (BD Biosciences)-coated 6-well plates.[189] HESC-cardiomyocytes were differentiated in RPMI 1640 + 1X B27 supplement without insulin (RPMI/B27 without insulin; Life Technologies) and maintained in RPMI/B27 (with insulin) with medium replaced every two days. After two weeks of differentiation, hESC-cardiomyocytes were harvested with 0.25% trypsin in 0.5 M EDTA (Life Technologies) and either incorporated into engineered tissues (Figures 1-5) or cryopreserved[190] for later use in single-cell experiments (Figures 6 and 7).

2.2 Flow cytometry

Cardiac purity was determined for each hESC-cardiomyocyte harvest. Cells were fixed in 4% PF and stained with antibodies against cardiac troponin T (cTnT, 2 μg/mL; Thermo Fisher Scientific) and alpha-smooth muscle actin (α-SMA, 0.5 μg/mL; Abcam) to identify cardiomyocytes (cTnT+), fibroblast-like cells (SMA+), and immature cardiomyocytes (double positive for cTnT and SMA).[191] Samples were analyzed with a FACSAria II cell sorter (BD Biosciences) and 10,000 events were recorded per sample. FACS data was analyzed used FlowJo software (Figure 1B) where gates were set based on isotype antibody controls.

2.3 Mold and tissue formation

Custom acrylic and polydimethylsiloxane (PDMS) molds were produced for ECT culture as previously reported.[192] Negative templates for tissue molds were created using a 100W CO_2 laser to etch a pattern generated in Adobe Illustrator into ¼" acrylic (TAP Plastics). Polydimethylsiloxane (PDMS, Thermo Fisher Scientific) was poured into acrylic negatives,

degassed, and cured overnight at 60°C (Figure 1C). Tissue molds were sterilized by autoclave and made hydrophilic with a BD-20A high frequency generator (Electro-Technic Products). Engineered tissues were created by combining $1x10^6$ hESC-cardiomyocytes 50%/50% vol/vol with 2.5 mg/mL rat tail collagen-I (Advanced Biomatrix) for a final concentration of 1.25 mg/mL collagen-I and pipetting into the prepared molds. Collagen-cell suspensions were allowed to gel for 45 minutes at 37°C before RPMI/B27 was added. Tissues were cultured in 6 well plates fitted with C-pace stimulator lids (IonOptix) and stimulated at 1 Hz, 4 ms pulse width, 5V/cm for 14 days immediately following tissue formation. Tissues contracted the collagen and began beating within 48 hours of formation (Figure 1D). Experimental groups were treated daily with 100 nM[39] insulin-like growth factor (PeproTech), 100 ng/mL[193] neuregulin-1 (R&D Systems), or both 100 nM IGF1 and 100 ng/mL NRG1. All experiments described used these concentrations where relevant. Media was replaced every other day, and tissues were cultured for two weeks. All constructs were treated with 10 μM bromodeoxyuridine (BrdU; Roche) 18-24 hours prior to fixation to label replicating DNA.

2.4 Mechanical testing

Cardiac tissues were cut into strips and their passive and active mechanical properties were measured with a custom mechanics setup as previously described.[194,16] Tissue strips were mounted on two hooks (attached to a force transducer and motor arm), bathed in Tyrode's solution containing 1.8 mM Ca^{2+} at 30-34°C, and electrically field stimulated via platinum electrodes. Force exerted by the tissue was measured with a 100 mN load cell (Aurora Scientific). Tissues were initially stretched to L_0, determined as the shortest length at which individual contractions could be detected by the force transducer. The tissues were then stretched by steps of 5% L_0 to 30% stretch (Figure 2A). Once at 30% stretch, tissues were paced at increasing frequencies and the fastest frequency they were able to follow was

measured and recorded as the maximum capture rate (MCR). Mechanical experiments were run in biological triplicate with three to four replicates in each group.

The following calculations were made based on the data obtained from mechanical testing. Active stress, σ_a, was determined at each length by averaging the amplitude of twitch force, F_a, of at least 5 contractions and normalizing by the cross-sectional area (CSA). The CSA of each tissue strip was assumed to be an ellipse with the measured preparation width and height corresponding to the major and minor axes, respectively. The fold increase in active stress was calculated from the active stress ($\sigma_{a,1}$) at the first length step ($L_1 = 1.05\ L_0$) and maximum active stress ($\sigma_{a,max}$) at 30% stretch ($L_6 = L_{max} = 1.30\ L_0$) using Equation 1 (Figure 2A).

$$Fold\ Increase = \frac{\sigma_{a,max} - \sigma_{a,1}}{\sigma_{a,1}} \quad \text{Eqn. 1}$$

Stiffness of each tissue strip was calculated by plotting the passive stress produced by each tissue against the strain (Figure 2C). Passive stress, σ_p, was calculated by normalizing the passive (or baseline) force produced by the tissue at each step, F_p, by the CSA and is reported in units of kPa. Strain, ε_x, at each step, L_x, was determined by Equation 2.

$$\varepsilon_x = \frac{L_x - L_0}{L_0} \quad \text{Eqn. 2}$$

A linear relationship of these data allowed for a regression line to be fit to each stress vs. strain plot (R^2 values of 0.749 to 0.998), and the stiffness (Young's modulus) is reported as the slope of the line for each ECT strip. Passive stiffness was difficult to measure in tissues due to uncontrolled drift in the baseline force during testing of some samples, resulting in reduced sample sizes of n=5-6.

Contraction kinetics were calculated from data traces acquired at 1000 Hz sampling rate in custom Lab View software using a custom analysis script in MATLAB®. The peak speed of

force development during contraction, upstroke velocity (v_{up}), was determined as the slope of the linear regression line to the steepest rise in stress and was averaged across at least 5 contractions (Figure 2B). The peak force of each contraction and the time to relax to 50% and 90% ($\sigma_{a,max}$, R_{50}, and R_{90}, respectively) were calculated and averaged across at least 5 contractions (Figure 2B).

2.5 Immunofluorescent and immunohistochemical staining

Engineered tissues were fixed in 4% paraformaldehyde (PF; Sigma-Aldrich), embedded in paraffin, and sectioned at 5μm. Sections were blocked in 1.5% normal goat serum in PBS and primary antibodies for cardiac troponin T to label cardiomyocytes (cTnT, 0.5 μg/mL; Thermo Fisher Scientific) and BrdU for cells in the S phase of the cell cycle (1.5 U/mL; Roche) were applied sequentially overnight with development using Vector Red and DAB (Vector Laboratories) according to manufacturer's instructions to color cTnT-positive cells pink and BrdU-positive nuclei brown. Hematoxylin (7 mg/mL; Sigma-Aldrich) was used as a nuclear counterstain. For cardiomyocyte proliferation studies, at least 100 cTnT-positive nuclei were counted per slide with proliferating cardiomyocytes identified as those with brown nuclei and senescent cardiomyocytes those with blue nuclei. Brightfield images were taken with an Olympus IX70 Inverted Microscope.

For immunofluorescent staining of ECT sections, slides first underwent antigen retrieval with a Proteinase K digest (10 μg/mL; Roche) for 12 minutes at 37°C. Mouse anti-alpha-actinin was used to identify cardiomyocyte z-discs of the myofibrils (1:800; Sigma-Aldrich) with Alexa Fluor® 488 goat anti-mouse secondary antibody (Life Technologies) and Hoechst 33342 to label nuclei (1.5 μg/mL; Sigma-Aldrich; Figure 1d). The same protocol was used for immunofluorescent staining of single cells with the Proteinase K digest replaced by a permeabilization step in Triton X-100 (0.25%; Sigma-Aldrich) for 6 minutes at room temperature. Confocal images were taken

with a Zeiss LSM 510 Meta Confocal Laser Scanning Microscope. Image processing and analysis was performed with ImageJ,[171] CellProfiler,[169] and MATLAB® (MathWorks).

2.6 RNA isolation and quantitative reverse transcriptase-polymerase chain reaction

MRNA was extracted from engineered tissues using the RNeasy Mini Kit (QIAGEN) and mRNA concentration was measured with a NanoDrop 1000 Spectrophotometer (Thermo Fisher Scientific). CDNA was synthesized from the same mass of mRNA per sample with the SuperScript III First-Strand Synthesis System (Life Technologies) and included genomic DNA digestion. CDNA samples were combined with primers (Thermo Fisher Scientific) and SYBR Master Mix (Life Technologies), and quantitative real-time PCR was run with an Applied Biosystems® 7900 fast real-time system (Life Technologies). Relative expression levels were calculated using the 2^(-ΔΔCt)[195] with HPRT as an internal control (Figure 4). Samples were run with biological and technical triplicates.

2.7 Mitochondrial content quantification

Single hESC-cardiomyocytes were plated on Matrigel-coated chamber slides (Thermo Fisher Scientific) at 22 x 10^3 cells/cm^2 on day 0, and treatment groups were pulsed daily with IGF1, NRG1, or IGF1+NRG1. On day 5, cells were treated with MitoTracker® Red FM (Life Technologies), incubated for 30 minutes at 37°C, and then fixed in 4% PF. Cells were imaged with an Eclipse Ti-E inverted fluorescence microscope (Nikon), and total integrated fluorescence per image, normalized by cell number, was calculated with a custom CellProfiler Pipeline. CellProfiler data was analyzed in MATLAB®.

2.8 Metabolic activity

HESC-cardiomyocytes were seeded at 40 x 10^3 cells/well of a Matrigel-coated XFe96 cell culture microplate (Seahorse Bioscience, North Billerica, MA, USA) and fed daily for two weeks.

Treatment groups were supplemented with IGF1, NRG1, or NRG1+IGF1 daily. On day 14, cells were switched to 175 µL/well assay media: XF Base Medium (Seahorse Bioscience), 4 mM GlutaMAX, 1 mM Sodium Pyruvate (Life Technologies), and 25 mM glucose (Sigma-Aldrich) and incubated for 90 minutes at 0% CO_2 and 37°C. Basal oxygen consumption rate (OCR) and extracellular acidification rate (ECAR) measurements were then made with an XFe96 Extracellular Flux Analyzer (Seahorse Bioscience).

2.9 Statistical analysis

Data are expressed as mean ± SEM or SD as indicated in figure legends. Statistical significance was determined by using Student unpaired *t*-tests (Figure 3A, 3B), one-way ANOVA with Dunnett's multiple comparisons (Figures 4-7), linear regression analysis (Figure 3B), or as indicated in the text. A *P*-value < 0.05 was considered statistically significant.

Results

3.1 Cardiac force-length relationship is recapitulated in ECTs

ECTs were formed in a collagen gel with 1.0 x 10^6 cells per tissue ranging from 81-95% cardiac purity by flow cytometry (Figure 1B) in custom PDMS molds (Figure 1C). We treated ECTs daily with 100 nM IGF1, 100 ng/mL NRG1, or both 100 nM IGF1 + 100 ng/mL NRG1 (IGF+NRG) and continuously paced ECTs at 1 Hz during their two-week culture period. ECTs contracted within the PDMS molds (Figure 1D) and assembled striated myofibrils (Figure 1E). To characterize the effects of biochemical treatment with IGF1 and NRG1 upon contractile function of ECTs, we used a custom mechanics apparatus to measure intact twitch forces and their kinetics under electrical stimulation. ECTs from all groups followed electrical stimulation at 1 Hz both in culture and during mechanical measurements, however, ECTs treated with NRG1 or IGF1+NRG1 exhibited a loss of spontaneous contractions (automaticity) when external pacing was paused after just one week in ECT culture. ECTs exhibited the classic Frank-Starling relationship[196] with

active twitch force, F_a, increasing as tissues were stretched up to 30% of their initial length, L_0 (Figure 2A). A fold change in active stress significantly greater than 1 indicates a positive force-length relationship. This signifies increased contractile force with stretch, consistent with the Frank-Starling relationship (Table 1). There was no significant difference in fold-change of active stress between control and treatment groups, indicating that biochemical stimulation neither enhanced nor inhibited the sensitivity of hESC-cardiomyocytes to increases in length. Passive tissue stiffness, defined as passive force normalized by cross-sectional area, ranged from 0.685 ± 0.265 kPa in control to 0.964 ± 0.158 kPa in NRG1-treated tissues (Figure 2C, Table 1). The maximum passive stiffness value measured, 1.928 kPa, was equal to that previously reported for scaffold-free engineered hESC-cardiac patches[16] and about ten-fold below that of human myocardium (~16 kPa).[197]

3.2 Active contractile force and force-frequency relationship are sensitive to biochemical stimulation

We hypothesized that cardiomyocyte maturation due to biochemical stimulation would be detected at the level of force production in ECTs. To test this, we measured active stress in tissue preparations up to 30% stretch, $\sigma_{a,max}$ (Table 1). Surprisingly, active stress was significantly decreased by 63%, 64%, and 65% of control with IGF1, NRG1, and IGF1+NRG1 treatment, respectively. The average $\sigma_{a,max}$ in the control group, 0.59 ± 0.14 mN/mm^2, is equivalent to other reported values in collagen-based engineered hESC-cardiac tissue[198] and two orders of magnitude below healthy human myocardium[199]. The force-frequency relationship, which is a positive relationship *in vivo* and one often missing *in vitro,*[201,200,198] was examined in our ECTs by calculating the fraction of the force produced at 1 Hz to that produced when pacing tissues at a range of stimulation frequencies (Figure 3A). We observed a negative force-frequency response in control and IGF1-treated tissues with significant decreases in force beyond 1.5 Hz and 1 Hz, respectively. In NRG1-treated tissues, we observed sustained force

amplitude with increasing frequency and measured a significant drop in force only at 3 Hz (180 beats per minute), which is close to the maximum rate captured. IGF1+NRG1 treated tissues showed the most positive force-frequency relationship, with force significantly higher at 1.5 Hz and no significant reduction in force with increasing frequency, similar to recently reported results when using electromechanical stimulation.[202,58] Lastly, the maximum capture rate (MCR) of each group was determined at 30% stretch (Table 1). The IGF1-treated group had the slowest MCR, while the NRG1-treated group had the fastest at 2.8 ± 0.3 Hz and was significantly greater than control.

3.3 Biochemical stimulation does not alter the kinetics of contraction and relaxation

To determine if biochemical stimulation altered contraction and relaxation kinetics independent of changes in force, we examined the speed of tissue contraction and relaxation. Peak rate of force development or upstroke velocity, v_{up} (Figure 2C), at 30% stretch was fastest in the control group, depressed with IGF1 treatment, and significantly slower in the NRG1 and IGF1+NRG1-treated groups (Table 2). The change in v_{up} with stretch was then examined and a slope significantly greater than 0 was observed in all groups, indicating a significant increase in v_{up} with stretch as is expected for increased twitch force amplitude. The slope was steepest in the control group and significantly reduced in treatment groups (Figure 3B). The control group had the slowest time to 50% and 90% relaxation from peak force (R_{50} and R_{90}, respectively; Figure 2B) and both R_{50} and R_{90} were decreased with NRG1 treatment (Table 2). However, the apparent changes in contraction upstroke velocity and relaxation kinetics with biochemical stimulation at maximal stretch can be explained by the lower maximal twitch force that biochemically stimulated tissues produced. Because force production in treated ECTs was 35% of control, we also examined v_{up}, R_{50}, and R_{90} in control ECTs at 35% of their maximal force production (at 10% stretch) where R_{50} and R_{90} were very similar to what has been previously reported for hESC-cardiomyocytes.[203] No significant differences were observed between

treatment groups and 35% control (Table 2). When examined over the range of maximal stress produced across all groups (Figure 3C), v_{up} does not differ with IGF1 and NRG1 treatment. This confirms that for a given $\sigma_{a,max}$, contraction kinetics are not altered with biochemical stimulation.

3.4 Biochemical stimulation induces increased gene expression of maturation markers in ECTs

To determine if our biochemical stimulation could induce changes at the molecular level in our ECTs, we used q-RT-PCR to examine mRNA expression levels of a panel of cardiac markers involved in force production, development, calcium handling, and resting membrane potential. Genes MYH6, MYH7, and TNNT2, which code for proteins α- and β-myosin heavy chain and cardiac troponin T, respectively, that are components of the contractile lattice, increased expression by about 4- to 6-fold without reaching significance when NRG1 was included in the stimulation cocktail (Figure 4A). Atrial and ventricular myosin light chain expression did not change significantly with stimulation (data not shown). NPPA and NPPB, coding for atrial (ANP) and brain (BNP) natriuretic peptides, had expression levels greater than 50-fold above control with NRG1 stimulation (Figure 4B). Their increased expression has been associated with cardiovascular development, where natriuretic peptides are expressed in the ventricles during gestation and in the cardiac conduction system after birth.[204] Phospholamban (PLN), whose low expression is characteristic of stem cell-derived cardiomyocytes but is required for proper calcium handling[205] also trended towards increased expression with NRG1 and IGF1+NRG1 treatment, which may contribute to decreased twitch amplitude in those groups. Ryanodine receptor 2 (RYR2), responsible for the release of Ca^{2+} from the sarcoplasmic reticulum, was not altered by treatment (Figure 4C). Two ion channels important for resting membrane potentials in cardiomyocytes were not altered by biochemical stimulation, namely the hyperpolarization-activated channel 4 (HCN4), responsible for the “funny current” and necessary for pacemaker action potentials in cardiomyocytes,[206] and the KCNJ2 gene, encoding the inward-rectifier

potassium ion channel, $K_{ir}2.1$ (Figure 4D). No gene expression differences were observed with IGF1 treatment alone and synergy between NRG1 and IGF1 was not observed. Together, this gene expression data suggests that the cardiac lineage may be pushed forward into a more mature phenotype in ECTs stimulated with NRG1.

3.6 IGF1 increases cardiomyocyte proliferation in ECTs

Because force production was decreased in biochemically stimulated ECTs, we sought to identify alternative molecular mechanisms occurring in IGF1- and NRG1-treated tissues. First, we examined proliferation rates in ECTs by quantifying the number of cardiomyocytes that had incorporated bromodeoxyuridine (BrdU) into their nuclei during DNA replication (S phase of the cell cycle; Figure 5A,B). This was done by incubating ECTs with BrdU overnight, prior to fixation, and staining tissue sections for cardiac troponin T and BrdU. Proliferation rates increased more than 3-fold over control with IGF1 treatment from 3.0 ± 0.6% to 12.3 ± 1.0% (Figure 5c). NRG1 treatment negated this effect, returning proliferation rates to that of control. As seen in both gene expression and mechanics data, NRG1 dominates the treatment effects when administered simultaneously with IGF1. Because treatment of hESC-cardiomyocytes with IGF1 in 2D culture results in increased cytokinesis, not karyogenesis, we hypothesize the same is the case in ECTs.

3.7 Cellular metabolic activity is modulated by NRG1 and IGF1 treatment

Because NRG1 signaling has been implicated in altering cellular respiration[207] and because we noticed increased media yellowing of ECTs treated with NRG1 and IGF1+NRG1, we investigated mitochondrial content and metabolic rates in hESC-cardiomyocytes. We first sought to confirm that overall mitochondria content was differentially affected by growth factor stimulation. Plated single cells were treated for 2 or 5 days with IGF1, NRG1, or IGF1+NRG1 and mitochondrial content per cell was then determined with MitoTracker® Red. No differences

were seen between groups treated for 2 days, but 5 days of NRG1 treatment significantly increased mitochondrial content 3.6 ± 0.6-fold over control (P<0.05, n=4). Either increased mitochondria size or biogenesis could explain this result, se we next sought to assess if increased mitochondrial content in NRG1-treated cells was associated with an increase in metabolic activity, we examined basal cardiomyocyte metabolic rates with an XFe96 Extracellular Flux Analyzer (Seahorse Bioscience). To emulate the 3D engineered tissue conditions as closely as possible, we plated cardiomyocytes as a confluent monolayer and treated for 2 weeks with IGF1, NRG1, or IGF1+NRG1 daily. On day 14 we measured the basal oxygen consumption rate (OCR, Figure 6A), extracellular acidification rate (ECAR), and calculated the ratio of the two measures (OCR/ECAR, Figure 6B) with all measures normalized to cell number. A significant increase in OCR over control was present in all treatment groups, indicating increased metabolic activity with each treatment. The OCR/ECAR ratio indicates relative levels of mitochondrial respiration and glycolysis, with an increased ratio reflecting an increase in mitochondrial respiration and a decreased ratio reflecting an increase in glycolysis. The IGF1-treated cells had a significantly lower OCR/ECAR ratio versus control, whereas NRG1-treated cells had a significantly higher OCR/ECAR ratio. IGF1+NRG1-treated cells displayed a trend towards an increased OCR/ECAR ratio, but this did not reach significance. These results align with previous studies that show proliferating cells have increased rates of glycolysis[208] and treatment with NRG1 increases oxidative phosphorylation subunits in mitochondria of rat skeletal muscle cells.[119]

3.8 NRG1 induces increased area at the single-cardiomyocyte level

Because both IGF1 and NRG1 have been implicated in cardiomyocyte hypertrophy through traditional 2D culture methods using single cells[210,209] we examined the morphological response of single hESC-cardiomyocytes plated in 2D to IGF1 and NRG1. Cells were treated daily with IGF1, NRG1, IGF1+NRG1 or a recently published hypertrophic cocktail “TID” (100 nM

triiodothyronine hormone, 100 ng/mL IGF1, 1 μM dexamethasone)[43] for five days. HESC-cardiomyocytes in every group show distinct striations with alpha-actinin labeling (Figure 7). Further, biochemical treatment for 5 days increased cell area by 2- to 2.6-fold of untreated control with a significant increase in NRG1, IGF1+NRG1, and TID groups (p<0.01, Figure 7). These results in 2D-plated hESC-cardiomyocytes do not predict the response of the same cell-type in 3D ECTs where there was no significant difference in alpha-actinin content per cardiomyocyte with growth factor stimulation (data not shown). This demonstrates the necessity of studying cardiomyocytes in the more physiological, 3D platform.

Discussion

This study describes the response of hESC-cardiomyocytes in engineered cardiac tissues (ECTs) to stimulation by developmentally important growth factors insulin-like growth factor 1 (IGF1) and neuregulin 1β (NRG1). The novel findings include (1) description of the amplitude and kinetics of twitch force development and the force-frequency relationship in ECTs stimulated with IGF1 and NRG1, (2) quantification of hESC-cardiomyocytes' proliferative response in 3D to IGF1 and NRG1, (3) characterization of the metabolic activity of biochemically stimulated hESC-cardiomyocytes, and (4) the observation that responses from cells in 2D and at the gene expression level do not predict 3D engineered tissue functional behavior. This study demonstrates that this ECT platform is an accessible and valuable 3D *in vitro* tool to analyze the response of hESC-cardiomyocytes to biologically important growth factors.

In an effort to develop a contractile tissue therapy for the heart, it is necessary to thoroughly understand the contractile function of engineered cardiac tissues. We used a variety of parameters to evaluate how growth factor treatment modulated ECT function. Across all groups we observed a positive relationship between stretch and both σ_a and v_{up}. The average active force produced by the control group (normalized only by cross-sectional area, CSA) of 0.59 ± 0.14 mN/mm^2 was higher than previously reported for hESC-cardiomyocyte-only, strip-like

tissues;[23,21] was equal to recently reported values;[198] and was lower than with patterned molds where overall tissue force production was normalized by CSA, porosity, and cellular orientation.[211] Notably, our tissues were formed without Matrigel or Geltrex and were cultured in serum-free conditions in contrast to these other studies, suggesting that it is possible to eliminate ill-defined protein components in the process of making engineered cardiac tissue. In our tissues, contraction kinetics are within 25% of what has been reported in both hESC-cardiomyocytes[203] and adult cardiomyocytes.[213,212] In order to boost both passive and active mechanical properties in our ECTs to physiologically relevant levels, it will be important to create a more stiff matrix environment that more closely mimics human myocardium, and these efforts are underway by our group and others.[214,215]

Cardiomyocyte proliferation can be significantly enhanced in ECTs treated with IGF1 to 12.3 ± 1.0% (3-fold above untreated control) as evidenced histologically and metabolically, far above rates in mature, adult myocardium which have a proliferation rate of <0.1% beyond 20 years of age.[216] This phenomena has been reported in human ESC-derived cardiomyocytes in both 2D[39] and *in vivo*,[4] but had yet to be confirmed in engineered tissues *in vitro* prior to this study. A balance between proliferation and differentiation of cardiomyocytes exists in the embryonic cardiovascular system[217] where the increase in one process precludes the other. This could explain why increased cardiomyocyte proliferation rates in ECTs stimulated by IGF1 was accompanied with a significant decrease in force production, which requires assembly and maturation of the contractile lattice. Although IGF1 results in decreased twitch force amplitude in ECTs, the ability of engineered cardiac tissue to respond to proliferative stimulation is a valuable asset because of the precious nature of hESC-cardiomyocytes. Producing hESC-cardiomyocytes is an expensive endeavor, and tools to maximize yield will be key to advancing cardiac tissue engineering technologies towards therapeutic applications. Because this study focused on the detailed evaluation of ECT response to biochemical stimulation, only one

treatment condition for each stimulant group was used. In the future, optimization of dose and timing could enable a more careful modulation of ECT response to growth factor stimulation to elicit a particular response. For example, IGF1 administered early in engineered tissue formation would facilitate proliferation of hESC-cardiomyocytes and could be followed by subsequent treatments or growth periods. Additionally, the B27 supplement used in this study contained insulin, which can bind and activate IGF receptors, and future studies may demonstrate increased sensitivity to IGF1 treatment with insulin-free supplement.

NRG1 treatment of ECTs produced additional novel benefits, enhancing electromechanical maturity, reflected in a non-negative force-frequency relationship up to 3 Hz and a maximum capture rate of 2.8 Hz, and promoting metabolic activity with an increase in both mitochondrial content and oxidative phosphorylation by 1.4 and 1.5-fold over control, respectively. Metabolic sensitivity to growth factor treatment has previously been reported in hiPSC-cardiomyocytes where tri-iodo-L-thryonine (T3) treatment increased oxygen consumption rate without an increase in mitochondrial content but with a corresponding increase in force production.[41] Similar results were reported with a cocktail of T3, IGF1, and dexamethasone (TID).[43] Our results also show that hESC-cardiomyocyte metabolism can be manipulated with biochemical stimulation, but in a manner that increases mitochondrial content (biogenesis). Recent work has demonstrated that mitochondria number increases during maturation of hPSC-cardiomyocytes in long-term culture, and our results suggest a means to expedite this process.[218] Currently, the field is limited to metabolic measurements of hESC-cardiomyocytes in 2D cultures, and yet we believe these data accurately represent the metabolic behavior of engineered 3D tissues because they provide plausible explanations for the phenomena observed in 3D, namely an increased rate of medium acidification (apparent with overnight color change to yellow in phenol red-containing culture medium) and decreased force production. With NRG1 stimulation, the increase in mitochondrial content and decrease in force production we observed suggests that

mitochondrial maturation was achieved with NRG1 while contractile maturation was paused or hindered. This result contrasts those of T3 stimulation[41] and TID stimulation,[43] suggesting that hESC-cardiomyocyte maturation is dependent upon the specific developmental stimulant. We hypothesize that metabolic maturation is required for increased contractile function of hESC-cardiomyocytes, but that removal of NRG1 stimulation to curb mitochondrial biogenesis may be required to promote contractile strength.

NRG1 stimulation in ECTs dramatically increased ANP and BNP expression greater than 50-fold over control, which suggests hypertrophic growth and is in stark contrast to the reduced maximal force we obtained with NRG1 stimulation. Spikes in ANP and BNP transcript levels are observed during important milestones in embryonic cardiac development.[219] The high levels of gene expression observed in ANP and BNP may be due to the biochemically-induced developmental environment we create *in vitro* through the addition of NRG1. NRG1 has also been implicated in maintaining metabolic homeostasis,[220] which could indicate the ANP and BNP upregulation correlates with the postnatal period. Alternatively, increased ANP and BNP serum levels have been clinically associated with heart failure,[221] so an alternative explanation for increased ANP and BNP levels, accompanied by decreased contractility, could be the induction of a pseudo disease state. Because NRG1 signaling is present in both development and disease,[220] we hypothesize that the spikes in ANP and BNP are likely akin to normal development (e.g., ANP/BNP spike at birth due to rapid changes in hemodynamics and atrial pressure) and cardiac homeostasis because of the immaturity of these hESC-cardiomyocytes as well as the positive metabolic effects NRG1 stimulation had on ECTs. Assessing the mechanistic importance of ANP and BNP in hiPSC-cardiomyocyte maturation will require verification of protein levels and activated signaling pathways.

Our data on cardiomyocyte area versus tissue force production support the idea that the morphological response of hESC-cardiomyocytes plated on stiff surfaces in 2D is not

necessarily predictive of hESC-cardiomyocyte functional maturity.[222] Biochemically treated cells showed a significantly larger area versus control in 2D and although gene expression profiles in ECTs suggested maturity, no significant change in α-actinin content was observed at the tissue level as assessed by α-actinin staining intensity normalized per nucleus in ECTs (data not shown). Further, functional analysis of active contractile strength in ECTs showed decreased twitch force amplitude with biochemical stimulation by IGF1, NRG1, or IGF1+NRG1. The discrepancy we find in cellular growth in 2D (increased) and force generation in 3D engineered tissue (decreased) is likely due to the different microenvironments (e.g., stiffness) that are provided to the cells in these two culture systems, which is a phenomenon that has been previously described and appears to affect cell phenotype across many cell types ranging from fibroblasts[223] and neurons[224] to primary cardiomyocytes.[225] Additionally, recent work from our group demonstrates that single hPSC-cardiomyocyte volume does not increase with area, which suggests that 2D area increase with biochemical stimulation does not truly indicate physiological hypertrophy of the cells but rather a morphological response to the microenvironment.[226]

In summary, this study describes how developmentally important growth factors can be used to elicit functional responses in 3D engineered cardiac tissues (ECTs) for therapeutic applications including increased cardiomyocyte proliferation by IGF1 and metabolic maturation by NRG1. We developed and characterized an hESC-derived cardiac tissue engineering platform that incorporates static stress and electrical stimulation during culture and utilize it as a test bed for cardiac tissue maturation. ECTs responded to NRG1 and IGF1 treatment at the biomolecular, metabolic, and functional levels, demonstrating the therapeutic potential of these biochemical stimulants. We speculate that the timing and combination of developmentally pertinent growth factors including IGF1 and NRG1 will reveal methods for maximizing ECT maturity and contractile performance.

5 Conclusion

Our results show that growth factors identified from development, IGF1 and NRG1, modulate hESC-derived cardiomyocyte physiology in 3D engineered cardiac tissues by increasing proliferation and maturing the metabolic phenotype, respectively. IGF1 and NRG1 together synergistically acted to create a positive force-frequency response. Further, we showed that when IGF1 and NRG1 were administered to single hESC-cardiomyocytes in 2D culture, NRG1 promoted increased cell area (often referred to as hypertrophy but potentially not the case with hPSC-cardiomyocytes),[226] which was different from the 3D hESC-cardiomyocyte response as measured by force production, highlighting the necessity of 3D platforms to characterize and develop tissues for therapeutic applications.

Author Contributions

C.E.R. and K.L.K.C. designed the project, performed experiments, and collected data. C.E.R. analyzed data and generated figures. C.E.R. and K.L.K.C. interpreted data and wrote the manuscript.

Acknowledgements

We gratefully acknowledge funding from NIH K99/R00 HL115123 (to K.L.K.C.) and the Brown University Eccleston Fellowship (to C.E.R.). We thank Dr. C. Murry (University of Washington) for advice on experiment design and data interpretation, Dr. M. Regnier (University of Washington) for mechanics support, and Dr. M. Tipping (Providence College) for technical assistance with Seahorse assays.

Conflict of interest

The authors have no financial interest in the subject matter discussed in this paper.

Ethics Statement

Studies were performed and the manuscript was assembled in accordance with the Journal of Tissue Engineering and Regenerative Medicine Ethical Policies.

Figures & Tables

Figure 1

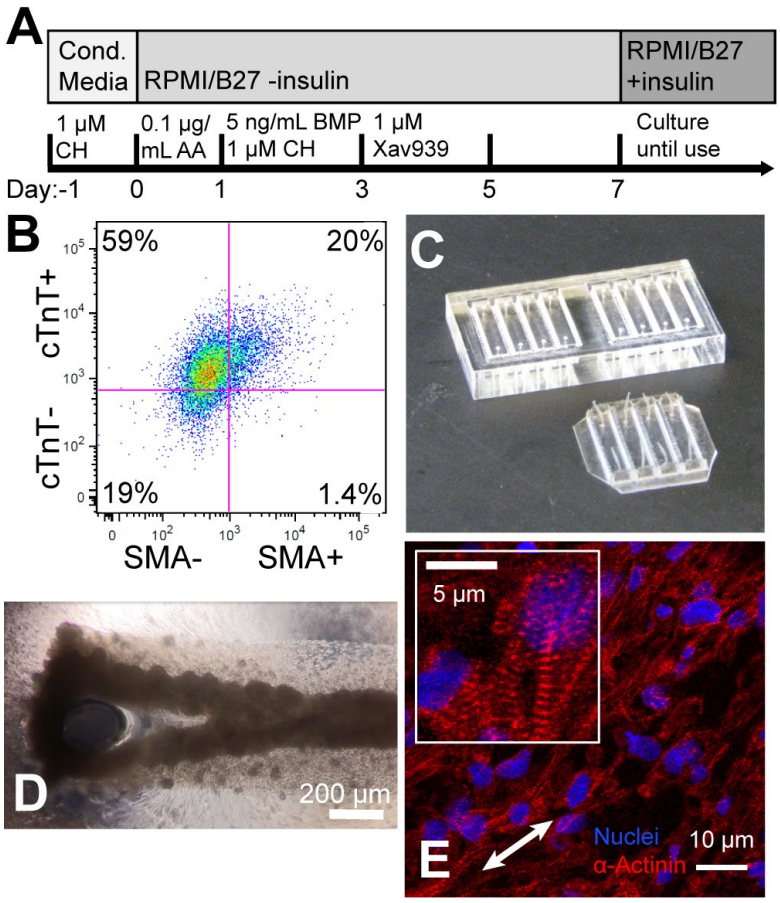

Figure 1. Directed differentiation of hESCs result in highly enriched cardiomyocyte populations which form beating tissues *in vitro*. (A) Timeline of differentiation of cardiomyocytes from hESCs (Cond. Media: MEF-conditioned media, CH: Chiron99021, AA: activin A, BMP: bone morphogenic protein 4). (B) Differentiated populations were immunofluorescently stained for cardiac troponin T (cTnT) and smooth muscle actin (SMA) and analyzed with flow cytometry. (C and D) Cardiomyocytes cultured with a collagen-1 matrix in PDMS molds cast from custom laser-etched acrylic negatives (C) remodeled the matrix and formed beating constructs within 48 hours (D). (E) Immunofluorescence of α-actinin (red) and nuclei (blue) in engineered tissue sections. Myofibril striations were visible (inset). White double-headed arrow indicates direction of uniaxial stress in tissue during culture.

Figure 2

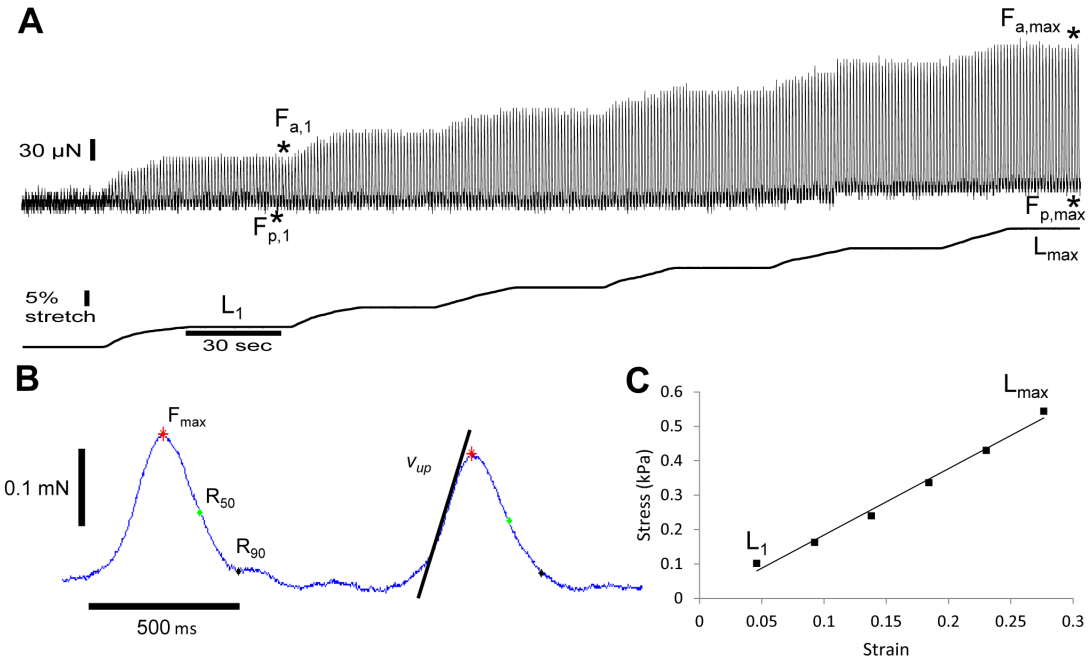

Figure 2. Engineered muscle displays robust twitch contractions. (A) Force (top) and length (bottom) trace of an ECT stretched to 130% of its initial length in 5% steps with individual twitch contractions recorded at each length**.** Active and passive force are indicated at 5% stretch (length step L_1) as $F_{a,1}$ and $F_{p,1}$ and at 30% stretch (L_{max}) as $F_{a,max}$ and $F_{p,max}$ as indicated by asterisks. (B) Traces of individual contractions were processed to identify maximal twitch stress ($\sigma_{a,max}$, red asterisk), time to 50% and 90% force relaxation (R_{50}, green asterisk, and R_{90}, black asterisk), and peak upstroke velocity (v_{up}). (C) Young's modulus (stiffness) of each tissue was determined by measuring passive stress, σ_p, from 5% stretch of initial length (L_1 = 0.05 strain) to 30% stretch (L_{max} = 0.30 strain) and calculating the slope of the line of best fit. In this example, Young's modulus = 1.93 kPa (R^2=0.99).

Figure 3

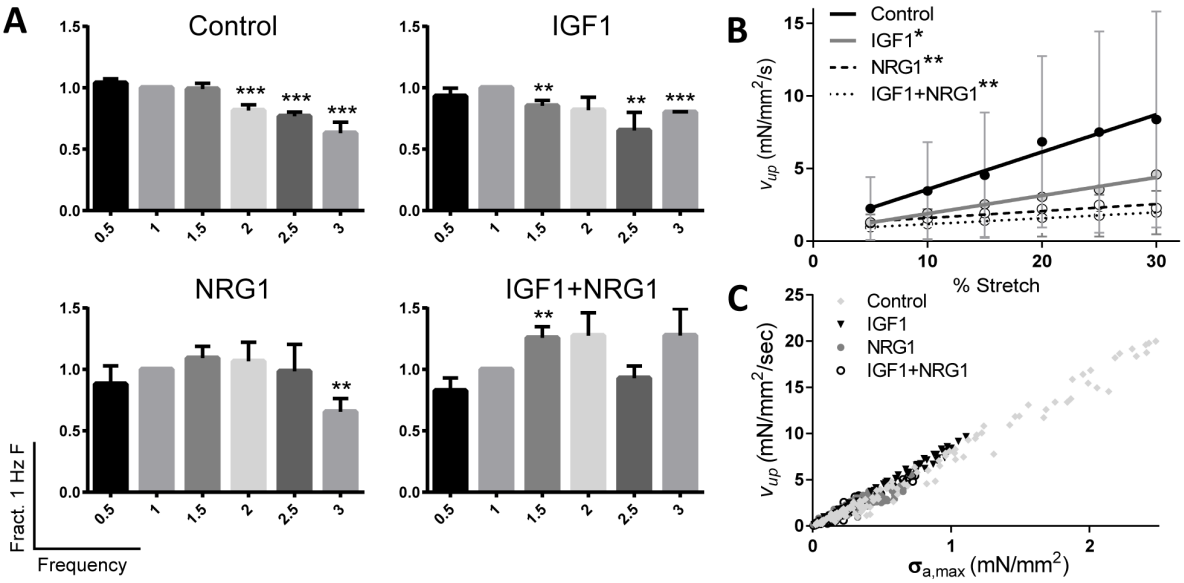

Figure 3. Engineered muscle displays a force-frequency response that is sensitive to biochemical stimulation. (A) Maximum active stress at 30% stretch was measured at increasing frequencies for control, IGF1, NRG1, and IGF1+NRG1. Data are shown normalized to active stress at 1 Hz and expressed as mean ± SEM. (B) The relationship between upstroke velocity (v_{up}) and percent stretch was plotted and fit with a regression line for each treatment group. Data are expressed as mean ± SEM at each length. (C) A scatterplot of v_{up} versus maximum active stress, $\sigma_{a,max}$, was plotted. n = 10 per group. *P < 0.05, **P < 0.01, ***P < 0.001 vs 1Hz of same group (A) or slope of line versus control (B).

Figure 4

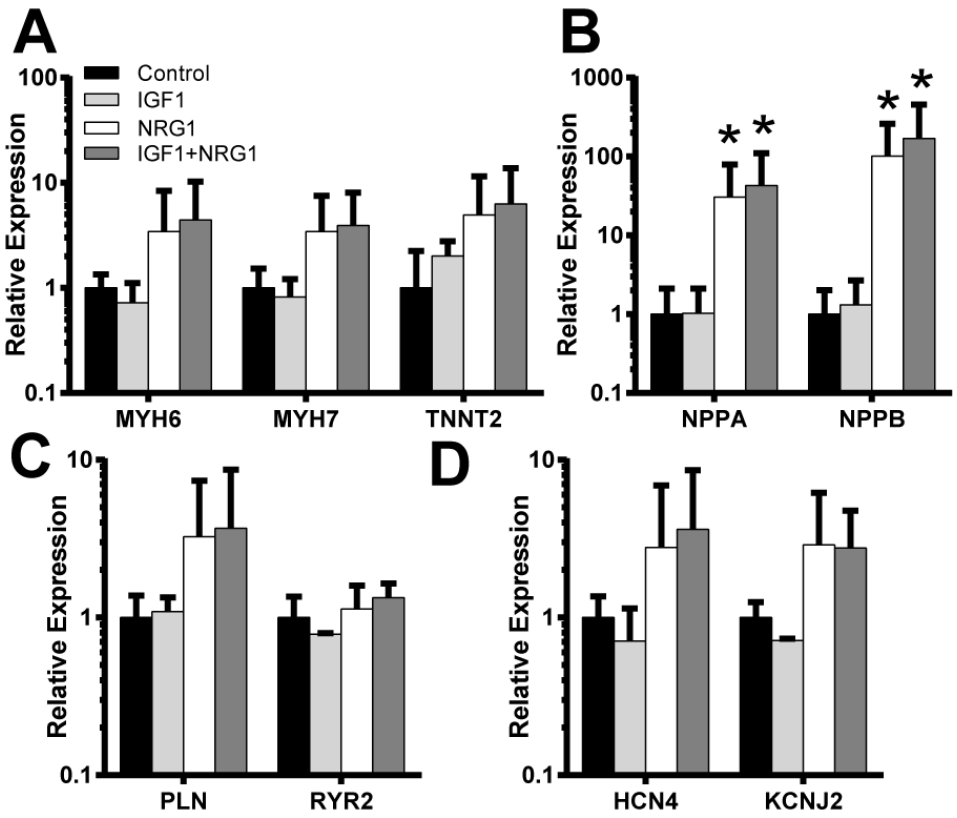

Figure 4. Engineered tissues alter their gene expression patterns by q-RT-PCR analysis in response to biochemical stimulation. Genes shown encode proteins associated with the contractile lattice (MYH6: α-myosin heavy chain, MYH7: β-myosin heavy chain, TNNT2: cardiac troponin T; A), development (NPPA: atrial natriuretic peptide, BNNP: brain natriuretic peptide; B), calcium handling (PLN: Phospholamban, RYR2: ryanodine receptor 2; C), and voltage-gated ion channels (HCN4: Hyperpolarization-activated cyclic nucleotide-gated channel, KCNJ2: inward-rectifier potassium ion channel; D). *n* = 3 per group; data are shown as fold induction of gene expression normalized to HPRT1 and expressed as mean ± SEM. **P* < 0.05.

Figure 5

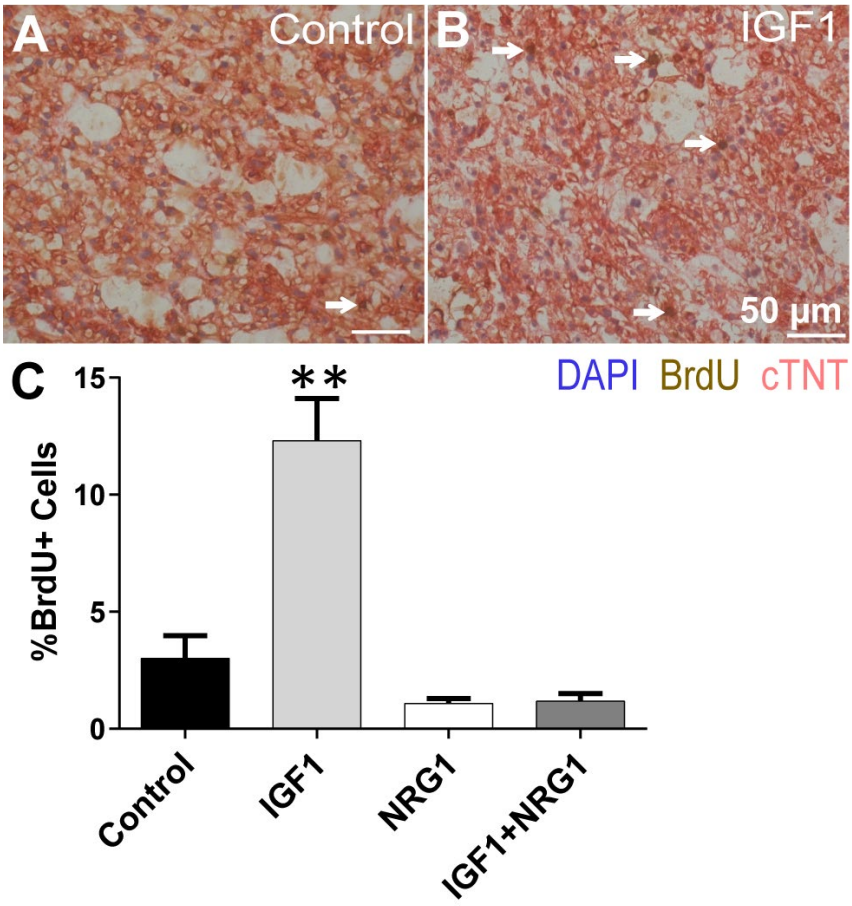

Figure 5. IGF1 stimulates cardiomyocyte proliferation in engineered tissues. (A and B) Immunohistological staining of cardiac troponin T (pink), nuclei (blue), and bromodeoxyuridine (BrdU)-positive nuclei (brown) in control (A) and IGF1-treated (B) ECTs. (C) Percent BrdU positive nuclei was calculated for each group by counting the number of BrdU positive cardiac nuclei of the total cardiac nuclei (n = 3 biological replicates with ≥ 100 cardiomyocytes counted per group). $^{**}P < 0.01$.

Figure 6

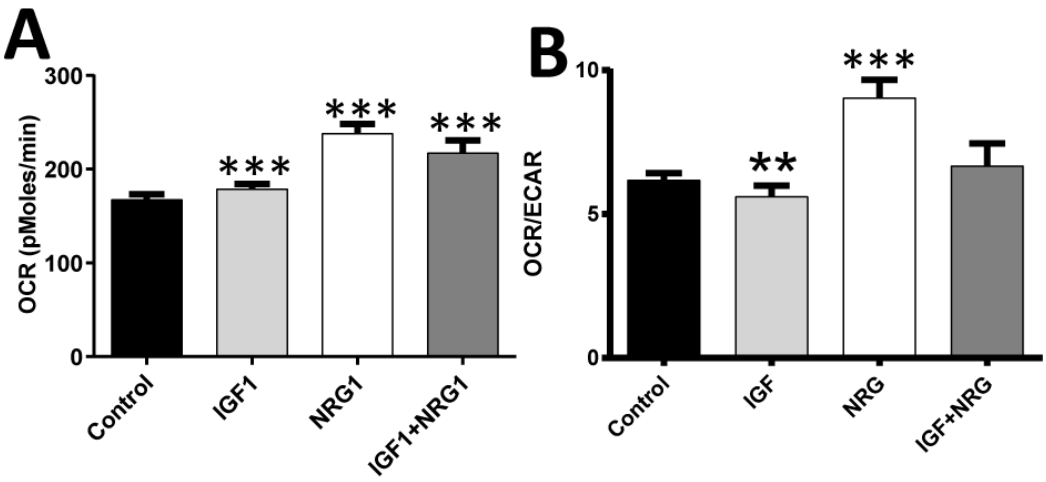

Figure 6. NRG1 treatment increases mitochondrial activity in cardiomyocytes. (A and B) Basal metabolic profiling of hESC-cardiomyocytes was normalized to live cells (with LIVE/DEAD® staining) to determine oxygen consumption rate (OCR; A), extracellular acidification rate (ECAR), and the OCR/ECAR ratio (B; $n = 6$). Data are expressed as mean ± SD. *$P < 0.05$, **$P < 0.01$, ***$P < 0.001$ versus control.

Figure 7

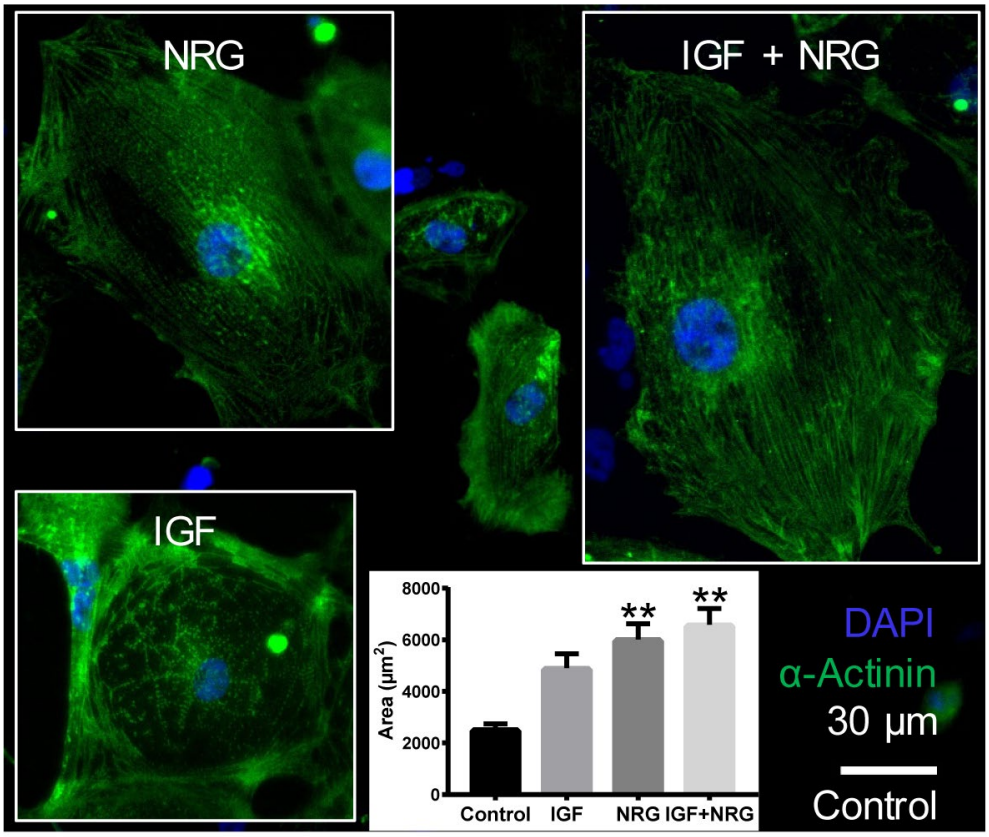

Figure 7. NRG-1 treatment stimulates growth in single hESC-cardiomyocytes. Immunofluorescence of α-actinin (green) and nuclei (blue) in control (center), IGF1 (bottom left), NRG1 (top left), or IGF1+NRG1 (top right) treated hESC-cardiomyocytes. Area was measured for each group (bottom center). $n \geq 38$ cells analyzed per group; data are expressed as mean ± SEM. $^{**}P < 0.01$.

Table 1. Contractile and mechanical characteristics of engineered tissues.

Group	Fold Increase	Stiffness (kPa)	$\sigma_{a,\,max}$ (mN/mm^2)	MCR (Hz)
Control	3.1 ± 0.3 (9)†	0.685 ± 0.265 (5)	0.59 ± 0.14 (10)	2.2 ± 0.2 (9)
IGF1	3.7 ± 0.5 (10)†	0.600 ± 0.177 (5)	0.22 ± 0.06 (10)*	1.9 ± 0.4 (8)
NRG1	2.3 ± 0.2 (10)†	0.964 ± 0.158 (6)	0.21 ± 0.01 (10)*	2.8 ± 0.3 (10)*
IGF1+NRG1	1.9 ± 0.2 (10)†	0.644 ± 0.163 (5)	0.19 ± 0.04 (10)*	2.4 ± 0.27 (10)

Peak active stress ($\sigma_{a,\,max}$) and maximum capture rate (MCR) were measured at 30% stretch. †$P < 0.05$ versus a value of 1 (no change). *$P < 0.05$ versus control. Data are displayed as mean ± SEM with sample size displayed in parentheses.

Table 2. Contraction and relaxation kinetics of engineered tissues.

Group	**Stretch (n)**	**v_{up} (mN/mm^2/s)**	**R_{50} (msec)**	**R_{90} (msec)**
Control	30% (13)	9.41 ± 2.14	167 ± 13	326 ± 24
Control	10% (12)	2.89 ± 0.93**	113 ± 13**	232 ± 15**
IGF1	30% (9)	5.01 ± 1.14	144 ± 10	277 ± 24
NRG1	30% (11)	2.38 ± 0.26**	120 ± 9**	243 ± 25*
IGF1+NRG1	30% (13)	2.19 ± 0.45**	139 ± 9	278 ± 28

Peak upstroke velocity (v_{up}) and time to 50% and 90% relaxation (R_{50} and R_{90}) of peak active stress, $\sigma_{a,max}$, was measured at the indicated stretch. Sample size is displayed in parentheses. *P < 0.05, **P < 0.01 versus control.

Chapter 5: Human cardiac fibroblasts uniquely modulate electromechanical function of hiPSC-cardiomyocytes in engineered myocardium

Submission Reference: Rupert CE, Kim TY, Choi B-R, Coulombe, KLK. Human cardiac fibroblasts uniquely modulate electromechanical function of hiPSC-cardiomyocytes in engineered myocardium. Stem Cell Reports. Submitted 2019-06-04

Supplemental material referenced in this chapter can be found in Appendix 1

Abstract

Cardiac tissue engineering using hiPSC-derived cardiomyocytes is a promising avenue for cardiovascular regeneration, pharmaceutical drug development, cardiotoxicity evaluation, and disease modeling, yet there still exist limitations to these applications due to functional immaturity of hiPSC-derived cells. It is well accepted that heterotypic cellular interactions alter the phenotype of cardiomyocytes. The current study evaluates the functional effects of co-culturing adult human cardiac fibroblasts (hCFs) in 3D engineered tissues and recapitulates healthy and diseased myocardium in vitro. A small population (5% of total cell number) of hCFs in tissues improves tissue formation, material properties, and contractile function that was unattainable with human dermal fibroblasts. However, two small perturbations to the hCF population creates disease-like phenotypes in engineered cardiac tissues. First, increasing the percentage of hCFs to 15% resulted in tissues with increased ectopic activity and spontaneous beating frequency. Second, hCFs undergo increased myofibroblast activation in traditional two-dimensional culture, and after prolonged culture, retain this altered phenotype when incorporated into engineered cardiac tissues to ablate functional benefits provided by their early-passage counterparts. Taken together, results of this study demonstrate that hCFs are a valuable cell source to manipulate engineered cardiac tissue physiological and pathophysiological function for downstream regenerative medicine applications.

Introduction

Tissue engineering approaches to cardiac modelling, therapeutic development, and regeneration are promising but have been hindered in part by the electromechanical immaturity of human pluripotent stem cell (hPSC)-derived cardiomyocytes. This immaturity has been documented in cardiovascular research from the single-cell level, where electrophysiological patch-clamp recordings have revealed a reduced inward rectifier potassium current (I_{K1}),[227] expression of pacemaker channels to cause frequent spontaneous contractions,[228] and low expression of L-type channels,[229] to implantation in animal models, where arrhythmia and insufficient coupling are reported with the injection of cells[160,230] and engineered tissues,[231,232,161] respectively. The ubiquity of these obstacles necessitates further exploration of how hPSC-cardiomyocyte electromechanical phenotype develops in response to differentiation protocols,[7,11] culture conditions, and heterocellular interactions, to name only a few. Non-cardiomyocytes have been shown to be necessary for achieving optimal mechanical performance of engineered cardiac tissues,[58] which makes the study of heterocellular interactions particularly invaluable to the cardiovascular engineering field.

As thoroughly summarized by Zhou and Pu,[233] the ratio of cardiomyocytes to non-cardiomyocytes in the heart varies widely depending on methodology of measurement. However, studies of the human ventricle come to a general consensus that cardiomyocytes contribute to about one third of the tissue by cell number,[234,235] with endothelial cells and cardiac fibroblasts comprising the majority of non-cardiomyocytes. A variety of human cell types have been used to replace this non-cardiomyocyte population in engineered tissues ranging from mesenchymal stem cells and umbilical vein endothelial cells[59,61,60] to brain pericytes[62], neonatal dermal fibroblasts[63,58], and simply relying on the non-cardiac population resulting from the differentiation process.[58] These support cell types provide functional benefit to engineered tissues including improved extracellular matrix (ECM) production and contractile force. However, they do not take into account native myocardial cellular heterogeneity, which provides

a physiologically relevant list of potential support cell candidates that may also impact cardiac function.

Among these candidates are cardiac fibroblasts (CFs), which comprise a significant portion of the heart by cell number.[233] Fibroblasts of the cardiac lineage in particular are critical for providing structural organization and support in homeostasis and are prominent modulators of acute and chronic cardiac injury.[236] In the healthy heart, CFs produce and maintain the ECM, specifically fibronectin, laminin, and collagens I, III, and IV.[238,237,19] In a disease state, CFs undergo activation to a myofibroblast phenotype, characterized by increased proliferation, contractility, and extracellular matrix production.[239] Myofibroblasts express gap junction proteins connexin 43 and 45, and at a low concentration, they speed conduction and upstroke velocity in vitro.[240,241] Recent studies also suggest myofibroblasts electrically couple to cardiomyocytes at the border zone of infarcted murine hearts.[243,242] Their active participation in myocardial structural maintenance and disease makes hCFs an excellent candidate for developing engineered cardiac tissues with more mature functionality while incorporating a physiologically relevant toolkit to model cardiac injury, aging, and fibrosis.

In this study, we demonstrate that adult human cardiac fibroblasts (hCFs) can be used to optimize engineered cardiac tissue electromechanical performance and that altering culture conditions produces arrhythmogenic phenotypes based on percentage and pre-conditioning of the hCF population. We demonstrate that, in our hands, neonatal human dermal fibroblasts (NHDFs) cannot be leveraged in the same way. We show that low hCF inclusion increases contractile force by three-fold compared to hiPSC-cardiomyocyte only control tissues, while higher percentages increase excitability and spontaneous beating rate. Additionally, we show that serial passaging and resulting increased myofibroblast activation is at least partially retained by hCFs in engineered cardiac tissues, negating the benefit to function that early-passage hCFs provide. We also report and characterize, for the first time, the appearance of

contractile alternans—the periodic alternation between full-force and partial-force contractions—and their pacing frequency dependence in engineered tissues. These data demonstrate that hCFs are a valuable cell type for manipulating the pathophysiological phenotype of engineered cardiac tissues and that our tissue engineering platform has the sensitivity to distinguish differences in functional performance in response to heterocellular interactions between hiPSC-cardiomyocytes and hCFs.

Methods

Cell Culture and Differentiation

Gibco® Human Episomal induced pluripotent stem cells (hiPSCs) were purchased from ThermoFisher Scientific. HiPSCs were cultured on plates coated with truncated human vitronectin in Essential 8 medium (ThermoFisher Scientific). Small molecule Wnt modulation was used for directed cardiac differentiation, as previously described.[226] In brief, hiPSCs were singularized, seeded on Matrigel-coated plates, and grown to approximately 70% coverage at which point chemically defined differentiation was started. Cells were sequentially treated with 6 μM CHIR 99021 follow by 5 μM IWP2 in RPMI 1640 supplemented with L-Ascorbic Acid and human serum albumin.[7] After one week of differentiation cells were maintained in RPMI 1640 supplemented with B27 (RPMI/B27). HiPSC-cardiomyocytes were harvested using 0.25% trypsin in 0.5 mM EDTA and used for engineered tissue experiments at 14 – 25 days of differentiation.

Healthy adult human ventricular cardiac fibroblasts (hCFs) were purchased from a commercial vendor (63-year-old female, lot #416Z048.9, PromoCell) and maintained in DMEM/F12 supplemented with 10% fetal bovine serum (FBS) and 1% penicillin-streptomycin (pen-strep). HCFs were expanded and used for downstream experiments (passages 3-9, reported with each data set in Results). For 2D myofibroblast activation experiments, coverslips were coated with polyacrylamide gels at 10% acrylamide and 0.1% bis-acrylamide for a stiffness of approximately

12 kPa.[244] Gels were functionalized with 0.2 mg/mL human Fibronectin and seeded with hCFs for 72 hours.

Flow Cytometry

Cells for flow cytometry analysis were singularized and fixed in 4% paraformaldehyde (PF) for 10 minutes at ambient temperature. Cells were stained with antibodies against cardiac troponin T (cTnT, 2 *μ*g/mL; Thermo Fisher Scientific) and alpha-smooth muscle actin (*α*SMA, 0.5 *μ*g/mL; Abcam). CTnT+ cells were considered cardiomyocytes, *α*SMA+ cells fibroblast-like, and double-positive cTnT+/ *α*SMA+ immature cardiomyocytes.[191] Samples were run on either an Attune NxT or BD FACSAria Flow Cytometer and analyzed with either FlowJo or Flowing software.

Quantitative RT-PCR

MRNA was extracted from cells and tissues using the RNeasy Mini Kit and mRNA concentration was measured with a NanoDrop 1000 Spectrophotometer. CDNA was synthesized from a normalized mass of mRNA for cells and tissues separately using the SuperScript III First-Strand Synthesis System. CDNA samples were combined with custom primers (Supplemental Table S1) and SYBR Master Mix, and quantitative real-time PCR was run on an Applied Biosystems® 7900 fast real-time system. HPRT was used as an internal control and relative expression was calculated using the 2^(-ΔΔCt) method.[195]

Mold and Tissue Formation

Molds and tissues were formed as previously described.[192,245] In brief, custom acrylic molds were fabricated using a 100W CO_2 laser and polydimethylsiloxane (PDMS) was poured into acrylic negatives and cured at 60°C. Tissues were form by combing $1x10^6$ hiPSC-cardiomyocytes and 0-15% hCFs with 2.5 mg/mL rat tail collagen-1 at a 50%/50% vol/vol ratio for a final concentration of approximately $16x10^6$ hiPSC-CMs/mL and 1.25 mg collagen/mL.

Cell-collagen solution was pipetted into PDMS molds, maintained in RPMI/B27, and stimulated with a 4 ms biphasic pulse at 1 Hz and 5 V/cm for the duration of culture.

Mechanics Testing

Mechanical measurements were performed after one or two weeks of culture as previously described.[245] Engineered tissues were cut in half and their passive and active mechanical properties were measured with an ASI 1600A system (Aurora Scientific). Strips were mounted on hooks attached to a 5 mN force transducer and high-speed motor arm, bathed in Tyrode's solution with 5 mM glucose and 1.8 mM $CaCl_2$ at 30-34°C, and electrically field stimulated with platinum electrodes. Tissues were stretched from their initial length, L_o (determined as just above slack length), by 5% steps to 130% L_o. At the final length, tissues were paced with increasing frequency, and the fastest pacing they followed was recorded as the maximum capture rate (MCR).

Calculations were made from the data recorded during mechanical testing to obtain the following values: Active stress, σ_a, was calculated by averaging the active twitch force of 10 contractions and normalizing by the cross-sectional area (CSA). CSA was calculated under the assumptions that tissue height was half the width and cross-sectional shape was an ellipse. Fold change was calculated from the ratio of the maximum active stress at 130% L_0 to active stress at the initial length L_0. Passive stress, σ_p, was calculated by normalizing the passive (baseline) force produced at each step by the CSA, and tissue stiffness (Young's modulus) was calculated as the slope of the line of best fit of passive stress versus strain at 5 – 30% strain.

Optical mapping of action potentials

ECTs were placed in a temperature regulated chamber (37.0 ± 0.2 °C) and perfused with 130 NaCl, 24 $NaHCO_3$, 1.0 $MgCl_2$, 4.0 KCl, 1.2 NaH_2PO_4, 5 Dextrose, 1.25 $CaCl_2$, gassed with 95% O_2 and 5% CO_2. ECTs were stained with voltage-sensitive dye, di-4-ANEPPS (Invitrogen) and 5

$\mu mol \cdot L^{-1}$ blebbistatin was added to the perfusate to reduce contraction artifact to fluorescence recording. Fluorescence images of APs were recorded from the anterior surface of the heart using a CMOS camera (100×100 pixels, 1000 frames/sec, 1.0 × 1.0 cm^2 field of view, Ultima-L, SciMedia, Japan). Activation maps and APD maps were generated using dF/dt for activation and dF^2/dt^2 for repolarization using digital image analysis routines as previously described.[246] The values are represented as mean ± standard deviation.

Statistical Analysis

Statistical analyses of the obtained data were performed using two-tailed unequal variance Student's t tests (Figures 2B, 2D, 2F), one-way ANOVA with Tukey's multiple comparisons tests (Figures 1A-C, 3A-D, 4C, 5A-D, 6B, 7B-C, S1A-B, ST2, ST4), two-way ANOVA with Tukey's multiple comparisons tests (Figures 4D, 6C, S5B, ST3, ST5), linear regression (Figures S2A-C, S4A-C) and non-linear regression (Figure 7A). Significance was considered as $P < 0.05$. Mean and standard deviation or standard error of the mean (as noted in each figure legend) were plotted using Graphpad Prism. Number of independent experiments (n) is indicated in the text and each figure legend.

Results

Neonatal human dermal fibroblasts are not sufficient to improve engineered myocardial function

Neonatal human dermal fibroblasts (NHDFs) are a widely available fibroblast cell source, so we first sought to utilize them in engineered cardiac tissues (ECTs) as a support cell type as recently shown by others.[58] Passage 4 NHDF's were doped into ECTs at 0% (control), 10%, or 20% of hiPSC-cardiomyocyte input and cultured for one week. NHDF's significantly increased tissue compaction as measured by cross-sectional area (CSA, $P<0.01$, $n\geq5$; Figure 1A). The

addition of 10% NHDFs increased tissue stiffness to 38 ± 9 kPa ($P<0.01$, $n\geq5$; Figure 1B). Most importantly, only in cardiomyocyte-only control tissues did the majority of ECTs form a beating syncytium, determined by tissue-level contractile response to 1 Hz field stimulation and by observation of holes and cell segregation in culture (Figure 1C-D, Movie S1, S2). Taken together, these data indicate that NHDFs are not an ideal support cell-type and that fibroblast origin may be critical for modulating the function of engineered myocardium.

Human cardiac fibroblasts undergo myofibroblast activation in monolayer culture

Based on our findings that neonatal human dermal fibroblasts (NHDFs) were insufficient for improving the function of engineered cardiac tissues (ECTs), we next identified adult human cardiac fibroblasts (hCFs) as a potential physiologically relevant support cell source. HCFs are a novel cell type to include in ECTs, so we first sought to validate their phenotype in 2D culture. Sensitivity of hCFs to stiffness-induced myofibroblast activation was determined by plating passage 3 or 4 (p3 or p4) hCFs on polyacrylamide gels or glass coverslips with stiffnesses of approximately 12kPa and 50GPa, respectively. After 72 hours of culture, hCFs were fixed and immunofluorescently labeled for vimentin, an intermediate filament protein in fibroblasts, and alpha smooth muscle actin (αSMA), an actin isoform whose increased expression is associated with myofibroblast activation (Figure 2A).[247] Expression of αSMA normalized by vimentin was 0.5-fold less in hCFs cultured on polyacrylamide gels of a physiological stiffness compared to those cultured on glass ($P<0.01$, $n=5$; Figure 2B), demonstrating hCF sensitivity to stiffness-induced activation in 2D culture.

We next assessed the ability of hCFs to be further activated via biochemical stimulation mimicking inflammation by treating passage 4 hCFs with 10 ng/mL TGF-β1 for 48 hours. Cells were subsequently fixed and fluorescently labeled for αSMA and vimentin (Figure 2C). TGF-β1-

treated hCFs had a 1.2-fold increase in normalized αSMA fluorescence compared to control ($P<0.01$, $n\geq10$; Figure 2D). These data show that in addition to stiffness-induced myofibroblast activation, biochemical activation of hCFs occurs in 2D culture.

To further evaluate hCF activation in response to prolonged exposure to a stiff substrate, cells were maintained on tissue culture plastic with a stiffness of approximately 100MPa from passage 4 (p4) to passage 9 (p9). Passage 9 hCFs showed a 1.3-fold increase in αSMA expression over p4 hCFs ($P<0.01$, $n\geq17$; Figure 2 E&F). MRNA was collected from p4 and p9 hCFs and p4 neonatal human dermal fibroblasts (NHDFs), and q-RT-PCR was run to assess transcript expression levels. Analysis revealed a significant increase in transcript levels of ACTA2, encoding αSMA, by 1.5-fold in p9 hCFs over p4 hCFs ($P<0.05$, $n\geq3$; Supplement Figure S1A). Additionally, GJA1, encoding connexin 43 (Cx43), which has been shown to be present in cardiac fibroblasts[249,241,248] and upregulated in parallel with αSMA,[250] increased by 4.6-fold in p9 over p4 hCFs ($P<0.01$, $n\geq3$; Figure S1A). Notably, expression levels of both ACTA2a and GJA1 were significantly lower in NHDFs than hCF groups, supporting the hypothesis that fibroblast lineage impacts cellular phenotype and heterotypic interactions.

Human cardiac fibroblast percentage modulates engineered tissue mechanics and kinetics

Addition of hCFs to our 3D ECT platform enabled examination of their effect on hiPSC-cardiomyocytes in a physiologically relevant 3D tissue microenvironment. In the human heart, cardiomyocytes compose ~20-30% of cells by number,[235] however, hiPSC-cardiomyocyte volume is approximately 1/3 of the adult human cardiomyocyte volume.[226] In order to recapitulate an appropriate volume ratio of cardiomyocytes to non-cardiomyocytes in ECTs, hCFs were doped in at a range of 0%-15% of input hiPSC-cardiomyocytes. HiPSC-

cardiomyocyte:hCF tissues were formed and cultured for one week. Tissues in all groups compacted the collagen matrix and formed a beating syncytium. HCFs increased ECT compaction as measured by cross-sectional area in a dose-dependent manner, resulting in a 25% to 63% decrease in cross-sectional area which reached significance with 10% and 15% hCFs ($P<0.01$, $n\geq7$; Figure 3A, Table S2).

Mechanical properties of ECTs were tested after 7 days of culture to determine the effect of ECT cellular composition on functional performance early after tissue formation before natural maturation processes progressed through longer-term culture periods. Tissues were mounted on a custom mechanical apparatus with 5 mN load cell (Aurora Scientific) and bathed in 37°C Tyrode's solution with 1.8 mM $CaCl_2$. Tissue stiffness was calculated from the linear portion of the stress-strain curve as ECTs were stretched from relaxed length (L_0) to 130% of L_0. Stiffness increased with the addition of hCFs in a dose-dependent manner by 3.7-fold with 5% hCFs, 5.2-fold with 10% hCFs, and significantly by 9.1-fold with 15% hCFs ($P<0.01$, $n\geq3$; Figure 3B, Table S2). Active stress, the contractile force produced during twitch contractions normalized by cross sectional area, was measured at 1 Hz stimulation and increased significantly with the inclusion of 5% hCFs. However, 10% and 15% hCFs did not differ significantly from control ($P<0.05$, $n\geq6$; Figure 3C, Table S2).

Because proliferation and migration of fibroblasts exist in the post-MI heart, we examined the effect of increasing hCF percentage on the contractile force and kinetics of engineered cardiac tissues during a frequency ramp protocol of 0.5 Hz increments from 1 Hz up to 4 Hz field stimulation. Because hCFs can electrically couple to cardiomyocytes via gap junctions to participate in electrical propagation in the healthy heart, we hypothesized their inclusion would not hinder electrical activity in ECTs. Maximum capture rate (MCR) was measured at peak tissue length and increased significantly in a dose-dependent manner with hCF percentage to

3.9 Hz with 15% hCFs, beyond that of physiological heart rates[251] ($P<0.05$, $n\geq7$; Figure 3D, Table S2).

The force-frequency relationship in engineered cardiac tissues was determined by measuring contractile force while pacing tissues from 1 Hz to 4 Hz at 0.5 Hz steps. Control ECTs showed reduction in force with increasing pacing frequency, as described in our previous studies with this platform.[245] Increasing hCF content did not alter the force-frequency performance, and tissues experienced a significant decrease in contractile force at 2-3.5 Hz compared to 1 Hz with 5%, 10%, 15% hCFs ($P<0.05$, $n\geq7$, Figure 3E, Table S3). Importantly, force amplitude of 5% and 10% hCF tissues was significantly greater than control ECTs by more than 6-fold between 1 and 2.5 Hz ($P<0.05$, $n\geq7$; Figure 3D, Table S3). Taken together, these data suggest that although control tissues maintain force amplitude to higher pacing frequencies than hCF-containing tissues, this is a result of their overall lower force production.[201,200,198,220]

To determine the frequency dependence of contraction and relaxation kinetics in ECTs, we analyzed the upstroke velocity (v_{up}, defined as the steepest slope of contraction rise), time to 50% relaxation of peak force (T50) and time to 90% relaxation of peak force (T90). V_{up} did not differ significantly between groups, however, relaxation kinetics changed significantly with the addition of hCFs. Faster repolarization kinetics are associated with anti-arrhythmia effects, a desirable characteristic in engineered tissues intended for translation. At 1 Hz, T50 was significantly faster in all hCF tissues, and T90 was significantly faster in 5% and 10% hCF tissues ($P<0.05$, $n\geq7$; Figure 3G-H, Table S3). Notably, T50 increased from 1 to 1.5 Hz in 15% hCF tissues and did not become significantly shorter than the 1 Hz value until reaching 3 Hz ($P<0.05$, $n=7$; Figure 3G, Table S3). This delayed repolarization is clinically considered a risk factor for arrhythmia, and indeed we observed evidence of EADs during *in vitro* testing (Supplement Figure S3A-B). In addition, optical mapping of ECTs with higher hCF concentrations frequently showed spontaneous beating frequencies greater than 1 Hz (Figure

S3C-J, Movie S3, S4), providing further evidence that too many fibroblasts disrupt electromechanical performance and that 5% hCFs were an optimal concentration for functionally normal ECTs.

Contractile alternans appear in engineered tissues during increased pacing frequency

In order to further elucidate how increasing human cardiac fibroblast percentage affected ECT frequency-dependent behavior, we analyzed the appearance and amplitude of contractile alternans, the regular alternation between consecutive contractions (Figure 4A). Alternans are highly correlated with cardiac arrythmia[252] but have been difficult to study in vivo, thus their appearance in our ECTs presented a valuable opportunity for their characterization. We hypothesized that because increasing hCF percentage improved maximum capture rate to higher frequencies, alternans would be reduced with the addition of hCFs. The fraction of ECTs with alternans present was not significantly different between groups (Figure 4B), however, the pacing frequency necessary to elicit alternans was significantly higher in 10% and 15% hCF tissues compared to control ($P<0.01$, $n\geq3$; Figure 4C). We then analyzed the frequency-dependence of the amplitude of alternans. No difference was present in the alternans makeup. 10% hCF tissues, at 3 and 4 Hz, and 15% hCF tissues, at 3.5 and 4 Hz, had a significantly smaller alternans amplitude compared to 5% hCF tissues ($P<0.05$, $n=3$, Figure 4D), correlating with the lower force amplitude exerted by these tissues. All groups studied included tissues exhibiting alternans, demonstrating that further conditioning is necessary to eliminate this phenomenon.

Cardiac fibroblast activation negates mechanical benefits of 5% hCF addition

Because 5% human cardiac fibroblasts (hCFs) resulted in tissues with the highest contractile function, we proceeded with studies at this concentration. To determine the sensitivity of our tissues to cardiac fibroblast activation state, we compared the effect of 5% early-passage (p4) hCFs and 5% serially passaged (p9) hCFs to control, cardiomyocyte-only tissues. Taking into account the results of our experiments in traditional 2D culture, we hypothesized that the increased myofibroblast-like activation state of p9 hCFs would negatively impact the function of ECTs in which they were included, determined by metrics of stiffness, compaction, contractile force, and maximum capture rate (MCR). Tissues were formed and cultured in the same manner described above and underwent mechanical testing after one week of culture. P4 hCFs significantly increased compaction, tissue stiffness, and contractile force, with no significant difference on MCR, matching the results seen in the earlier doping experiments ($P<0.05$, $n\geq15$; Figure 5A-D; Table S4). P9 hCFs, however, showed no significant difference from control, ablating the positive impact provided by early-passage hCFs.

Activated cardiac fibroblasts modulate contraction and relaxation kinetics

The frequency dependence of force production, contraction velocity, and relaxation times was measured with the addition of 5% p4 or p9 hCFs. As with previous experiments, p4 hCF tissues produced significantly more force by 1.6-fold over control tissues from 1 Hz to 2.5 Hz. The addition of p9 hCFs, however, resulted in a signification decrease in force compared to control (1 Hz and 1.5 Hz) and to p4 hCF tissues (1 Hz to 3 Hz) ($P<0.05$, $n\geq16$; Figure 5E, Table S5). While control and p4 hCF tissues retained a non-negative force-frequency relationship from 1 Hz to 2 Hz, p9 hCF tissues maintained this relationship to 3 Hz at the cost of force production.

Upstroke velocity was significantly faster in control tissues at 1 Hz and 1.5 Hz and decreased more quickly with decreasing force than p4 hCF and p9 hCF tissues ($P<0.05$, $n\geq16$; Figure S4;

Table S5). Relaxation times were not significantly different between groups, however, p9 hCF tissues had a significantly larger slope for the linear regression calculated for T50 and T90 versus contractile stress ($P<0.01$, $n\geq16$; Figure S4). In other words, for a given increase in contractile stress, p9 tissues displayed a significantly larger increase in relaxation time, reminiscent of increased relaxation times in cardiac infarct scar tissue.

Contractile alternans reflect force-frequency response

In order to determine how cardiac fibroblast activation state affected alternans behavior in ECTs, we analyzed the fraction, onset, and amplitude of alternans during pacing from 1 Hz to 4 Hz. The fraction of tissues exhibiting alternans and the frequency at which they appeared did not differ significantly between groups ($n\geq15$; Figure 6A-B). Onset of alternans occurred at 3.4 Hz pacing in all groups, well above the average adult's maximum heart rate. Control and p4 hCF tissues had a significant increase in alternans amplitude at 4 Hz ($P<0.01$, $n\geq5$, Figure 6C). However, the amplitude of alternans increased with overall contractile force and was not significantly different among the groups, suggesting that the changes in alternans were a reflection of each group's force-frequency response. To confirm the presence of alternans, we performed simultaneous force and Ca^{2+} measurements using Rhod-2 Ca^{2+}-sensitive dye and video recording of the fluorescence signal. Alternans in contraction amplitude were paralleled in Ca^{2+} transience amplitude in all groups and trended toward increasing amplitude with increasing stimulation frequency, reaching significance in control tissues ($P<0.05$, $n=3$, Figure S5). Taken together, this data demonstrates that ECTs of all groups exhibit alternans and that the amplitude of alternans is dependent on overall contractile force and thus the force-frequency response of tissues.

Human cardiac fibroblasts do not alter calcium handling in hiPSC-cardiomyocyte engineered tissue

HCFs did not significantly affect the appearance and onset of alternans or the force-alternans relationship in ECTs. Additionally, they did not alter Ca^{2+} alternans, leading to the hypothesis that hCFs do not alter hiPSC-cardiomyocyte calcium handling (Supplemental Figure S5B). To test this, we performed a force-Ca^{2+} protocol by increasing [Ca^{2+}] from 0.1 mM to 4 mM under 1 Hz stimulation. Force-Ca^{2+} data were fit with a nonlinear regression with R^2 values >0.92 (Figure 7A). EC_{50} and Hill's slope were calculated for each engineered tissue and did not differ significantly between groups (n.s., n≥3, Figure 7B-C). Taken together, these data demonstrate that addition of 5% hCFs did not affect hiPSC-cardiomyocyte sensitivity to calcium.

Discussion

Electromechanical immaturity of stem cell-derived cardiomyocytes is a significant limitation in the advancement of cardiac tissue engineering toward translation applications, and novel support cell types provide an exciting tool to overcome this limitation. This study describes the functional effects of human cardiac fibroblasts (hCFs) on hiPSC-cardiomyocyte engineered tissue contractility. We demonstrate that doping and serial passaging of hCFs are effective approaches to engineer physiological and pathophysiological models of human myocardium in vitro. Novel findings of this research include (1) evidence of primary adult human cardiac fibroblast activation in 2D culture through mechanical, biochemical, and serial passaging methods; (2) identification of 5% hCF content in engineered cardiac tissues for optimal functional performance; (3) demonstration that higher hCF content significantly increases spontaneous beating frequency and leads to a smaller fraction of engineered tissues capable of following physiological pacing; (4) evidence that functional benefits imparted by early-passage

hCFs are ablated when late-passage hCFs are used' and (5) the first report, to these authors' knowledge, of contractile and calcium alternans in human engineered cardiac tissues.

Because primary human cardiac fibroblasts have only recently been adopted as support cells for human cardiac tissues and it is well known that culture conditions can modulate cellular phenotype,[253,254] it is necessary to evaluate hCF behavior in traditional, two-dimensional culture. To do this, we used previously studied techniques to induce myofibroblast-like activation and deactivation. Transition from a soft, polyacrylamide gel to stiff, tissue-culture plastic has been shown to promote stiffness-induced myofibroblast differentiation in human lung fibroblasts,[253] a reversible process,[254] and one we were able to replicate with hCFs. We next demonstrated the biochemical activation of hCFs to a myofibroblast-like state using TGF-ß1.[255] This growth factor has been demonstrated to differentiate human adipose-derived stem cells to myofibroblasts as evidenced by increased αSMA expression after TGF-ß1 stimulation,[256] results we were able to replicate with hCFs. Finally, we sought to validate increased myofibroblast activation with serial passaging, a phenomena which has been reported in rodent cardiac fibroblasts.[257] Through long-term culture hCFs, we were able to achieve a significant increase in αSMA expression and define states of low and high activation for use in engineered tissues.

Cardiomyocytes make up approximately 70 to 80% of the volumetric fraction of the heart,[258,197] and we have previously shown that the volume of newly differentiated cardiomyocytes is roughly one third that of neonatal cardiomyocytes.[226] In order to maintain the physiological volume ratio in our engineered tissues, we chose to dope in hCFs at a range of 5-15% of hiPSC-cardiomyocyte number. Tissues with 5% hCFs produced significantly higher contractile forces than any other group, and we used this ratio for subsequent cardiac tissue engineering experiments. Although 10% and 15% hCFs increased tissue compaction, stiffness, and maximum capture rate more significantly than 5% hCFs, the prolongation of their relaxation time and increasing frequencies and appearance of EADs, made these higher percentages less

desirable for engineering a healthy cardiac tissue. Additionally, the fraction of beats captured at 1 Hz stimulation was significantly decreased in 10% and 15% tissues compared to control, which suggest this higher percentage of fibroblasts disrupts the electromechanical behavior of the tissues (Figure S4). Notably, we found that neonatal human dermal fibroblasts (NHDFs) in the same concentration range disrupted ECT formation and function, demonstrating that fibroblast origin uniquely determines fibroblast behavior. This finding is in agreement with previous reports that fibroblasts originating from different organs possess unique transcription profiles which can be distinctly grouped to dermal and non-dermal fibroblasts.[259]

Engineered cardiac tissues were sensitive to hCF concentration across multiple metrics, indicating the importance of heterotypic interactions between hiPSC-cardiomyocytes and hCFs. Tissue compaction, stiffness, and maximum capture rate (MCR) responded to increasing hCF concentration in a dose-dependent manner. Increased compaction and stiffness were expected, as cardiac fibroblasts are a remodeling and ECM-producing cell type; however, the increased MCR was surprising, given the previous reports that cardiac fibroblasts are insulating cells which decrease beating rate with increasing percentage.[260] A possible explanation is that the higher fibroblast content disrupts tissue-level electromechanical function, resulting in increased spontaneous activity of ECTs with 10% and 15% hCFs.

In order to determine the sensitivity of our ECTs to the activation state of hCFs, we compared their performance with 5% early-passage (p4) hCFs to those with 5% late-passage (p9) hCFs. P9 hCFs abrogated the benefits p4 hCFs provided in ECT compaction, stiffness, and force production after one week of culture, indicating that serial passaging leading to increased myofibroblast activation was at least partially retained during that time in three-dimensional culture. Previous work has shown that myofibroblast deactivation, in the form of decreased αSMA expression, occurs within 24 to 48 hours when p1,[261] p2,[262] or p2-p7[263] fibroblasts are transferred from stiff, two-dimensional substrates to three-dimensional culture platforms. The

results presented in this study suggest that activation of p9 hCFs 2D culture affects hiPSC-cardiomyocyte function in 3D engineered tissues out to at least one week. This provides an exciting avenue for engineering human myocardium of different pathophysiologies based solely on the pre-conditioning of hCFs.

Upon careful analysis, we discovered that the majority of our ECTs display contractile alternans whose amplitude increased with increasing frequency. Cardiac alternans have been well documented clinically, and they are considered an indicator of arrhythmogenic risk.[252,264] Potential involvement of CFs in modulating cardiac alternans, therefore, has been of great interest to develop effective anti-arrhythmic therapy.[267,265,266] Cardiac fibroblasts can alter dynamics of alternans, but the mechanisms are complex. Paracrine effect from CFs can influence alternans dynamics through causing electrophysiological remodeling of cardiomyocytes.[71] Electrical coupling through gap junctions is another important factor that can accentuate the effect of CFs on myocyte action potential. Interestingly, p9 hCF shows increased GJA1 expression in line with gap junction remodeling in CFs from infarcted hearts.[268] Coupling between CF and cardiomyocytes can either promote or suppress cardiac alternans, depending on two competing effects on repolarization and Ca^{2+} cycling.[269] Further, lack of proper electromechanical integration of hiPSC-cardiomyocytes in animal models has been attributed to the electrical immaturity of cardiomyocytes,[160] and the ubiquity of alternans in engineered tissues in this study suggests that this in vitro platform provides a robust pre-transplantation venue to study and reduce arrhythmogenicity of cardiomyocytes, and that early-passage cardiac fibroblasts may be a prime candidate for that purpose.

In summary, this study demonstrates the functional impact of human cardiac fibroblasts on hiPSC-derived cardiomyocytes in engineered cardiac tissue. The addition of 5% resulted in an optimized, highly contractile engineered tissue. Further, we showed that increasing percentages of hCFs led to higher spontaneous beating rates and increased maximum capture rate,

demonstrating their integral role in hiPSC-cardiomyocyte electrical behavior and whole-myocardium function. We showed that the functional benefits imparted by 5% hFCs were lost when hCFs were activated through serial passaging, which caused a disease-like state. Finally, we report for the first time the presence of alternans in hiPSC-cardiomyocyte engineered tissues, which is invaluable information as these tissue engineering approaches advance toward clinical application. Taken together, these results demonstrate the utility of human cardiac fibroblasts for manipulating hiPSC-cardiomyocyte function to produce physiological and pathophysiological myocardial phenotypes in vitro.

Author Contributions

CER and KLKC designed the project. CER performed the experiments and collected the data, analyzed the data, and generated figures. TYK performed the optical mapping experiment and data analysis. BRC interpreted the optical mapping data and edited the manuscript. CER and KLKC interpreted the data and wrote the manuscript.

Acknowledgments

The authors gratefully acknowledge funding from the US Department of Education GAANN Fellowship (to CER) and from the NIH R01 HL135091 (to KLKC).

Figures
Figure 1

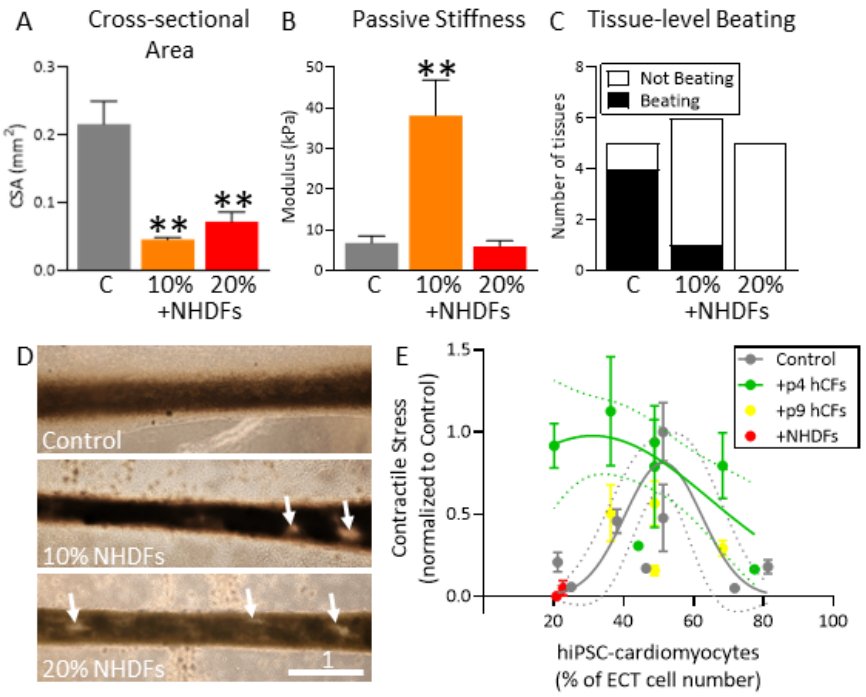

Figure 1. Neonatal Human Dermal Fibroblasts disrupt engineered cardiac tissue function. HiPSC-derived cardiomyocytes only (Control) or doped with 10% neonatal human dermal fibroblasts (NHDFs) or 20% NHDFs were cultured for one week. (A-B) Cross-sectional area (CSA, A) and passive stiffness (B) were measured after one week (**P<0.01 by one-way ANOVA, n≥5 tissues per group, data are represented as mean ± SEM. (C) Fraction of tissues beating (black) or not beating (white) in syncytium with 1 Hz field stimulation. (D) Phase contrast micrographs of control (top), 10% NHDF-added (middle), and 20% NHDF-added tissues at 5 days of culture. White arrows indicate holes in tissues, scale bar is 1 mm. (E) Contractile stress normalized to maximum stress of control (hiPSC-cardiomyocyte only) tissues as a function of engineered cardiac tissue (ECT) cardiomyocyte purity. Gaussian curves fitted to Control and +p4 hCFs with dotted lines indicating 95% confidence interval. +p4 and +p9 hCFs: passage 4 and passage 9 human cardiac fibroblasts. N ranges from 3 to 6 tissues at each purity and experimental group; data are represented as mean ± SEM. *See also Figure S1.*

Figure 2

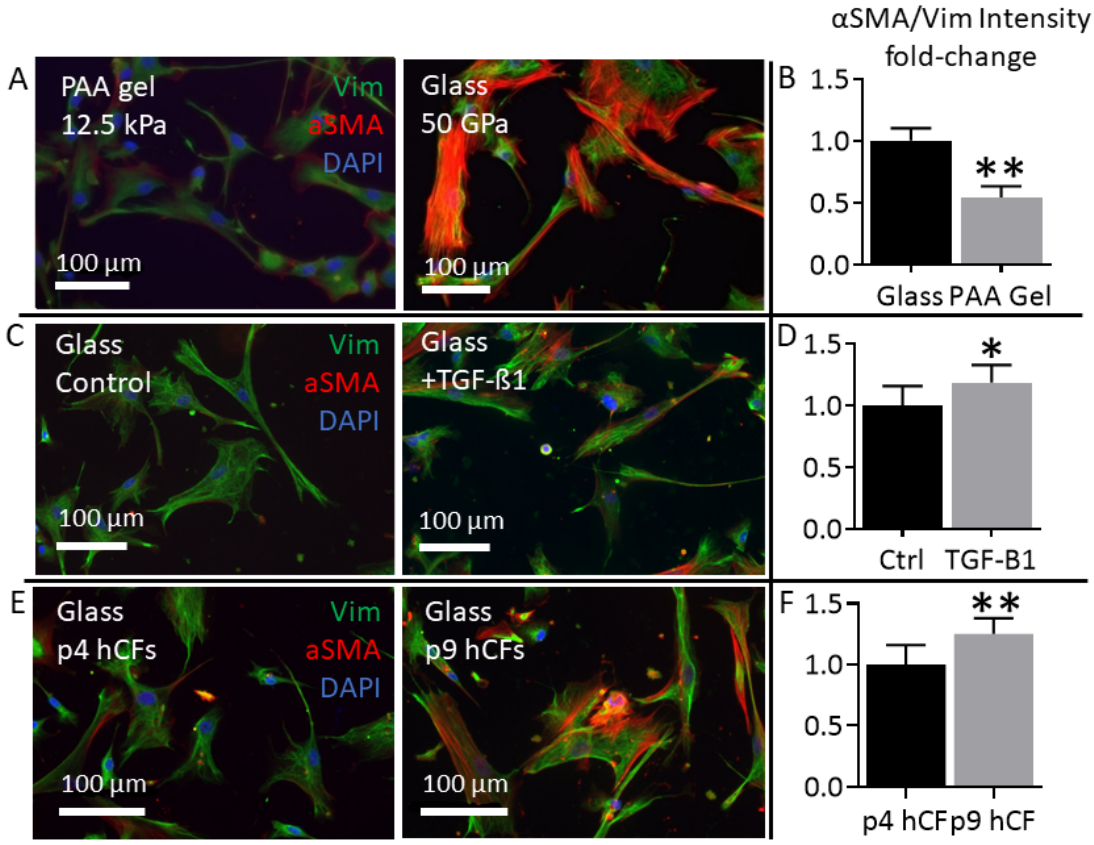

Figure 2. Human cardiac fibroblasts display classic signs of activation in monolayer culture. (A-B) HCFs cultured on soft 12.5 kPa polyacrylamide gels or stiff 50 GPa glass were stained for vimentin (Vim) and α-smooth muscle actin (αSMA; A), and fluorescence intensity was quantified (B; **P<0.01, n=5). (C-D) HCFs cultured on glass were stimulated with TGF-ß1, stained (C), and quantified (D; *P<0.05, n≥10). (E-F) Early passage (p4) and late passage (p9) human cardiac fibroblasts (P<0.01, n≥17). Data are represented as mean ± SD. *See also Figure S2.*

Figure 3

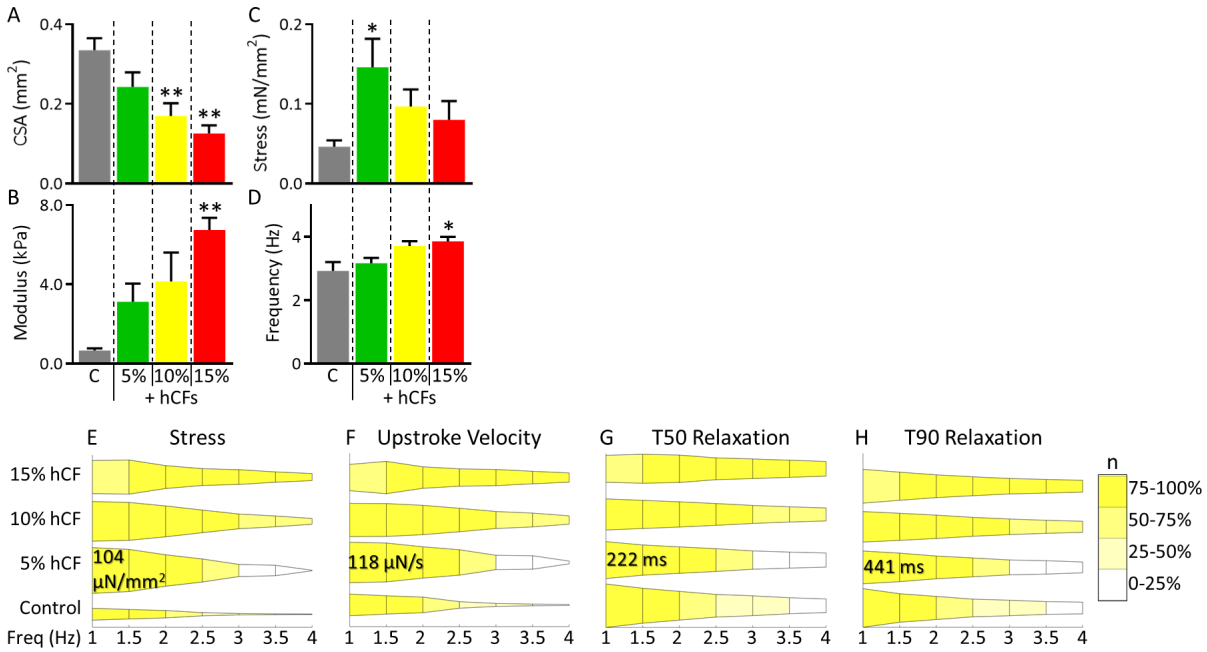

Figure 3. Mechanical and kinetic properties of engineered tissues are sensitive to hCF doping after one week of culture. (A) Cross-sectional area (CSA) of tissues was measured at relaxed length (n≥7). (B) Young's Modulus was measured by stretching tissues from relaxed length to 130% (n≥3). (C) Active stress was measured as the average peak contractile twitch force of tissues paced at 1 Hz field stimulation (n≥6). (D) Maximum capture rate of tissues was measured during pacing from 1 Hz to 4 Hz field stimulation (n≥7). *P<0.05, **P<0.01. Data are represented as mean ± SEM. (E-H) Tissue force amplitude and kinetics were measured as a function of increasing pacing frequency. Active stress (E), upstroke velocity (F), time to 50% relaxation from peak stress (T50, G), and time to 90% relaxation from peak stress (T90, H) are shown normalized to 5% hCF tissues at 1 Hz (value reported on graphs). Width of bars represents relative amplitude and color of bars represents the percentage of tissues following the pacing with 1:1 capture rate compared to 1 Hz (n = 3 – 12). C: cardiomyocyte-only control, 5%, 10%, 15%: addition of 5%, 10%, or 15% human cardiac fibroblasts, respectively, with constant number of cardiomyocytes. *See also Figure S3, Table S2, Table S3.*

Figure 4

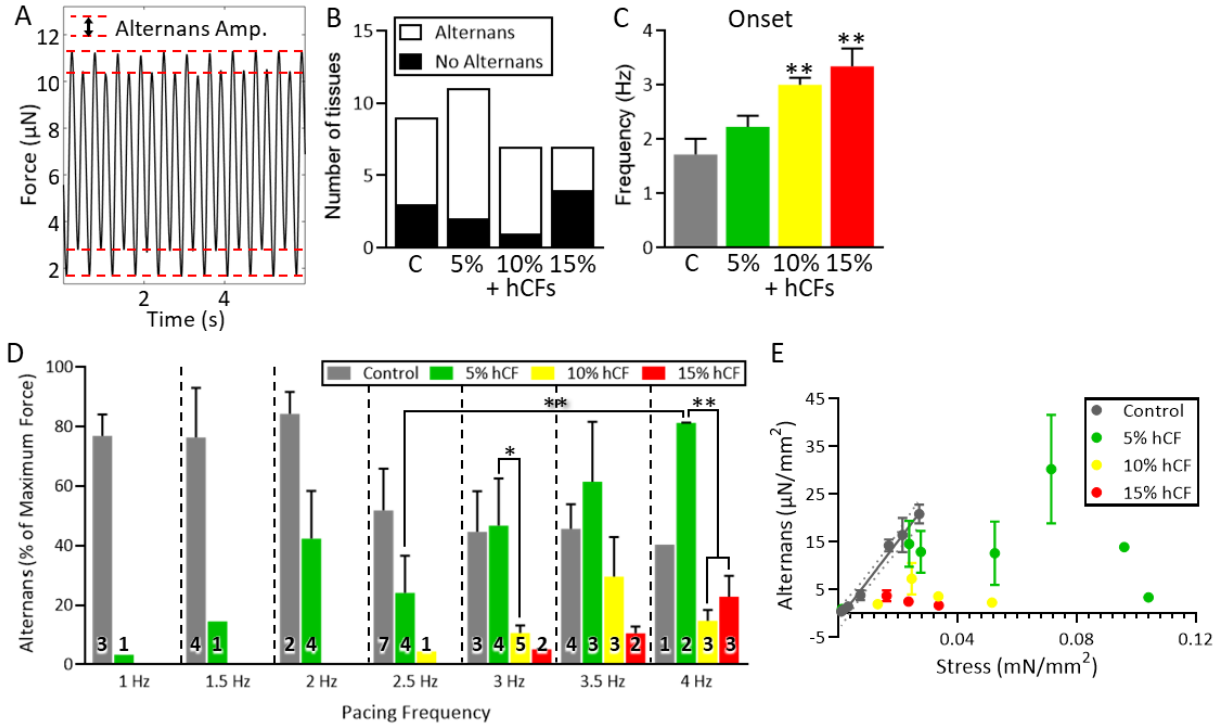

Figure 4. Alternans appear in engineered cardiac tissues dependent on pacing frequency and hCF percentage. (A) Raw force trace acquired during field stimulation at 2.5 Hz. Dashed lines indicate the difference in force amplitude between alternating contractions in systolic alternans (top) and diastolic alternans (bottom). (B) Number of tissues with (white) and without (black) alternans. (C) The onset of alternans was measured as the pacing frequency at which alternans amplitude reached ≥5% of the total force amplitude (n≥3 tissue per group). (D) Amplitude of alternans was measured during field stimulation of increasing frequency, and the fraction of full-force contractions was calculated. N ranged from 1 to 7 depending on group and frequency and are indicated on each bar. (E) Amplitude of alternans was plotted as a function of full-force contractile amplitude. Only control tissues could be fitted with a linear regression, R^2=0.85, dotted lines indicate 95% confidence interval. C: Control, 5%: +5% hCFs, 10%: +10% hCFs, 15: +15% hCFs. *P<0.05, **P<0.01; data are represented as mean ± SEM.

Figure 5

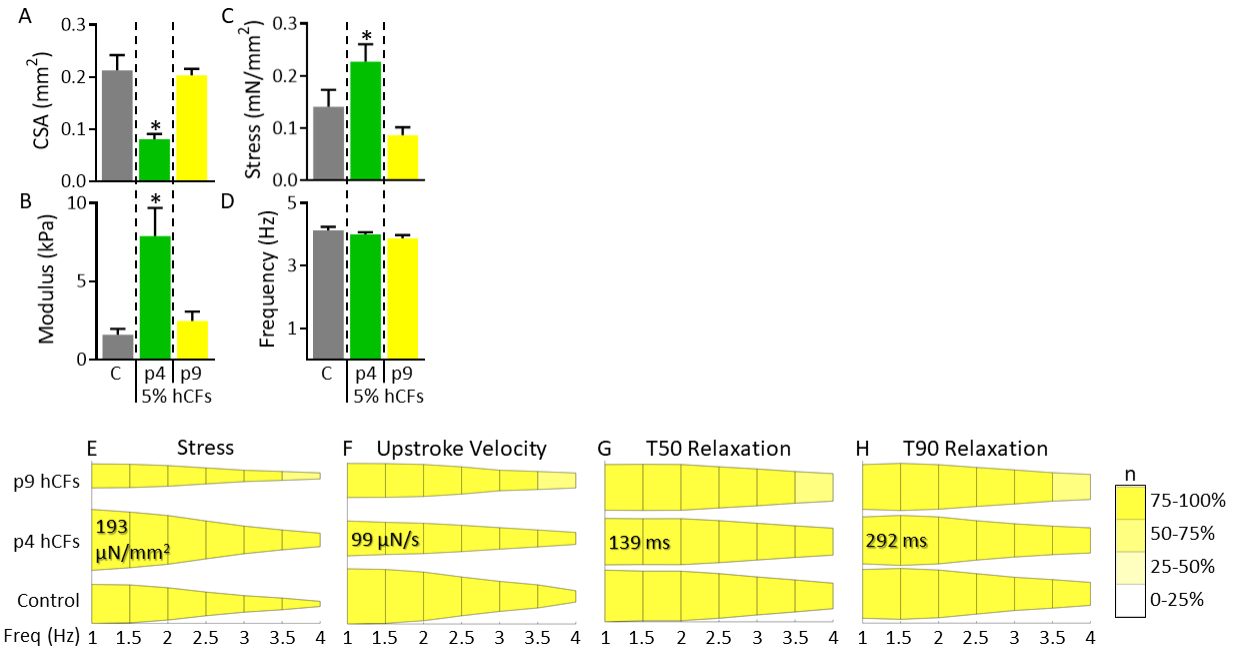

Figure 5. P9 hCFs reduce mechanical performance but maintain kinetic properties imparted by p4 hCFs after one week of culture. (A) Cross-sectional area (CSA) of tissues was measured at relaxed length (n≥18). (B) Young's Modulus was measured by stretching tissues from relaxed length to 130% (n≥14). (C) Active stress was measured as the average peak contractile force of tissues paced at 1 Hz field stimulation (n≥15). (D) Maximum capture rate of tissues was measured during pacing from 1 Hz to 4 Hz field stimulation (n≥16). *P<0.05, data are represented as mean ± SEM. (E-H) Tissue force amplitude and kinetics were measured as a function of increasing pacing frequency. Active stress (E), upstroke velocity (F), time to 50% relaxation from peak stress (T50, G), and time to 90% relaxation from peak stress (T90, H) are shown normalized to value of a given experimental condition at 1 Hz. Width of bars represents relative amplitude and color of bars represents the percentage of tissues following compared to 1 Hz (n = 13 – 20). *See also Figure S4, Table S4, Table S5.*

Figure 6

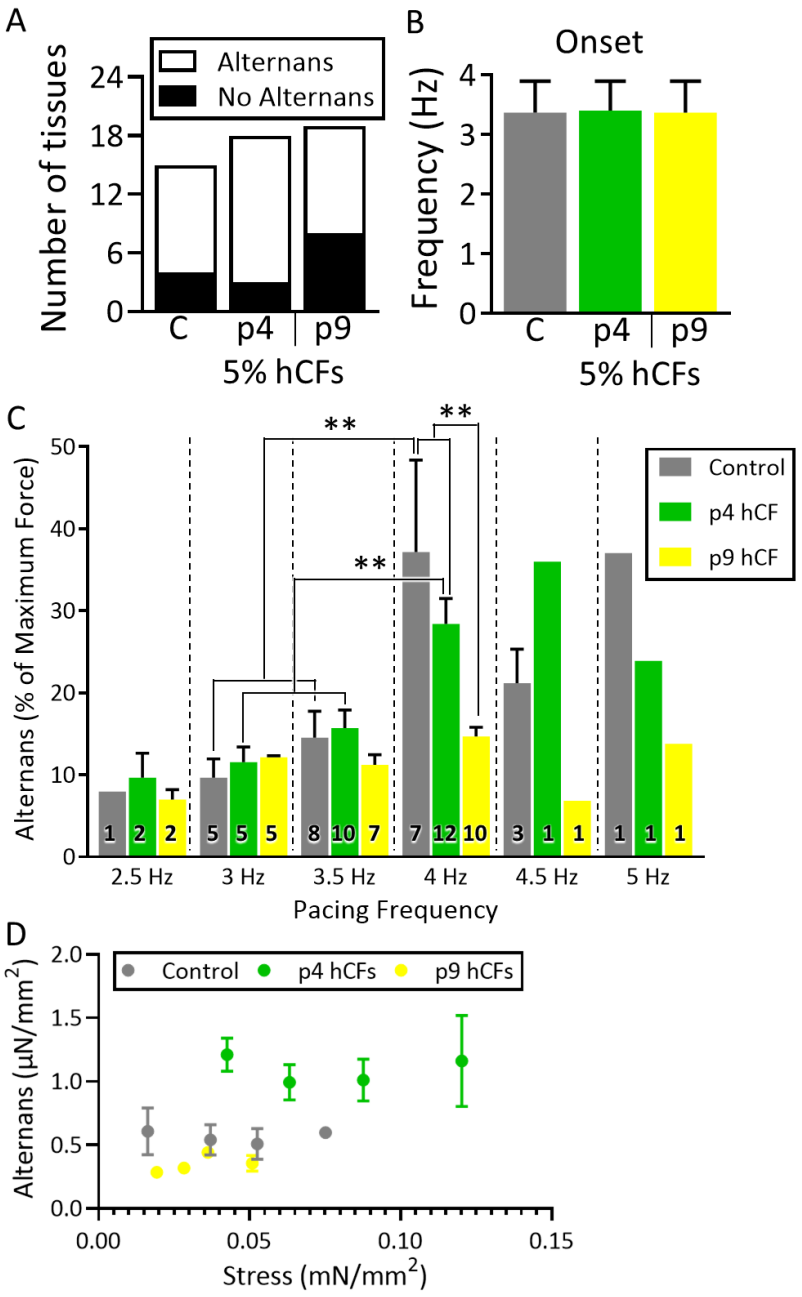

Figure 6. Contractile alternans appear independently of early or late passage hCFs but have a higher force threshold in early-passage tissues. (A) Number of tissues with (white) and without (black) alternans. (B) The onset of alternans was measured as the pacing frequency at which alternans amplitude reached ≥5% of the total force amplitude (n≥11 tissue per group). (C) Amplitude of alternans was measured during field stimulation of increasing frequency and represented as percentage of full-force contractile amplitude. N ranged from 1 to 12 depending on group and frequency, individual n values are indicated on respective bars. (D) Alternans amplitude was plotted as a function of full-force contractile amplitude. C: Control cardiomyocyte-only tissues, p4: 5% p4 hCF-added tissues, p9: 5% p9 hCF-added tissues; **P<0.01; data are represented as mean ± SEM. *See also Figure S5.*

Figure 7

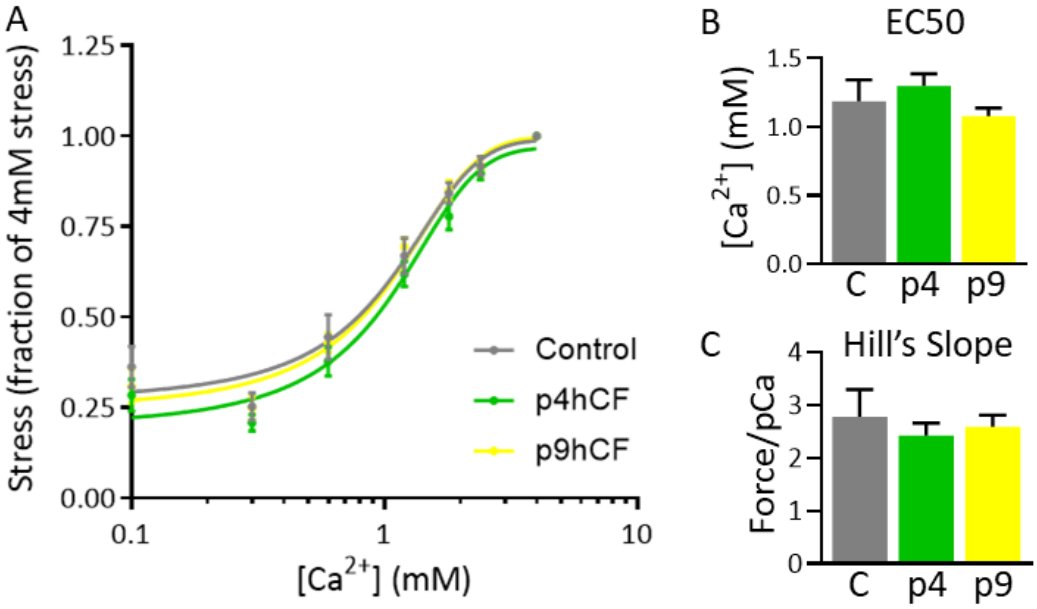

Figure 7. Human cardiac fibroblasts do not disrupt intact engineered tissues' sensitivity to extracellular Ca^{2+} concentration. (A) Intact engineered tissues were exposed to 0.1 mM to 4mM Ca^{2+} under 1 Hz pacing and contractile stress was measured. (B) EC_{50} was calculated as the extracellular Ca^{2+} concentration necessary to reach 1.5 times baseline force. (C) Hill coefficient was calculated from the linear portion of the force-pCa curve. N≥3; data are represented as mean ± SEM.

Chapter 6: Practical adoption of state-of-the-art hiPSC-cardiomyocyte differentiation techniques

Cassady Rupert, Chinedu Irofuala, Kareen Coulombe

Submission Reference: Rupert CE, Irofuala C, Coulombe, KLK. Practical adoption of state-of-the-art hiPSC-cardiomyocyte differentiation techniques. Annals of Biomedical Engineering. Submitted 2019-07-05

Abstract

Human induced pluripotent stem cell (hiPSC)-derived cardiomyocytes are a valuable resource for cardiac therapeutic development; however, generation of these cells in large numbers and high purity has been a point of limitation in widespread adoption. In this study, design of experiments (DOE) is used to explore the cardiac differentiation space of three hiPSC lines, and image analysis is subsequently used to validate optimal plate coverage predicted by the DOE models. Metabolic selection via lactate in culture medium is used to purify hiPSC-cardiomyocyte populations, and the bioenergetic phenotype and engineered tissue performance of purified and unpurified hiPSC-cardiomyocytes are compared. Findings demonstrate that when using a scheme to initiate differentiation one day after hiPSC plating, ~40% plate coverage results in peak cardiac purity (which varies by hiPSC line), which is in agreement with DOE predictions. Additionally, results show that metabolic selection with lactate increases hiPSC-cardiomyocyte oxygen consumption rate and oxidative phosphorylation compared to age- and batch-matched control hiPSC-cardiomyocytes (grown in glucose medium), but that this more mature metabolic phenotype does not result in a more mature contractile phenotype in engineered cardiac tissues at an early time point (one week) of culture in 3D tissues. This study provides widely adaptable methods and parameters for performing hiPSC-cardiomyocyte differentiation and describes the practical implications of metabolic selection as a purification technique.

Introduction

Human induced pluripotent stem cell (hiPSC)-derived cardiomyocytes are a promising cell source for cardiac regeneration, therapeutic development, and disease modeling. These cells, however, are difficult and costly to generate, which limits their accessibility. In order for the full potential of hiPSC-cardiomyocytes to be realized, careful and widely adaptable characterization of differentiation and purification techniques must be undertaken and made available.

Though cardiomyocyte differentiation from hiPSCs has advanced significantly, there remain challenges to its reliability and reproducibility both within and across research groups. Differentiation was first described in the spontaneous differentiation of human embryonic stem cells (hESCs) in embryoid bodies3 and evolved rapidly to a monolayer culture method, relying on the application of recombinant human proteins to module activin/nodal and BMP signaling to mimic embryonic heart development.9 Most recently, small molecules have been used to modulate the biphasic Wnt signaling pathway that is both necessary and sufficient for cardiac specification in a chemically defined differentiation process.2,11 While these advances have made cardiomyocyte differentiation increasingly feasible and amenable to clinical translation, they have arisen in parallel with the field's increasing use of human induced pluripotent rather than embryonic stem cells.6 HiPSCs have a less stable pluripotent state15 which we hypothesize results in increased heterogeneity of cell types from directed cardiac differentiation compared to hESCs.

There are several factors particularly critical for successful generation of hiPSC-cardiomyocytes during small-molecule differentiation. Cardiac differentiation is initiated with the application of a GSK3 inhibitor to activate Wnt signaling,22 and the concentration required to initiate the mesodermal lineage depends most significantly on the proportion of hPSCs in the S/G2/M stage of the cell cycle.10 This proportion, in turn, depends on cell density, colony size, and time in culture.17 These relationships have been uncovered using endpoint analysis of differentiation

runs. For practical application, methods to estimate cell cycle state and choose GSK3 inhibitor concentration prior to the initiation of cardiac differentiation must be developed.

HiPSC-cardiomyocyte generation and purification are nuanced processes that can be prohibitively difficult for widespread adoption. In this study, we evaluate heterogeneity of cardiac differentiation, provide tools to optimize cardiac purity, and investigate shortcomings of these processes. We use a design of experiments (DOE) approach to model optimal cardiac differentiation conditions across multiple hiPSC lines; develop an image analysis pipeline to identify the range of hiPSC densities in which directed differentiation is successful; and demonstrate that, although metabolic selection matures hiPSC-cardiomyocyte bioenergetic phenotype in two-dimensional culture, the process alone does not improve engineered cardiac tissue function. These findings provide a valuable resource for groups already performing cardiac differentiation as well as those new to the field. We provide useful tools to standardize differentiation and important insights into how hiPSC-cardiomyocyte purification affects cell phenotype.

Methods

Stem cell culture

Three human induced pluripotent stem cell (hiPSC) lines were used: GiPSC, NCRM-5, WTC11 (Table 1). Cells were culture on 10 cm tissue culture plastic dishes (Fisher) coated with truncated human vitronectin (VTN-N, ThermoFisher) in essential 8 media (E8™, ThermoFisher). Media was changed daily, and cells were passaged every 4 to 5 days at a 1:10 split ratio using in-house versine (DPBS, ThermoFisher, with 0.5mM EDTA and 1.1mM dextrose, Sigma-Aldrich).

Cardiomyocyte differentiation and purification

HiPSC-cardiomyocytes were differentiated as previously described.18 In brief, hiPSCs were broken into small colonies and seeded on Matrigel-coated 6 or 24 well plates in E8™ with 5μM Y-27632 (ROCK inhibitor, Fisher). Media was changed daily until initiation of differentiation (day 0), when cells were switched to CDM31 and treated sequentially with 6 μM (unless otherwise indicated) of GSK3 inhibitor CHIR 99021 (Chiron, Fisher), and 5 μM inhibitor of Wnt protein 2 (IWP2, Fisher).12 Cells were switched to RPMI 1640 + B27 supplement with insulin (RPMI/B27) at day 9 of differentiation. Both unpurified control cells and cells undergoing lactate purification were replated at 5-6 x106 cells/cm2 on Matrigel-coated 6 well plates after widespread appearance of beating in RPMI/B27. Cells for purification were then cultured for four days in LPM (lactate purification medium: glucose-free DMEM + 4mM L-glutamine, 1X non-essential amino acids, 1X GlutaMAX™, and 4 mM lactate).21 Unpurified control cells were maintained in RPMI/B27 during this period. All hiPSC-cardiomyocytes were maintained in RPMI/B27 until use between 14 and 24 days of differentiation.

Adult human cardiac fibroblast culture

Healthy adult human ventricular cardiac fibroblasts (hCFs; PromoCell) were maintained on tissue culture plastic in DMEM/F12 with 10% FBS and 1% penicillin-streptomycin (ThermoFisher). Cells were passaged upon reaching confluency in versine with 0.05% trypsin (ThermoFisher). HCFs were used in engineered tissues at passage 4 (p4).

Engineered cardiac tissue formation

Engineered cardiac tissues (ECTs) were formed as previously described.19 Briefly, hiPSC-cardiomyocytes were harvested at day 24 of differentiation and combined with 1.25 mg/mL rat-tail collagen-1 at 1x106 cells per tissue + 5% hCFs. ECTs were cultured under static stress14 in RPMI/B27 with 1% penicillin-streptomycin and field-stimulated at a 1 Hz (IonOptix). ECTs were cultured for one week before further experiments.

Metabolic characterization

Unpurified and lactate purified hiPSC-cardiomyocytes were harvested at day 24 of differentiation and seeded at 40 x 103 cells/well of a Matrigel-coated XFe96 cell culture microplate (Agilent). On day 27, cells were switched to 175 µL/well assay media: XF Base Medium (Agilent), 4 mM GlutaMAX™, 1 mM Sodium Pyruvate (ThermoFisher), and 25 mM glucose (Sigma-Aldrich) and incubated for 90 minutes at 0% CO2 and 37°C. Basal oxygen consumption rate (OCR) and extracellular acidification rate (ECAR) measurements were made with a Seahorse XFe96 Extracellular Flux Analyzer (Agilent).

Image analysis

Analysis of phase contrast images taken on day 0 of differentiation with a Canon EOS 6D was performed using MATLAB (R2019a, MathWorks). Each image was divided into 16 subimages, individually thresholded using Otsu's method, and binarized to calculate a fraction of well coverage. Code is available through the Brown University Dataverse in the Harvard Dataverse, DOI: https://doi.org/10.7910/DVN/KWI737.

Flow cytometry

Cardiac purity was determined for each hiPSC-cardiomyocyte differentiation run. Cells were fixed in 4% paraformaldehyde and stained for the cardiac marker cardiac troponin T (cTnT, 2 µg/mL; ThermoFisher) Samples were analyzed with a FACSAriaIIIu cell sorter (BD Biosciences) and 10,000 events were recorded per sample. Flow cytometry data was analyzed used opensource Flowing Software (Turku Centre for Biotechnology), and gates were set based on isotype antibody controls.

Mechanics testing

Engineered cardiac tissues (ECTs) underwent mechanics testing after one week of culture as previously described.19 Tissues were mounted on one side to a 5 mN load cell and on the other to a high-speed length controller (Aurora Scientific). ECTs were bathed in continuously perfused Tyrode's solution with 1.8 mM Ca2+ between 32 and 35°C. Cross-sectional area (CSA) was measured at relaxed length (L0), and CSA shape was assumed to be elliptical. Tissues were field stimulated at 1 Hz and stretched from L0 to 130% of L0 in 5% length steps, with twitch contractile force measured at each step. At 130% L0, ECTs were paced from 1 Hz to 4 Hz at 0.5 Hz steps.

Statistics

Quadratic models for differentiation optimization experiments were calculated using DOE, and goodness of fit was analyzed with ANOVA (Figure 1). Statistical analyses of the obtained data in lactate purification studies were performed using two-tailed unequal variance Student's t-tests. Significance was considered as $P < 0.05$. Mean and standard error of the mean were plotted using Graphpad Prism. Sample size (n) is indicated in the text and each figure.

Results

Seeding density and Chiron concentration determine cardiac differentiation outcome

In order to establish the relationship between Chiron concentration, seeding density, and cardiomyocyte purity, we used a DOE approach to explore the experimental space for three hiPSC lines: GiPSC, NCRM-5, and WTC11. HiPSCs were seeded at 60, 66, or 72 x103 cells/cm2, and differentiation was started the following day with the application of 3, 6, or 9 μM Chiron. Cells were dissociated into single cells and fixed at day 14 of differentiation, and cardiomyocyte purity was measured with flow cytometry, using the cardiac marker cardiac troponin T (cTnT). DOE software was used to correlate differentiation outcomes with the nine different starting conditions with R2 values of 0.86 for GIPSC, 0.93 for NCRM-5, and 0.87 for WTC11 ($N=9$, $P<0.01$, Figure 1). Lower Chiron concentration and higher seeding density

increased cardiomyocyte purity across all lines. Importantly, the highest purity was attained with low Chiron in all lines and dropped off steeply with increased Chiron concentration. These findings demonstrate common trends across hiPSC lines but also reveal important differences in sensitivity to differentiation conditions.

Thresholding of day 0 phase contrast images reveals optimal range of plate coverage

Because seeding density proved a critical factor in hiPSC-cardiomyocyte differentiation, we next sought to develop a robust and widely adaptable method to measure hiPSC density at the initiation of differentiation. Person-to-person variability in cell singularization and counting can greatly affect seeding density, so image analysis of day 0 hiPSCs was identified as a more uniform method to assess plate coverage. Phase contrast images of hiPSCs at day 0 were thresholded using a custom MATLAB code to determine a relative fraction of plate coverage (Figure 2A-D). Brightfield images were used because of their ease of acquisition, yet unbiased, automated image analysis is challenging; namely, dark cell bodies are not included in masked area, thus underestimating true cell confluency. Thus, we define a “relative fraction plate coverage” as a metric for confluency. These results were compared to flow cytometry data of cardiomyocyte purity after 14 days of differentiation with 6 μM Chiron to determine the optimal density range for this standard concentration (N=11, Figure 2E). This analysis shows that a relative fraction plate coverage of 0.31 to 0.44 consistently produces successful differentiation runs, and that, in the case of 6 μM Chiron differentiation initiation, cell densities above or below this range yield little to no hiPSC-cardiomyocytes.

Lactate purification enriches for hiPSC-cardiomyocyte and affects metabolic phenotype

The relative fraction of plate coverage determined with image analysis revealed a range for successful differentiation, but hiPSC-cardiomyocyte purity within this range varied from 15% to 60% purity. Previous work demonstrates that for optimal engineered cardiac tissue function,

input hPSC-cardiomyocyte purity should roughly be between 40% and 75%.20 In order to attain this level of purity, we investigated how the enrichment method of metabolic selection, or "lactate purification," performed in our hands. We adapted the previously published protocol (Figure 2A)21 to fit our differentiation pipeline, to attain hiPSC-cardiomyocyte populations of >80% purity (Figure 2B).

During the lactate purification process, we observed increased spontaneous beating of lactate-treated hiPSC-cardiomyocytes. Because lactate purification relies on the unique metabolic versatility of cardiomyocytes, we hypothesized that the enrichment process changed the population-level metabolic phenotype of hiPSC-cardiomyocytes. To test this, we cultured unpurified cardiomyocytes and lactate-purified cardiomyocytes in parallel and measured their rates of oxygen consumption (OCR) and extracellular acidification (ECAR) with a Seahorse Xfe96 Analyzer. OCR increased by 1.5-fold in lactate-purified hiPSC-cardiomyocytes compared to unpurified control, indicating an overall increase in metabolic rate ($n=10$, $P<0.01$, Figure 2C). The ratio of OCR over ECAR increased by 1.8-fold in lactate-purified hiPSC-cardiomyocytes compared to unpurified control ($n=10$, $P<0.05$, Figure 2D). The shift of this ratio toward OCR indicates an increased metabolic reliance on oxidative phosphorylation versus glycolysis, a trademark of more metabolically mature cardiomyocytes. Taken together, these findings indicate that although lactate purification is an efficient means to enrich for hiPSC-cardiomyocytes, it significantly changes the metabolic phenotype of the output population.

Engineered tissues form and function independently of cardiomyocyte purification status

To determine if the metabolic shift in lactate-purified hiPSC-cardiomyocytes affected functional output, we formed engineered cardiac tissues (ECTs) from purified (82% cTnT+, n=4) or non-purified (38% cTnT+, n=8) hiPSC-cardiomyocytes. In addition, 5% adult human cardiac fibroblasts (hCFs; passage 4) were included to aid tissue formation and function. ECTs were cultured for one week during which time all tissues formed and began to beat in syncytia (Figure

4A). At one week, tissues underwent mechanical testing to analyze functional performance. Cross-sectional area (CSA), a surrogate measure of tissues compaction, was not different between groups, which all compacted to approximately one third of initial tissue CSA (P=0.73, Figure 4B). Maximum twitch contraction stress (contractile force normalized by CSA) was measured under 1 Hz stimulation and did not differ significantly between groups (P=0.70, Figure 4C). Lastly, the maximum capture rate, determined as the pacing frequency at which ECTs could capture at least 5 consecutive stimuli, was measured by pacing ECTs from 1 Hz to 4 Hz. Once again, ECTs showed no difference between groups (P=0.24, Figure 4D). These results suggest that the metabolic shift resulting from lactate purification is not reflected in engineered cardiac tissue performance.

Discussion

Nuances and variability in cardiomyocyte differentiation and purification from human pluripotent stem cells has challenged widespread adoption. In this study, we optimize differentiation conditions and investigate the functional implications of hiPSC-cardiomyocyte enrichment through metabolic selection. Our results show that (1) cell seeding density and Chiron concentration impact cardiomyocyte differentiation in a similar way across hiPSC lines, but that the resulting range of hiPSC-cardiomyocyte purity is unique to each line; (2) analysis of phase-contrast images taken at day 0 of differentiation gives a range of plate coverage values to successfully differentiate hiPSC-cardiomyocytes; (3) modified lactate purification enriches for hiPSC-cardiomyocytes while shifting the population metabolic phenotype; and (4) the metabolic shift in lactate-purified cardiomyocytes does not significantly improve engineered cardiac tissue force production.

For cardiomyocyte differentiation to be successful, the mesodermal lineage must first be induced in hiPSCs, a process achieved through the application of Chiron in the protocol used for these experiments.12 Laco et al. recently demonstrated that the efficacy and optimal

concentration of Chiron in hPSC-cardiomyocyte differentiation depends on the proportion of the hPSC population in the S/G2/M phase of the cell cycle.10 Additionally, the group showed that the confluency of hPSCs in culture correlates with the distribution of cell cycle stages in the population. Our results suggest that, across three hiPSC lines, low (3 μM) Chiron concentrations with higher seeding density groups performed better than lower seeding density at any higher Chiron concentration. This is in agreement with Laco's finding that 3 μM Chiron in low S/G2/M populations (high density) produced roughly 40% pure hESC-cardiomyocyte populations while in high S/G2/M populations (low density), produced <5% pure hESC-cardiomyocyte populations. Interestingly, the study reports the biggest difference in differentiation outcomes based on both Chiron concentration and S/G2/M levels between 5 μM and 6 μM Chiron.

Though important to determine if and how Chiron concentration and seeding density affected cardiomyocyte differentiation outcomes across multiple hiPSC lines in our hands, it was equally important to develop methods to use this information in order to reliably and repeatably perform successful differentiation runs. Because Chiron concentration is far more easily controlled than seeding density, we developed an easily adoptable image analysis protocol to determine relative plate coverage from brightfield phase-contrast images. In this study, we tested one hiPSC line (GiPSCs) at one Chiron concentration (6 μM) to find the range of cell densities for successful differentiation. By determining the fraction coverage necessary for a range Chiron concentrations to produce hiPSC-cardiomyocytes, the method can then be reversed, and, given a cell density, the proper Chiron concentration can be applied to ensure successful hiPSC-cardiomyocyte differentiation or culture time extended to reach an optimal plate coverage. This methodology could thus potentially eliminate one of the greatest sources of variability in the differentiation process.

High purity hiPSC-cardiomyocyte populations of greater than 80% are currently considered the standard for clinical translation,5 which necessitates the use of enrichment protocols for most

differentiation runs. These methods take the form of genetic selection,23 antibody-based selection,4 and most commonly, metabolic selection.21 However, little is known about if and how these enrichment processes select for specific hiPSC-cardiomyocyte phenotypes or sub-populations. We show that, in the case of lactate purification, the enriched cell population shifts towards a higher dependence on oxidative phosphorylation. Within one post-natal week, human fetal cardiomyocytes shift from mostly glycolysis to oxidative phosphorylation due to increased metabolic demand,24 and hPSC-cardiomyocytes have been shown, similar to fetal cardiomyocytes, to utilize mostly glycolysis for energy production.7,16 The high expression level of HIF1α in hPSC-cardiomyocytes has been implicated in their immature metabolic phenotype, and culture in glucose-deprived media reduces HIF1α expression.7 This suggests that the metabolic stress induced during metabolic selection is responsible for the shift toward oxidative phosphorylation in our lactate-purified hiPSC-cardiomyocytes.

Though metabolic phenotype is one indication of maturation, for therapeutic purposes, cardiomyocyte electromechanical maturity is a critically important metric.8 To determine if increased metabolic maturation resulted in tissues with increased functional output, we compared contractile force of engineered cardiac tissues composed of unpurified or purified cardiomyocytes. Because ECTs reach peak performance with 40%-70% cardiomyocyte purity, we included 5% adult human cardiac fibroblasts. We observed no significant differences in tissue compaction, maximum contractile twitch stress, or maximum capture rate, which may be explained by multiple factors. Firstly, metabolic function is not a surrogate measure for electromechanical function. The conditions, namely glucose-deprived culture medium used for metabolic maturation in lactate-purified hiPSC-cardiomyocytes did not include stimulants for electromechanical maturation. Secondly, both unpurified and purified cardiomyocyte-containing ECTs were subjected to the same static uniaxial stress and 1 Hz electrical pacing during the one week of culture time. Thirdly, because ECT electromechanical function is closely linked to

cardiomyocyte purity,20,13 the purity of control and lactate purified ECTs, which fall on either side of the ideal cardiomyocyte purity of roughly 50-60%,20 may mask changes resulting from cardiomyocyte bioenergetic phenotype. Our findings suggest that though lactate purification changes hiPSC-cardiomyocyte metabolic phenotype, a corresponding matured electromechanical phenotype is not present after short culture periods (1 week), a phenomena similar to our previous work.19

In summary, this study provides insights for the widespread adoption of hPSC-cardiomyocyte differentiation and purification for translational applications. By harnessing the power of DOE and automated image analysis, we develop optimized differentiation models for multiple hiPSC lines, suggest low Chiron (3 M) and high cell density provide highest cardiac purity when directed differentiation is initiated 24 hours after cell seeding, and provide a practical means to implement these models at the bench. As hPSC-cardiomyocyte therapies reach clinical translation, it is critical for the cardiovascular engineering field to pursue reproducible, transparent means of generating high purity cell populations with well-defined phenotypes. The findings presented here provide important tools and advances to achieve that goal.

Author Contributions

CER, CI and KLKC designed the project. CER and CI performed the experiments and collected and analyzed data. CER generated figures. CER and KLKC interpreted the data and wrote the manuscript.

Acknowledgments

The authors gratefully acknowledge funding from the US Department of Education GAANN Fellowship (to CER), the Romer Undergraduate Teaching and Research Award (CI), and from the NIH R01 HL135091 (to KLKC). We also thank Dr. Marla Tipping (Providence College) for technical assistance with Seahorse assays.

Figures and Tables

Figure 1

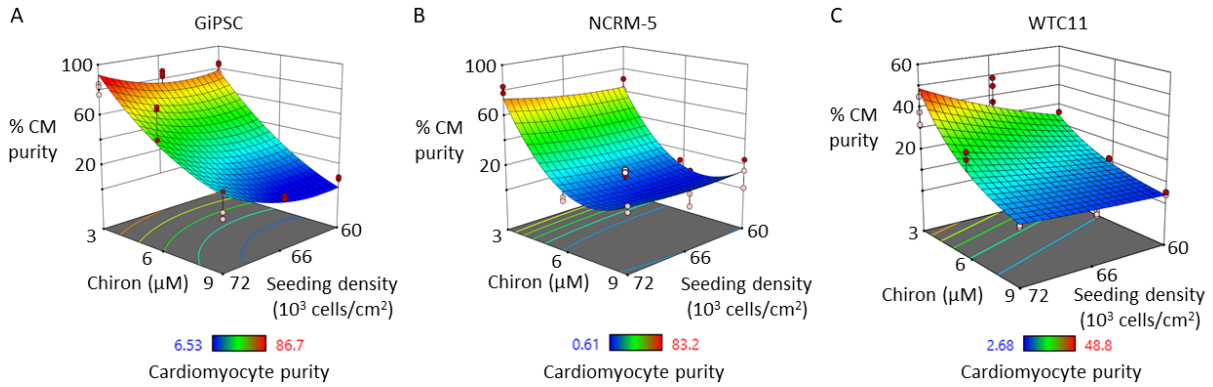

Figure 1. Chiron concentration and seeding density uniquely affect cardiac differentiation outcome. DOE (design of experiments) surface plots of directed differentiation outcomes in human induced pluripotent stem cell lines obtained from commercial (GiPSC; A), national bank (NCRM-5; B), and research institution (WTC11 ; C) sources. Red and pink circles indicate design points above and below predicted values, respectively. N=9 per group per condition from 3 biological replicates (i.e., batches of hiPSC-cardiomyocytes).

Figure 2

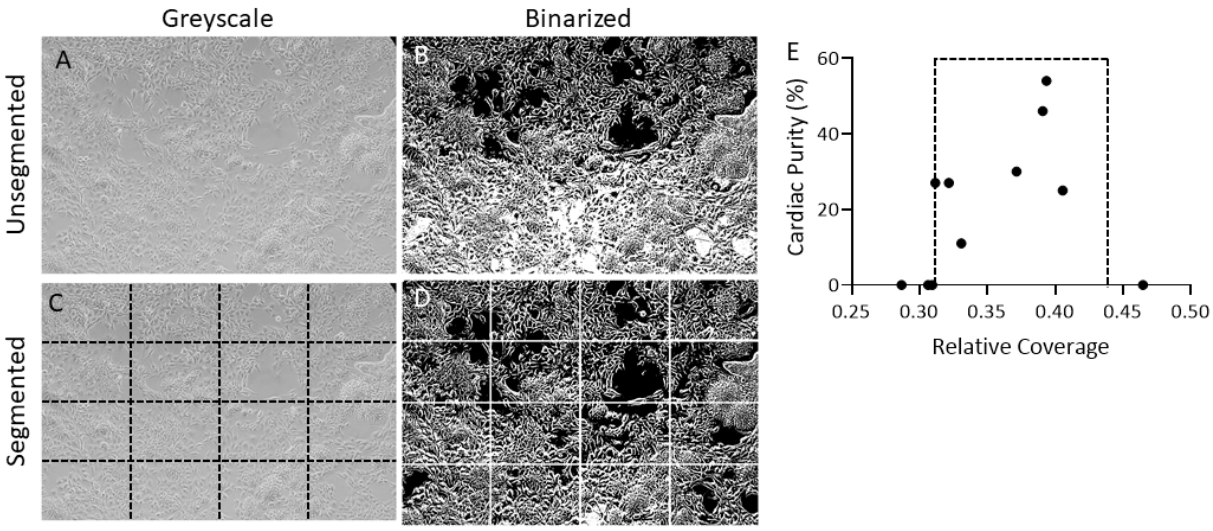

Figure 2. Segmented thresholding shows range of plate coverage for cardiomyocyte differentiation using 6 μM Chiron. (A) Brightfield image of Gibco hiPSCs (GiPSCs) at day 0 of differentiation. (B) Threshold of image without prior segmentation. (C) Segmented image, indicated by dashed black lines, and (D) reconstructed image after thresholding of segments. (E) GiPSC-cardiomyocyte purity plotted as a function of relative coverage at day 0, dashed box indicated range of plate coverage in which differentiation runs produced cardiomyocytes. N = 11 independent differentiation runs; data points represent single differentiation run outcomes.

Figure 3

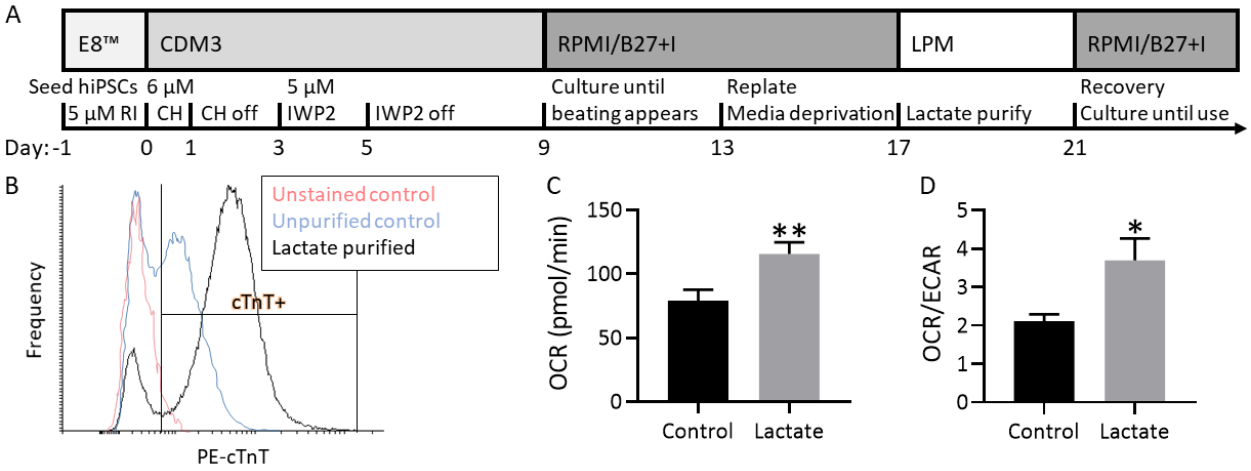

Figure 3. HiPSC-cardiomyocytes increase oxidative phosphorylation with lactate purification. (A) Cardiomyocytes were differentiated from Gibco hiPSCs (GiPSCs). (B) Control cells (blue, 51% cTnT+) were cultured for the same duration (with no starvation) and fed glucose medium, and lactate purified cells (black, 82% cTnT+) underwent glucose starvation and lactate purification from day 13 to 21 of culture. (C and D) Oxygen consumption rate (OCR; C), extracellular acidification rate (ECAR), and the ratio (OCR/ECAR; D) were measured at basal metabolic levels using a Seahorse XFe96 Analyzer, and values were normalized to live cell number using a LIVE/DEAD stain. *P<0.05, **P<0.01, n=10 per group, data are represented as mean ± SEM. (RI: rock inhibitor, CH: Chiron, IWP2: inhibitor of Wnt protein 2, CDM3: cardiac differentiation media 3, RPMI/B27 +I: RPMI/B27 with insulin, LPM: lactate purification media, cTnT: cardiac troponin T.)

Figure 4

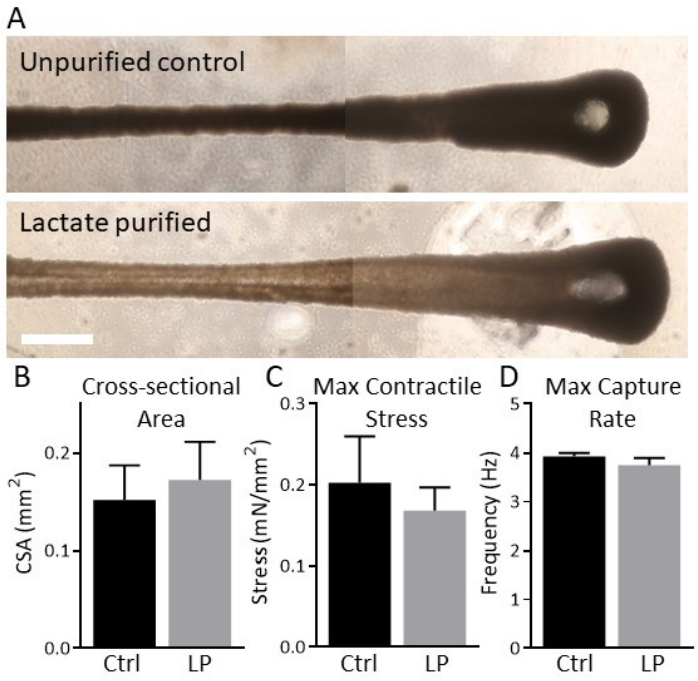

Figure 4. Lactate purified cardiomyocytes do not inhibit tissue formation via compaction and electromechanical function at one week. (A) Engineered cardiac tissues made with 5% human cardiac fibroblasts (hCFs) and unpurified hiPSC-cardiomyocytes (38% cTnT+; top) or lactate purified hiPSC-cardiomyocytes (82% cTnT+; bottom) were cultured for one week. Scale bar: 1 mm; images stitched together. (B-D) Control tissues (Ctrl, n=8) and tissues with lactate purified cells (LP, n=4) underwent mechanical evaluation after 1 week of culture. Cross-sectional area (B), maximum twitch contraction stress (C), and maximum capture rate (D) are not different between control (Ctrl) and lactate purified (LP) groups. Data are represented as mean ± SEM.

Table 1

Table 1. Human induced pluripotent stem cell lines

In-House name	**Line name**	**Source**	**Donor Source**	**Reprogramming method**
GiPSC	Gibco® Episomal hiPSC Line	ThermoFisher Scientific (Catalog #A18944)	Female, CD34+ cord blood	Episomal
NCRM-5	NCRM-5	NIH Center for Regenerative Medicine	Male, CD34+ cord blood	Episomal
WTC11	WTC11, GM25256	Gladstone Institute of Cardiovascular Disease, UCSF	Male, dermal fibroblasts	Episomal

Chapter 7: Discussion

The field of cardiac tissue engineering is faced with numerous challenges in producing robust, physiological tissues from human pluripotent stem cell (hPSC)-derived cardiomyocytes. The research described in this dissertation provides advances to the field both by questioning long-standing assumptions and by demonstrating novel, bioinspired methods for engineering cardiac tissue. Important findings include (1) the finding that hPSC-cardiomyocyte cytosolic and myofibril volume are not surrogate measures for each other; (2) evidence that developmental growth factors insulin-like growth factor 1 (IGF1) and neuregulin 1ß (NRG1) affect hPSC-cardiomyocyte proliferation and electromechanical maturity, respectively, in two and three dimensions; (3) the novel use of adult human ventricular cardiac fibroblasts (hCFs) to produce physiological and pathophysiological phenotypes in engineered cardiac tissues; and (4) the description of widely-adaptable differentiation optimization through image analysis. These findings impact research both in the Coulombe lab and the field as a whole; and they provide insights into and benefit from progress in areas of cell heterogeneity, hPSC-cardiomyocyte maturation and in vitro model development.

Stem cell heterogeneity

The complexity of human pluripotent stem cell (hPSC) biology and heterogeneity has been progressively uncovered, and the impact on hPSC-based research and therapies is only beginning to be realized. Many areas are being reexamined in light of these discoveries. Issues of particular relevance to the research described in this dissertation are (1) hPSC heterogeneity arising from cell source and culture conditions, (2) the line-dependent proclivity for differentiation down particular cell lineages, and (3) the functional differences in cells derived from different hPSC lines, research groups, and individual differentiation runs.

Heterogeneity in hPSCs arising from cell source and culture conditions were long noted in an observational manner but have recently been described more rigorously with advances in the “omics” and microfluidics fields. This heterogeneity is present at the mRNA transcript level,

where analysis of pluripotent marker expression in single human embryonic and induced pluripotent stem cells differed significantly among cells.[270] The heterogeneity within a population was more pronounced in hiPSCs, indicating a less stable pluripotent state. These findings support observations in our lab where cells of progressive passages lead to decreased differentiation potential in hiPSCs but not hESCs. In short, it is likely that the decreased pluripotent stability of hiPSCs is responsible for increased spontaneous differentiation during extended culture and decreased potential for directed differentiation into the cardiac fate.

The description of heterogeneity in hPSC pluripotency provides an explanation for heterogeneity in differentiation efficiency. However, the ultimate way stem cell-based research benefits is from the ability to identify, prior to differentiation, the pluripotency of an hPSC population. A broader study of hiPSC transcript profiles using single-cell RNA sequencing demonstrated transcriptional heterogeneity exists among hiPSCs across the entire transcriptome, not just across pluripotent markers.[271] Using unbiased clustering, the authors identify four hiPSC subpopulations of relative pluripotency, and they develop a multigenic prediction model to classify single cells into each of these populations. These findings, though critical to the field, must be condensed and streamlined in a manner that will allow bench scientists to adapt genetic profiling as a feasible, high-throughput predictor of pluripotency in their own hPSC cultures as they grow and deviate (potentially) on a weekly basis.

It is critical to consider not only cellular heterogeneity, but culture heterogeneity, when putting the results described in this dissertation into context. Though more difficult to quantify, there is a level of heterogeneity that arises from the culture conditions employed by different research groups. Shinya Yamanaka, Nobel laureate for his discovery of the transcription factors to induce pluripotency in differentiated cells, described at the International Society for Stem Cell Research Annual Meeting of 2016,[3] his efforts to evaluate cell culture geographical location on hiPSC heterogeneity.[272] The Center for iPS Cell Research and Application, Kyoto University (CiRA),

founded by Yamanaka, has undertaken the process of distributing iPSC stocks to both institutional and commercial labs and obtaining samples of these same cells after second-party culture. Though final results are not available, initial findings demonstrated mutations arising in iPSC samples from different groups.[272] These findings highlight the importance of careful and consistent analysis when comparing results of stem cell research across groups. As such, though the hPSC lines used in this dissertation research are used by other groups for similar studies,[273,231,274,41] it is important to note that the starting cell populations are not truly identical.

Another notable manifestation of hPSC heterogeneity represented in this work is the broad range of outcomes in cardiac directed differentiation. Because cardiac purity has the most significant impact on engineered tissue formation and function,[275] it is critical for the field to understand the source of this heterogeneity and to account for it when analyzing results. Recent work reported that cardiomyocytes differentiated from 181 hiPSC lines have unique expression patterns and differentiation outcomes, and upon single-cell RNA sequencing of 8 lines, showed that within differentiated cell populations, cells from the same line remained clustered.[276] This study demonstrates that some hiPSC lines have a more “primed” cardiogenic phenotype and that even after differentiation, hiPSC lines retain unique expression profiles. Individual studies in this dissertation each employ a single hPSC line.

In light of the findings referenced above, it is necessary to consider these studies, as well as the multitude of others in the field performed with a single hPSC line, as only partially representative of cardiomyocyte biology. In the early years (2008-2010) of hiPSC research, the field imposed higher standards for repeatability across hPSC types with roughly 80% of hiPSC papers including an hESC line.[277] This percentage has dropped precipitously in the past ten years to less than 30%, indicating an increased trust in hiPSCs as bona fide pluripotent stem cells, However, this trend may limit how robust, repeatable, and representative hiPSC research articles. The extent to which unique hiPSC-cardiomyocyte expression profiles impacts cell

function is not yet, and may never be, fully known. For the time being, it is another factor to consider when comparing and interpreting results across hPSC lines and research groups.

A downstream result of variability in differentiation efficiency across hPSC lines and research groups is the variability in cardiomyocyte purity in engineered tissues made in these different conditions. Setting aside the matter of heterogeneity among hPSC-cardiomyocytes, questions that still plague the field are (1) what are the non-cardiomyocytes and (2) what is their functional impact? My research presented in Chapter 4, and that of others,[58,211] shows a bimodal response of engineered tissue contractile force to hPSC-cardiomyocyte purity, demonstrating that the non-cardiomyocytes are important players in tissue function. Single-cell RNA sequencing and mRNA expression analysis suggest these non-cardiomyocytes exhibit a fibroblast-like expression profile,[276,8] but there is still little known about the mechanistic role of these cells in engineered cardiac tissue formation and function. The field as a whole, in cooperation with regulatory agencies, will have to determine the acceptable levels of contaminant cell types and the degree to which they must be characterized for predictive and therapeutic application of hPSC-cardiomyocytes.

Approaches to engineering maturity in cardiac tissues

The research described in this dissertation was performed in the rapidly evolving field of tissue engineering, and through its progression (2013-2019), reflects some of the trends developing in this area. In particular these studies were performed in consideration of (1) development of optimized native polymeric scaffolds; (2) advances in the chemical engineering of tailored scaffolds; and (3) new approaches to stimulate maturation of engineered cardiac tissues during culture. Both the composition and culture conditions of engineered cardiac tissues can drastically change their formation and function. Though there is unlikely to be one combination that produces engineered muscle far superior to the rest, certain trends have begun to arise that consistently produce higher-performing tissues.

Native polymeric scaffolds collagen and fibrin have come to stand out as top candidates in cardiac tissue engineering. In the adult ventricle, collagen-1 is the most abundant of the extracellular matrix (ECM) proteins, representing over one third of the total ECM protein content.[278] As such, it is commonly used as the scaffold protein in engineered tissues,[279] as it is in all the work presented in this thesis. A shortcoming of collagen-1 hydrogels, however, is its limited mechanical tunability, which forces biomedical engineers to rely on cells within the tissue to provide structural support. In cardiomyocyte-only engineered tissues, this can lead to tissues with a stiffness 10 to 100-fold lower than that of the adult ventricle, making the tissues challenging to handle and reducing the load they experience during culture. Fibrin, which undergoes a stochastic polymerization process, has been widely used as an ECM component to tune engineered tissue stiffness in a more controlled manner. Though fibrin can provide some additional structural support in engineered tissues, it is rapidly degraded by proteolysis and cell remodeling makes this process somewhat unpredictable, with different cell compositions remodeling surrounding ECM at variable rates.[275] This complication is exacerbated by the heterogeneity of hPSC-cardiomyocyte input populations. Due to this lack of control, despite the use of proteolysis inhibitors, some groups have turned toward more highly controlled scaffolds.

Synthetic polymeric scaffolds have provided a means to directly manipulate the extracellular environment of engineered cardiac tissues. In particular, functionalization of synthetic scaffolds to elicit specific responses is a promising approach for some areas of cardiovascular engineering. Conductive polymer scaffolds have gained popularity as a means to engineer scaffolds with electrotonic properties that more closely mimic the native myocardium. These polymers have been used in multiple forms, including electrospun fibers[280,281] and injectable hydrogels,[283,282] to improve electrical performance of cardiomyocytes. Some of the most innovative and involved advances in this realm have been pioneered by Tal Dvir (Tel Aviv University), including the recent report of engineered cardiac tissues with integrated

electronics.[284] Though synthetic polymers have proven to be a useful tool for the controlled formation and manipulation of engineered tissues, a corresponding increase in control of cardiomyocyte and cardiac tissue electromechanical function is not evident. This may be attributable to the very nature of the polymers as a non-native scaffold, a frustrating conclusion to be sure.

Because synthetic components may hinder the improved functional performance of engineered cardiac tissues due to high stiffness, lack of biocompatibility, non-physiologic degradation products, etc., the field has turned its attention toward bioinspired techniques for “pre-conditioning” or maturing tissues. The idea of improving tissue force production by “exercising” them during culture has been implemented through several techniques and is prevalent in this dissertation research. The load and the frequency of the load to which a tissue is subjected in culture can be used to exercise a tissue in culture. The load can be adjusted by changing the geometry and stiffness of an engineered tissue, and the frequency adjusted by simply changing the pacing frequency during culture.[286,45,25,21,285] The research described in this dissertation employs uniaxial stress through posts to establish load in culture and support cells to increase tissue stiffness and subsequent load. Though these methods go a ways toward exercising tissues during culture, others in the lab and field more broadly have employed different geometries, stretching protocols, and ECM stiffness (to name a few) to increase the minimum load experienced in culture.[192,25] An alternative approach to mechanical conditioning is electrical conditioning to increase the frequency of cardiac contractions, such as a frequency ramp pacing protocol (from standard, human-like 1 Hz pacing up to supra-human 6 Hz pacing over about 10 days), though these results for “exercising” tissues have yet to be replicated by other groups.[48]

One final but inconvenient bioinspired approach to improving tissue function is allowing tissues to mature in culture over longer periods of time. Engineered tissues in my research were cultured for one (Chapter 4) to two (Chapter 3) weeks, however, tissues producing higher force

levels have been reported at 4, 6, 8, and out to 10 weeks.[48,23,58] For many in vitro applications, it is only necessary to use tissues of sufficient maturity to detect functional differences in response to the chosen stimuli, though it is important to keep in mind that hPSC-cardiomyocyte response may change with overall maturation state. For engineered cardiac tissues to be repeatably and reliably effective tools for in vitro modeling and in vivo therapies, a functional benchmark will have to be determined, and combinations of composition and culture techniques will continue to evolve to reach that benchmark. The research presented in this dissertation is a significant contribution to the body of work that will ultimately lead to the field's definition of "mature" tissue for various translational applications and realization of these translational goals.

In vitro engineered cardiac tissue models

The development of in vitro models for evaluating cardiotoxicity and therapeutic efficacy (e.g., novel pharmaceuticals) is described as the "low hanging fruit" of cardiovascular engineering. As my work demonstrates, the complexity of these in vitro systems requires careful consideration of how they should be used and how to interpret their outputs. In particular, it is necessary to consider the throughput against the sensitivity of in vitro models, how truly predictive and representative results obtained from them are, and the most realistic and appropriate applications for these models.

One presumed requirement of in vitro models for therapeutic testing and development is high throughput, however, this often comes at the cost of sensitivity. HPSC-cardiomyocyte spheroids are gaining popularity for their simple assembly in a 96-well plate format and compatibility with already developed tools of analysis such as high-content imaging[287] and metabolic assays.[288] This model, however, is limited in two significant ways. Firstly, the spheroids cannot be subjected to load during culture, and as previously discussed, this is a critical culture condition for the development of hPSC-cardiomyocyte contractility. Secondly, the types of measurements that can be made on spheroids are limited primarily to visual outputs. At this time, contractile

force cannot be directly measured, leaving out a critical metric of cardiac function from any spheroid assay. Slightly lower throughput assays using PDMS posts or wires to provide load during engineered tissue culture can measure force indirectly using video analysis of post deflection, however, this method assumes PDMS posts are manufactured with reliable and repeatable stiffness, and the calculated force data is limited by the camera spatial resolution and capture speed.[289,25]

As my research demonstrates, significant changes in contraction and relaxation kinetics and appearance of contractile alternans can occur in very small ranges of force, necessitating a sensitive means of measuring force. This increase in sensitivity comes at the cost of throughput, with the platform used in this dissertation research producing between 10 and 20 tissues per experimental group compared with the 100s of tissues of spheroid platforms. Given this tradeoff, it is likely that a multilevel approach will be necessary to engineer experimentally feasible (high throughput, tier 1) and sufficiently sensitive (low throughput, tier 2) modeling systems.

Another important consideration of in vitro models is the interpretation of output data. In vitro platforms of engineered cardiac tissue are an inevitable simplification of human myocardium and are thus limited, to some extent, in their physiological relevance. hPSC-cardiomyocytes posses a high level of phenotypic plasticity, and it is critical to understand unintended or unseen shifts in cardiac phenotype resulting from culture conditions. My work demonstrates that hPSC-cardiomyocytes respond to growth factors and cardiac fibroblasts to produce both physiological and pathophysiological phenotypes (Chapters 4 and 5), a critical distinction for modeling and regeneration. Because the fetal gene program is reactivated during heart failure,[290] it is of particular importance to validate models that rely heavily on metrics of gene expression.

Finally, as the field of in vitro modeling develops new, more sophisticated assays, their realistic uses and applications must be kept in mind. These models will be only one step in the process of cytotoxicity testing and therapeutic development, and as the field moves toward

implementation of these models, it is important they are developed with consideration of context within the overall healthcare pipeline. The US Food and Drug Administration (FDA) has highlighted cell purity, biomarker expression, and metabolic activity as key metrics for predicting the quality of tissue engineered products.[291] As previously discussed, hPSC-cardiomyocyte purity is varied between batches and groups, significantly affects tissue function, and is most widely manipulated through metabolic selection. In vitro models must be sufficiently validated or "qualified" to withstand variability in hPSC-cardiomyocytes or developed in a way to control for this variability.

New tools in biomedical engineering

There are a multitude of technologies from which cardiac tissue engineering can benefit, and the impact and scope of the research described in this dissertation is no exception. In particular, single-cell RNA sequencing and liquid chromatography-mass spectrometry (LC-MS) could provide valuable additional information in the areas discussed above, including hPSC-cardiomyocyte heterogeneity and engineered tissue composition and maturation state.

Single-cell RNA sequencing (SC-RNAseq) is a powerful tool to examine transcript profiles of multiple cell populations in an unbiased manner. Though the findings in this dissertation are supported with analysis of transcript levels of specific mRNA targets when appropriate, the old adage "you don't know what you don't know" comes to mind. In particular, population averages of gene expression will dilute out the nuances of single cell behavior and variability. SC-RNAseq could be used to characterize hPSC-cardiomyocytes and non-cardiomyocytes as well as adult cardiac fibroblasts prior to and after inclusion in engineered tissues. This would allow us to ask and more fully answer the questions: what cells are we putting into our tissues, and what are they doing once they are there? As in any area with an ultimate goal of engineering functional tissues, it is critical that the results of SC-RNAseq experiments be interpreted in the context of the functional output of engineered cardiac tissues. An exhaustive transcript profile of cells from

engineered cardiac tissues will be of little use without an understanding of their functional phenotype.

Another tool that would allow us to more fully analyze what happens to cells in engineered cardiac tissues is liquid chromatography-mass spectrometry (LC-MS). LC-MS can be used as a bottom-up approach to proteomics, particularly helpful in analyzing complex mixtures of proteins. The ECM components used in tissue engineering are varied, as described above, and though the work in this dissertation uses only collagen-1, it also employs fibroblasts, a cell type that produces and remodels ECM. By correlating LC-MS data of ECM composition with cell composition and resulting engineered mechanical phenotype, we could gain insight into ECM, support-cell, and culture combinations that produce the most robust engineered tissues.

In conclusion, the research described in this thesis provides important insights to the field of cardiac tissue engineering as it marches closer to practical applications. Findings stress the importance of accounting for cellular heterogeneity (Chapters 2, 3, and 6) and explores strategies for manipulating engineered tissue composition and culture to produce healthy and disease phenotypes (Chapters 4 and 5). As the field advances toward translation to impact human health and wellness, these results highlight the need for careful consideration of engineered cardiac tissue composition and function in light of hPSC-cardiomyocytes' tendency to defy expectations.

Appendix I

Supplementary data associated with Chapter 5

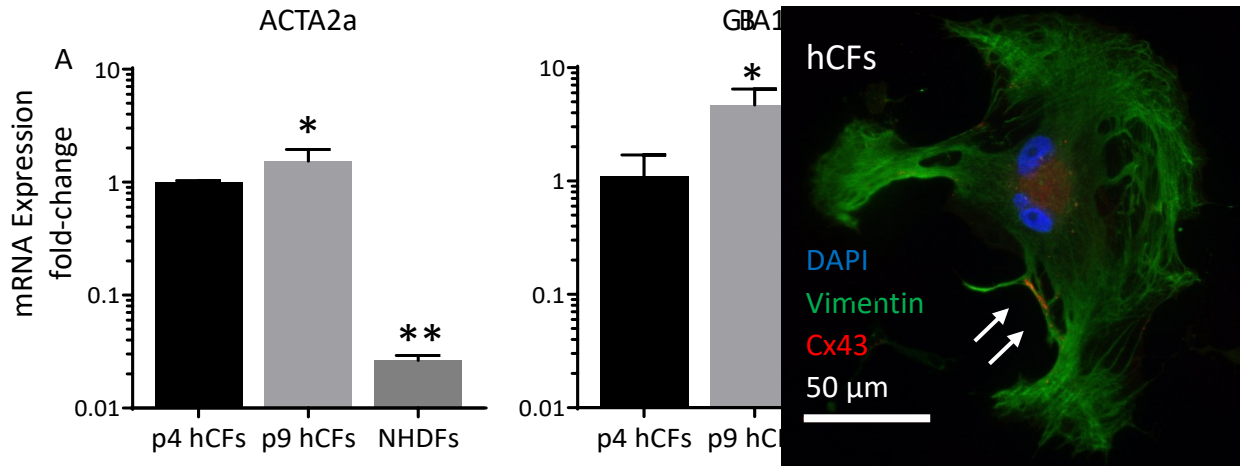

Figure S1. Myofibroblast markers upregulated in serially passaged human cardiac fibroblasts (hCFs). *Related to Figure 1.* (A) MRNA collected from monolayer hCFs at passage 4 (p4), passage 9 (p9), or from passage 4 neonatal human dermal fibroblasts (NHDFs) was analyzed with q-RT-PCR for expression levels of ACTA2a (left, encoding α-smooth muscle actin) and GJA1 (right, encoding connexin 43). Data are presented as a fold-change of p4 hCF expression levels and are represented as mean ± SD, *P<0.05, **P<0.01, n≥3. (B) Passage 9 human cardiac fibroblasts (hCFs) have localized gap junctions. HCFs are labeled for vimentin (green) to identify fibroblasts, connexin 43 (Cx43, red) to identify gap junctions, and DAPI (blue) to label nuclei. Cells express both diffuse Cx43 in a peri-nuclear region (e.g., Golgi) and punctate Cx43 gap junctions at cell edges (white arrows).

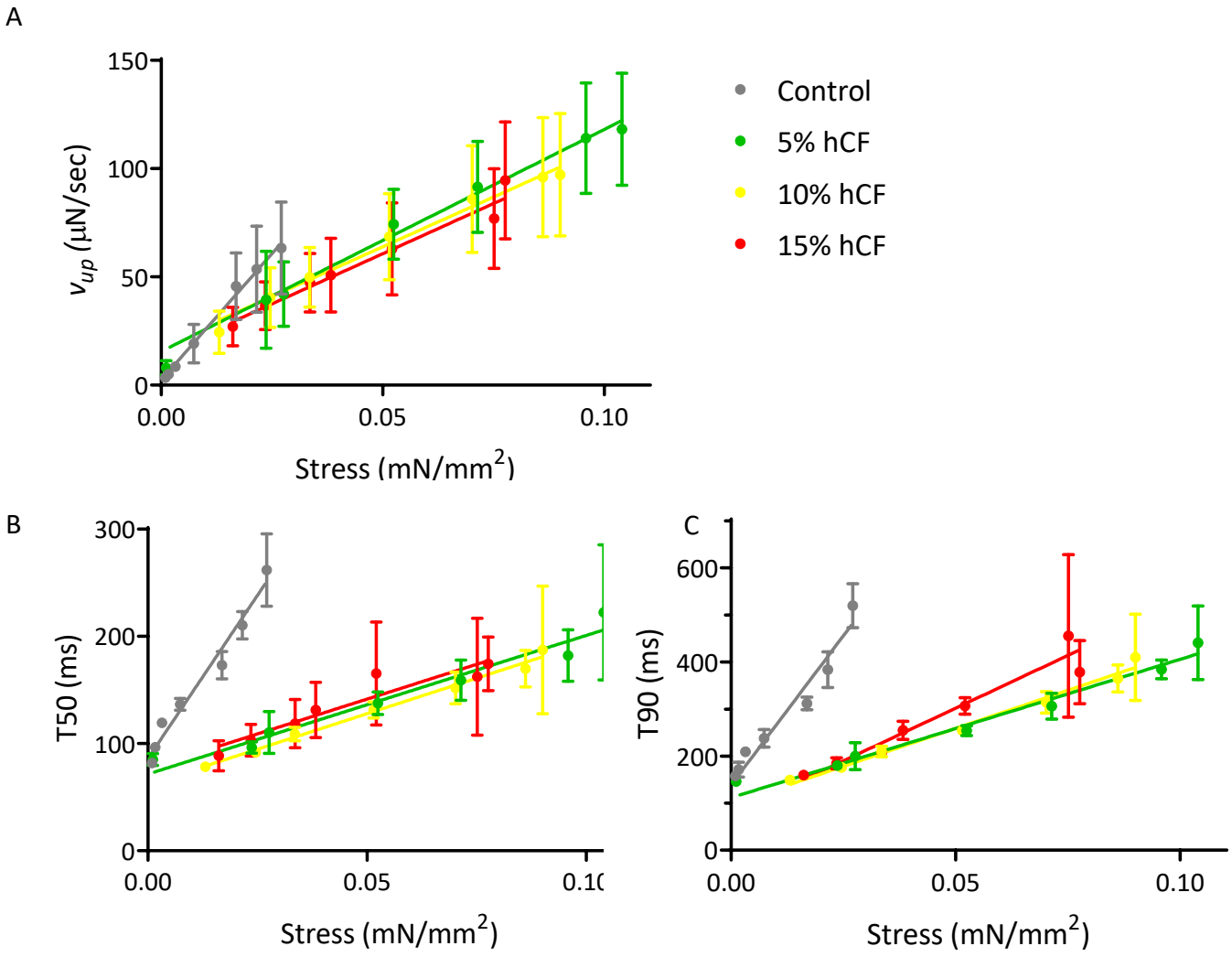

Figure S2. Contraction and relaxation kinetics of engineered cardiac tissues change with human cardiac fibroblast (hCF) addition. *Related to Figure 2.* (A) Upstroke velocity in cardiomyocyte-only ECTs (Control), 5% hCF added ECTs (5% hCF), 10% hCF added ECTs, or 15% hCF added ECTs plotted as a function of contractile stress amplitude. (B-C) Time to 50% relaxation from peak contractile amplitude (T50; B) and time to 90% relaxation (T90; C) plotted as a function of contractile stress. The slope of the linear regression was significantly greater in control tissues compared to p4 and p9 hCF tissues. $P<0.05$, $n\geq7$, data shown as mean ± SEM (A) or SD (B-C) for ease of viewing.

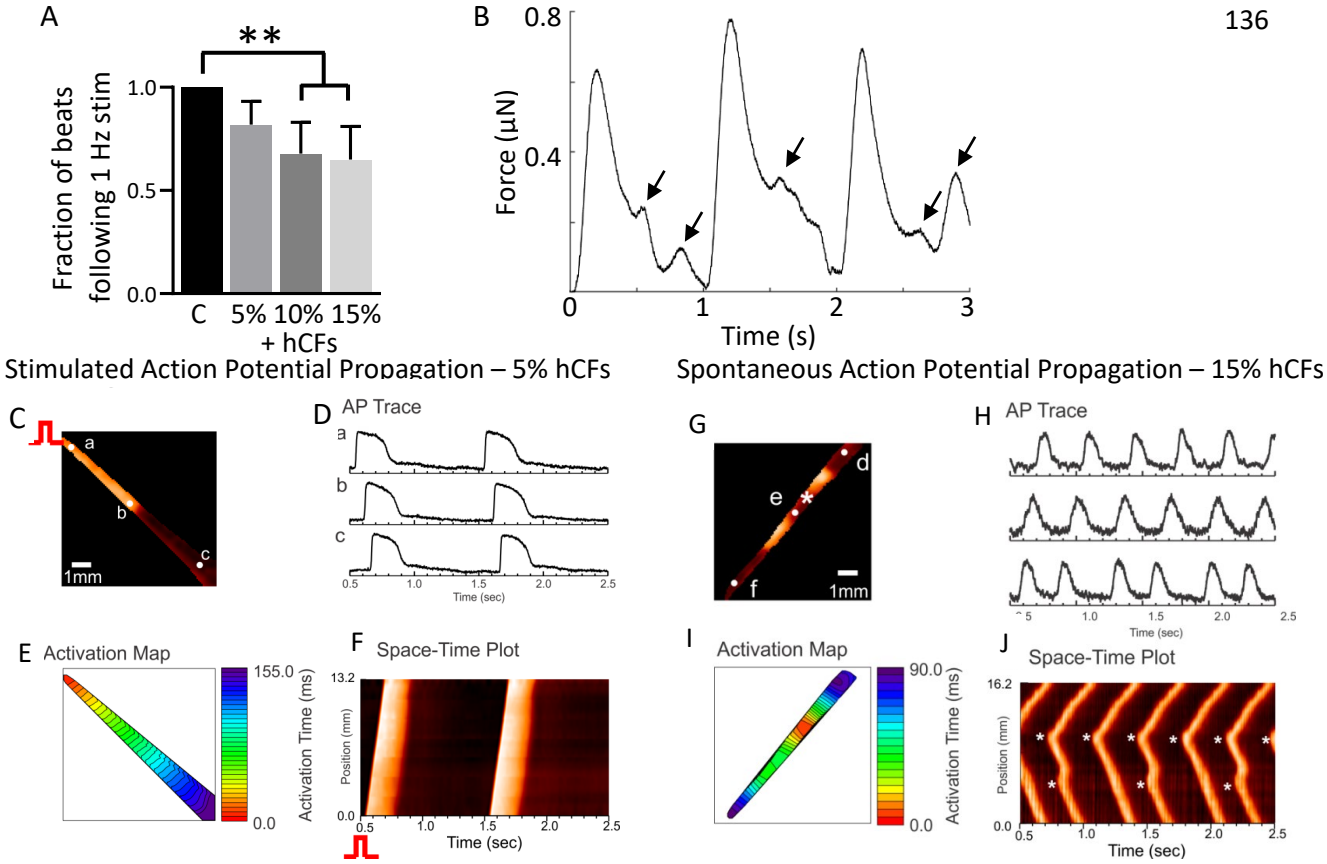

Figure S3. Higher percentages of human cardiac fibroblasts increase spontaneous beating activity. *Related to Figure 3.* (A) Fraction of beats captured by cardiomyocyte-only control (C), 5%, 10%, or 15% added cardiac fibroblast (+hCFs) tissues at 1 Hz pacing at 130% L_0 (**P<0.01, n≥4, data represent mean ± SEM). (B) Example raw trace of 15% hCF tissue during 1 Hz pacing. Arrows indicate early afterdepolarizations (EADs). (C-J) Representative maps of action potential propagation of paced or spontaneous beats. (C) Fluorescence image of paced beat from 5% hCF ECT, stimulated from the left upper corner. (D) Sample action potential traces from the locations marked with ‘a’, ‘b’, ‘c’ in panel C. (E) Action potential propagation map. (F) Space-time plot of action potential propagation (Conduction Velocity(CV) = 6.42 cm/s). (G) Fluorescence image of spontaneous beat from the 15% hCF ECT. (H) Sample action potential traces from the locations marked with ‘d’, ‘e’, ‘f’ in panel G. (I) Action potential propagation map. (J) Space-time plot of action potential propagation (CV = 2.59 cm/s). Note that the spontaneous beats originated from the center of the ECT marked with white stars (*) and propagated in both directions.

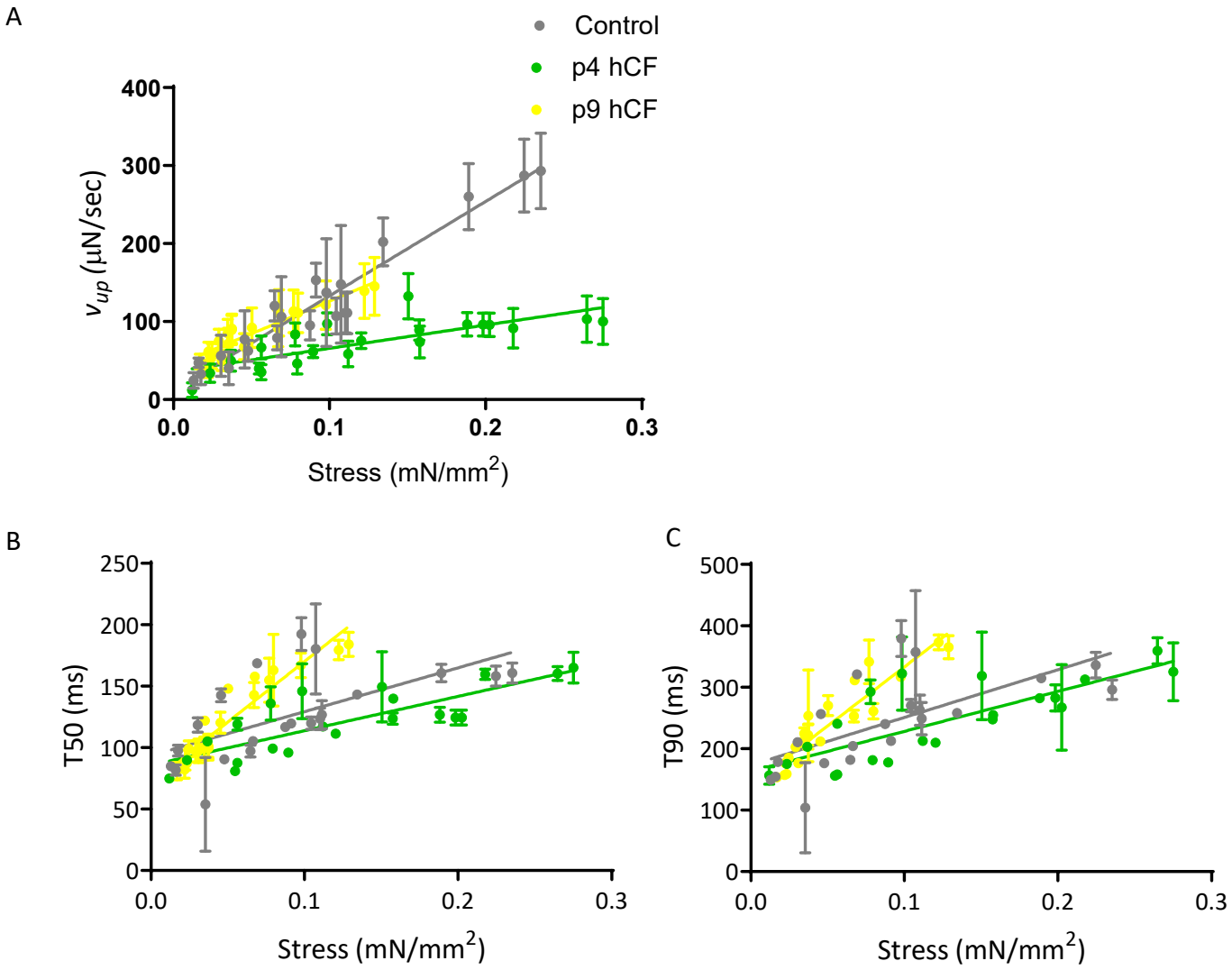

Figure S4. Contraction and relaxation kinetics of engineered cardiac tissues sensitive human cardiac fibroblast (hCF) level of activation. *Related to Figure 5.* (A) Upstroke velocity in cardiomyocyte-only ECTs (Control), 5% p4 hCF ECTs (p4 hCF), 5% p9 hCF added ECTs (p9 hCF) plotted as a function of contractile stress amplitude. The slope of the linear regression was significantly different between all groups. (B-C) Time to 50% relaxation from peak contractile amplitude (T50; B) and time to 90% relaxation (T90; C) plotted as a function of contractile stress. The slope of the linear regression of p9 hCF tissues was significantly greater than control and p4 hCF tissues for both T50 and T90. $P<0.05$, $n\geq16$, data shown as mean ± SEM (A) or SD (B-C) for ease of viewing.

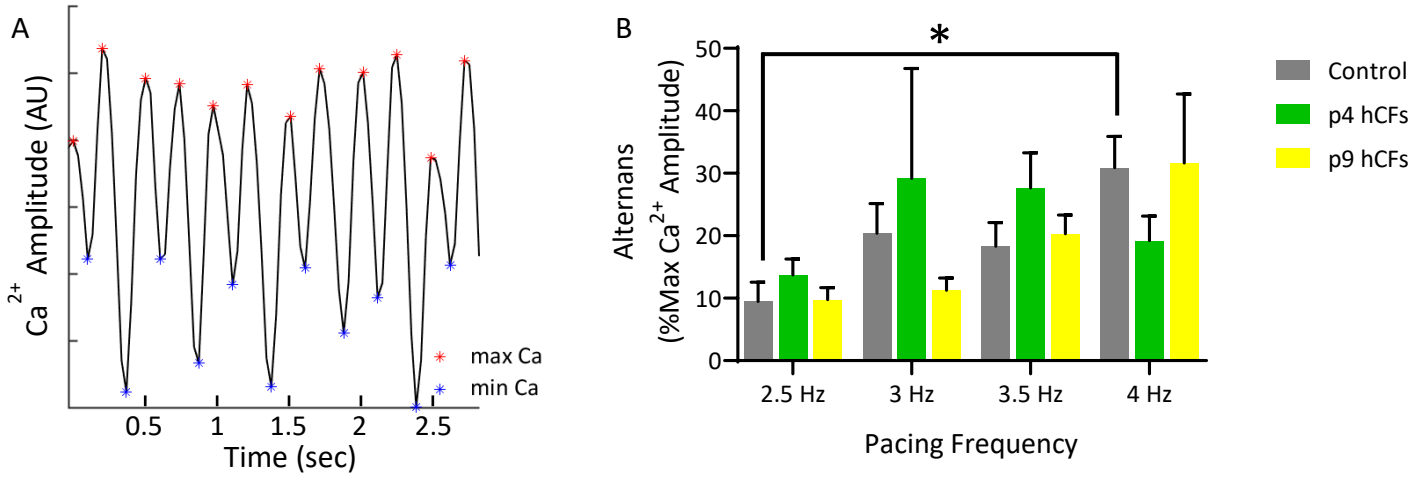

Figure S5. Calcium alternans increase with pacing frequency in engineered cardiac tissues. *Related to Figure 6*. Control, cardiomyocyte-only tissues, 5% p4 hCF-doped tissues, and 5% p9 hCF-doped tissues were treated with Ca^{2+}-sensitive, Rhod-2 dye and paced at increasing frequencies while fluorescence signal was obtained. Alternans were determined as alternating transients with a difference ≥5% of maximum Ca^{2+} amplitude. (A) Example raw trace of Ca^{2+} signal recorded at 4 Hz stimulation in a p4 hCF tissues. Red and blue asterisks mark local maxima and minima, respectively. (B) Alternans amplitude was calculated for Control, p4 hCF, and p9 hCF tissues up to 4 Hz pacing ($P<0.05$, n=3, data are represented as mean ± SEM).

Table S1. Custom primers used for real-time quantitative PCR. *Related to experimental procedures.*

Target	Sequence
ACTA2a (α-smooth muscle actin)	Forward: CCGACCGAATGCAGAAGGA
	Reverse: ACAGAGTATTTGCGCTCCGAA
GJA1 (connexin 43)	Forward: CTTTTGGAGTGACCAGCAAC
	Reverse: TGAAGCTGAACATGACCGTA

Table S2. hCF Doping Experiments 1 Hz Mechanics Summary. *Related to Figure 3.*

Measure	Group		Mean (n)	SEM
Cross-sectional area (mm^2)	Control		0.335 (7)	0.030
	5%	+ hCFs	0.243 (12)	0.036
	10%		0.170 (7)	0.032
	15%		0.126 (8)	0.021
Young's Modulus (kPa)	Control		0.67 (6)	0.11
	5%	+ hCFs	3.12 (6)	0.92
	10%		4.16 (4)	1.45
	15%		6.75 (3)	0.62
Maximum active stress (mN/mm^2)	Control		0.046 (7)	0.008
	5%	+ hCFs	0.123 (10)	0.032
	10%		0.097 (7)	0.021
	15%		0.080 (6)	0.024
Maximum capture rate (Hz)	Control		2.93 (7)	0.28
	5%	+ hCFs	3.17 (12)	0.17
	10%		3.71 (7)	0.15
	15%		3.86 (7)	0.14

Significant vs. Control	Significant vs. Ctrl and 5% hCF

Table S3. hCF Doping Experiments Force-Frequency Summary. *Related to Figure 3.*

	Frequency		**1Hz**		**1.5 Hz**		**2 Hz**		**2.5 Hz**	
Measure	**Group**		**Mean (n)**	**SEM**	**Mean (n)**	**SEM**	**Mean (n)**	**SEM**	**Mean (n)**	**SEM**
Stress (μN/ mm²)	Control		27.1 (7)	5.0	21.5 (7)	4.2	16.9 (5)	3.7	7.4 (6)	1.7
	5%	+hCF	104.0 (12)	11.8	95.9 (12)	11.1	71.4 (12)*	9.4	52.5 (11)**	7.5
	10%		90.1 (7)	18.1	86.1 (7)	17.9	70.2 (7)	15.0	51.5 (7)	10.9
	15%		75.2 (7)	15.5	77.6 (5)	21.6	52.1 (7)	12.6	38.3 (7)	9.3
Vup (μN/s)	Control		63.4 (7)	21.3	53.5 (7)	20.0	45.7 (5)	15.3	19.2 (6)	8.9
	5%	+hCF	118.2 (12)	25.9	113.7 (12)	25.6	91.6 (12)	21.0	74.3 (11)	16.2
	10%		97.2 (7)	28.3	96.1 (7)	27.5	85.9 (7)	24.7	68.6 (7)	19.9
	15%		76.9 (7)	23.0	94.5 (5)	27.1	62.9 (7)	21.3	50.8 (7)	17.0
T50 (ms)	Control		261.8 (7)	12.7	210.5 (7)**	4.9	173.0 (5)**	5.8	136.6 (6)**	2.3
	5%	+hCF	222.3 (12)	18.2	182.2 (12)**	6.9	159.1 (12)**	5.4	137.5 (11)**	3.2
	10%		187.4 (7)	22.5	169.8 (7)	6.4	151.9 (7)	5.6	131.4 (7)**	2.8
	15%		162.5 (7)	20.6	174.3 (5)	11.3	165.4 (7)	18.1	131.3 (7)	9.8
T90 (ms)	Control		519.7 (7)	17.7	383.6 (7)**	14.4	311.5 (5)**	6.2	237.6 (6)**	7.7
	5%	+hCF	440.7 (12)	22.6	383.9 (12)*	5.8	306.0 (12)**	8.0	253.9 (11)**	3.3
	10%		409.6 (7)	34.6	364.6 (7)	11.0	314.2 (7)**	8.5	254.4 (7)**	3.7
	15%		455.1 (7)	65.3	378.5 (5)*	30.0	306.6 (7)**	6.7	254.8 (7)**	7.3

	Frequency		3 Hz		3.5 Hz		4 Hz	
Measure	**Group**		**Mean (n)**	**SEM**	**Mean (n)**	**SEM**	**Mean (n)**	**SEM**
Force (μN/ mm²)	Control		3.2 (2)	0.9	1.7 (3)	0.9	1.0 (1)	N/A
	5%	+hCF	27.6 (8)**	5.3	23.7 (3)**	1.0	1.1 (3)**	0.9
	10 %		33.5 (7)**	6.9	24.6 (5)**	6.8	13.1 (4)**	5.6
	15 %		33.6 (6)	7.9	23.5 (6)	5.9*	16.2 (6)**	4.4
Vup (μN/s)	Control		8.6 (2)	1.5	5.1 (3)	1.7	3.4 (1)	N/A
	5%	+hCF	42.0 (8)*	15.0	39.4 (3)	22.4	8.1 (3)*	3.3
	10 %		49.8 (7)	13.8	40.4 (5)	13.8	24.4 (4)	9.8
	15 %		47.3 (6)	13.5	36.7 (6)	11.0	27.1 (6)	8.9
T50 (ms)	Control		119.4 (2)**	3.0	96.5 (3)**	1.0	81.9 (1)	N/A
	5%	+hCF	110.5 (8)**	6.9	96.4 (3)**	3.0	85.1 (3)**	3.1
	10 %		108.8 (7)**	2.4	91.9 (5)**	1.6	78.5 (4)**	1.7
	15 %		118.6 (6)*	9.2	103.0 (6)**	6.1	88.7 (6)**	5.7
T90 (ms)	Control		209.2 (2)**	4.4	171.3 (3)**	9.2	157.8 (1)	N/A
	5%	+hCF	200.0 (8)**	10.1	179.8 (3)**	2.9	145.9 (3)**	3.9
	10 %		209.9 (7)**	4.3	175.7 (5)**	2.0	149.0 (4)**	3.6
	15 %		208.2 (6)**	3.3	184.4 (6)**	4.9	159.3 (6)**	2.7

Significant vs. Control	Significant vs. Ctrl and 5% hCF

Table S4. p4 v p9 hCF Experiments 1 Hz Mechanics Summary. *Related to Figure 5.*

Measure	**Group**		**Mean (n)**	**SEM**
Cross-sectional area (mm^2)	Control		0.213 (18)	0.028
	P4	+ hCFs	0.081 (18)	0.010
	P9		0.203 (20)	0.012
Young's Modulus (kPa)	Control		1.59 (14)	0.36
	P4	+ hCFs	7.89 (16)	1.74
	P9		2.47 (16)	0.58
Maximum active stress (mN/mm^2)	Control		0.141 (15)	0.031
	P4	+ hCFs	0.227 (18)	0.033
	P9		0.087 (20)	0.015
Maximum capture rate (Hz)	Control		4.13 (16)	0.11
	P4	+ hCFs	4.00 (18)	0.07
	P9		3.87 (19)	0.10

Significant vs. Control	Significant vs. Ctrl and p9 hCF	Significant vs. Ctrl and p4 hCF	Significant vs. p9 hCF	Significant vs. p4 hCF

Table S5. p4 v p9 hCF Experiments Force-Frequency Summary. *Related to Figure 5.*

	Frequency		**1 Hz**		**1.5 Hz**		**2 Hz**		**2.5 Hz**	
Measure	**Group**		**Mean (n)**	**SEM**	**Mean (n)**	**SEM**	**Mean (n)**	**SEM**	**Mean (n)**	**SEM**
Stress ($\mu N/mm^2$)	Control		123.4 (16)	19.1	120.4 (16)	18.7	102.2 (16)	15.2	75.1 (16)*	10.5
	P4	+hCFs	193.0 (18)	25.5	176.4 (18)	21.7	154.4 (18)	18.3	120.2 (18)**	13.9
	P9		76.3 (20)	7.7	74.1 (20)	7.4	65.6 (20)	6.7	50.9 (20)	5.7
Vup ($\mu N/s$)	Control		156.5 (16)	35.2	152.9 (16)	34.2	138.0 (16)	30.5	110.1 (16)	22.9
	P4	+hCFs	99.1 (18)	12.5	91.5 (18)	10.3	86.1 (18)	9.6	74.8 (18)	8.5
	P9		96.7 (20)	12.4	95.7 (20)	12.1	90.8 (20)	11.1	77.3 (20)	9.4
T50 (ms)	Control		154.4 (16)	11.3	148.3 (16)	7.0	148.0 (16)	5.5	133.4 (16)*	5.5
	P4	+hCFs	138.8 (18)	5.5	137.1 (18)	4.5	137.6 (18)	3.8	125.7 (18)	2.9
	P9		136.5 (20)	8.0	137.9 (20)	7.7	136.9 (20)	6.8	123.1 (20)	4.8
T90 (ms)	Control		303.1 (16)	26.0	316.5 (16)	12.5	296.6 (16)	5.4	251.2 (16)**	1.9
	P4	+hCFs	291.6 (18)	16.2	311.2 (18)	10.4	292.0 (18)	3.8	244.6 (18)**	3.0
	P9		278.2 (20)	14.5	293.3 (20)	14.8	276.9 (20)	9.1	242.6 (20)*	4.2

	Frequency		3 Hz		3.5 Hz		4 Hz	
Measure	**Group**		**Mean (n)**	**SEM**	**Mean (n)**	**SEM**	**Mean (n)**	**SEM**
Stress ($\mu N/mm^2$)	Control		52.5 (16)**	7.1	37.0 (16)**	4.8	16.3 (13)**	1.9
	P4	+hCFs	87.6 (18)**	10.1	63.2 (18)**	7.2	42.6 (16)**	5.5
	P9		36.2 (20)	4.6	28.3 (17)*	4.0	19.3 (15)**	2.3
Vup (μN/s)	Control		85.1 (16)*	16.9	65.5 (16)**	13.1	32.2 (13)**	5.6
	P4	+hCFs	61.1 (18)	7.1	48.0 (18)	6.0	33.9 (16)*	4.4
	P9		58.3 (20)	7.7	51.2 (17)	6.7	42.4 (15)	5.4
T50 (ms)	Control		113.6 (16)**	2.2	95.6 (16)**	1.6	76.3 (13)**	5.8
	P4	+hCFs	109.9 (18)**	1.9	94.4 (18)**	1.1	80.5 (16)**	1.2
	P9		110.1 (20)**	3.3	94.8 (17)**	2.2	82.2 (15)**	1.9
T90 (ms)	Control		206.7 (16)**	2.7	177.5 (16)**	2.3	142.8 (13)**	10.7
	P4	+hCFs	206.9 (18)**	1.7	177.5 (18)**	1.0	156.5 (16)**	1.7
	P9		211.5 (20)**	3.6	177.3 (17)**	1.8	155.8 (15)**	15

Significant vs. Control	Significant vs. Ctrl and p9 hCF	Significant vs. Ctrl and p4 hCF	Significant vs. p9 hCF	Significant vs. p4 hCF

Bibliography

1. MALTSEV V, ROHWEDEL J, HESCHELER J, WOBUS A. Embryonic stem cells differentiate in vitro into cardiomyocytes representing sinusnodal, atrial and ventricular cell types. *Mech Dev*. 1993;44(1):41-50. doi:10.1016/0925-4773(93)90015-P

2. Yu J, Vodyanik MA, Smuga-Otto K, et al. Induced pluripotent stem cell lines derived from human somatic cells. *Science*. 2007;318(5858):1917-1920. doi:10.1126/science.1151526

3. Takahashi K, Tanabe K, Ohnuki M, et al. Induction of pluripotent stem cells from adult human fibroblasts by defined factors. *Cell*. 2007;131(5):861-872. doi:10.1016/j.cell.2007.11.019

4. Laflamme M a, Chen KY, Naumova A V, et al. Cardiomyocytes derived from human embryonic stem cells in pro-survival factors enhance function of infarcted rat hearts. *Nat Biotechnol*. 2007;25(9):1015-1024. doi:10.1038/nbt1327

5. Kattman SJ, Witty AD, Gagliardi M, et al. Stage-specific optimization of activin/nodal and BMP signaling promotes cardiac differentiation of mouse and human pluripotent stem cell lines. *Cell Stem Cell*. 2011;8(2):228-240. doi:10.1016/j.stem.2010.12.008

6. Lian X, Hsiao C, Wilson G, et al. Robust cardiomyocyte differentiation from human pluripotent stem cells via temporal modulation of canonical Wnt signaling. *Proc Natl Acad Sci U S A*. 2012;109(27):E1848-57. doi:10.1073/pnas.1200250109

7. Burridge PW, Matsa E, Shukla P, et al. Chemically defined generation of human cardiomyocytes. *Nat Methods*. 2014;11(8):855-860. doi:10.1038/nmeth.2999

8. Friedman CE, Nguyen Q, Lukowski SW, et al. Single-Cell Transcriptomic Analysis of Cardiac Differentiation from Human PSCs Reveals HOPX-Dependent Cardiomyocyte Maturation. *Cell Stem Cell*. 2018;23(4):586-598.e8. doi:10.1016/j.stem.2018.09.009

9. Churko JM, Garg P, Treutlein B, et al. Defining human cardiac transcription factor hierarchies using integrated single-cell heterogeneity analysis. *Nat Commun*. 2018;9(1):4906. doi:10.1038/s41467-018-07333-4

10. Werner JC, Sicard RE. Lactate Metabolism of Isolated, Perfused Fetal, and Newborn Pig Hearts. *Pediatr Res*. 1987;22(5):552-556. doi:10.1203/00006450-198711000-00016

11. Tohyama S, Hattori F, Sano M, et al. Distinct metabolic flow enables large-scale purification of mouse and human pluripotent stem cell-derived cardiomyocytes. *Cell Stem Cell*. 2013;12(1):127-137. doi:10.1016/j.stem.2012.09.013

12. Xu XQ, Zweigerdt R, Soo SY, et al. Highly enriched cardiomyocytes from human embryonic stem cells. *Cytotherapy*. 2008;10(4):376-389. doi:10.1080/14653240802105307

13. Dubois NC, Craft AM, Sharma P, et al. SIRPA is a specific cell-surface marker for isolating cardiomyocytes derived from human pluripotent stem cells. *Nat Biotechnol*. 2011;29(11):1011-1018. doi:10.1038/nbt.2005

14. Eschenhagen T, Bolli R, Braun T, et al. Cardiomyocyte Regeneration: A Consensus Statement. *Circulation*. 2017;136(7):680-686. doi:10.1161/CIRCULATIONAHA.117.029343

15. Stevens KR, Pabon L, Muskheli V, Murry CE. Scaffold-free human cardiac tissue patch created from embryonic stem cells. *Tissue Eng Part A*. 2009;15(6):1211-1222. doi:10.1089/ten.tea.2008.0151

16. Stevens KR, Kreutziger KL, Dupras SK, et al. Physiological function and transplantation of scaffold-free and vascularized human cardiac muscle tissue. *Proc Natl Acad Sci U S A*. 2009;106(39):16568-16573. doi:10.1073/pnas.0908381106

17. Kreutziger KL, Muskheli V, Johnson P, Braun K, Wight TN, Murry CE. Developing vasculature and stroma in engineered human myocardium. *Tissue Eng Part A*. 2011;17(9-10):1219-1228. doi:10.1089/ten.TEA.2010.0557

18. Masumoto H, Ikuno T, Takeda M, et al. Human iPS cell-engineered cardiac tissue sheets with cardiomyocytes and vascular cells for cardiac regeneration. *Sci Rep*. 2014;4:6716. doi:10.1038/srep06716

19. Sullivan KE, Quinn KP, Tang KM, Georgakoudi I, Black LD. Extracellular matrix remodeling following myocardial infarction influences the therapeutic potential of mesenchymal stem cells. *Stem Cell Res Ther*. 2014;5(1):14. doi:10.1186/scrt403

20. Kensah G, Roa Lara A, Dahlmann J, et al. Murine and human pluripotent stem cell-derived cardiac bodies form contractile myocardial tissue in vitro. *Eur Heart J*. 2013;34(15):1134-1146. doi:10.1093/eurheartj/ehs349

21. Tulloch NL, Muskheli V, Razumova M V, et al. Growth of engineered human myocardium with mechanical loading and vascular coculture. *Circ Res*. 2011;109(1):47-59. doi:10.1161/CIRCRESAHA.110.237206

22. Streckfuss-Bömeke K, Wolf F, Azizian A, et al. Comparative study of human-induced pluripotent stem cells derived from bone marrow cells, hair keratinocytes, and skin fibroblasts. *Eur Heart J*. 2013;34(33):2618-2629. doi:10.1093/eurheartj/ehs203

23. Schaaf S, Shibamiya A, Mewe M, et al. Human engineered heart tissue as a versatile tool in basic research and preclinical toxicology. *PLoS One*. 2011;6(10):e26397. doi:10.1371/journal.pone.0026397

24. Hirt MN, Sörensen NA, Bartholdt LM, et al. Increased afterload induces pathological cardiac hypertrophy: a new in vitro model. *Basic Res Cardiol*. 2012;107(6):307.

doi:10.1007/s00395-012-0307-z

25. Thavandiran N, Margulies KB, Borochin M a., et al. A Microfabricated Platform to Measure and Manipulate the Mechanics of Engineered Cardiac Microtissues. *Tissue Eng Part A*. 2012;18(9-10):910-919. doi:10.1089/ten.TEA.2011.0341

26. Duan Y, Liu Z, O'Neill J, Wan LQ, Freytes DO, Vunjak-Novakovic G. Hybrid gel composed of native heart matrix and collagen induces cardiac differentiation of human embryonic stem cells without supplemental growth factors. *J Cardiovasc Transl Res*. 2011;4(5):605-615. doi:10.1007/s12265-011-9304-0

27. Silva AKA, Juenet M, Meddahi-Pellé A, Letourneur D. Polysaccharide-based strategies for heart tissue engineering. *Carbohydr Polym*. 2015;116:267-277. doi:10.1016/j.carbpol.2014.06.010

28. Dar A, Shachar M, Leor J, Cohen S. Optimization of cardiac cell seeding and distribution in 3D porous alginate scaffolds. *Biotechnol Bioeng*. 2002;80(3):305-312. doi:10.1002/bit.10372

29. Shachar M, Tsur-Gang O, Dvir T, Leor J, Cohen S. The effect of immobilized RGD peptide in alginate scaffolds on cardiac tissue engineering. *Acta Biomater*. 2011;7(1):152-162. doi:10.1016/j.actbio.2010.07.034

30. Sapir Y, Kryukov O, Cohen S. Integration of multiple cell-matrix interactions into alginate scaffolds for promoting cardiac tissue regeneration. *Biomaterials*. 2011;32(7):1838-1847. doi:10.1016/j.biomaterials.2010.11.008

31. Hussain A, Collins G, Yip D, Cho CH. Functional 3-D cardiac co-culture model using bioactive chitosan nanofiber scaffolds. *Biotechnol Bioeng*. 2013;110(2):637-647. doi:10.1002/bit.24727

32. Li J, Shu Y, Hao T, et al. A chitosan-glutathione based injectable hydrogel for suppression of oxidative stress damage in cardiomyocytes. *Biomaterials*. 2013;34(36):9071-9081. doi:10.1016/j.biomaterials.2013.08.031

33. Marsano A, Maidhof R, Wan LQ, et al. Scaffold stiffness affects the contractile function of three-dimensional engineered cardiac constructs. *Biotechnol Prog*. 26(5):1382-1390. doi:10.1002/btpr.435

34. Carrier RL, Papadaki M, Rupnick M, et al. Cardiac tissue engineering: cell seeding, cultivation parameters, and tissue construct characterization. *Biotechnol Bioeng*. 1999;64(5):580-589. http://www.ncbi.nlm.nih.gov/pubmed/10404238. Accessed May 25, 2015.

35. Lesman A, Habib M, Caspi O, et al. Transplantation of a tissue-engineered human vascularized cardiac muscle. *Tissue Eng Part A*. 2010;16(1):115-125. doi:10.1089/ten.TEA.2009.0130

36. Mukherjee S, Reddy Venugopal J, Ravichandran R, Ramakrishna S, Raghunath M. Evaluation of the Biocompatibility of PLACL/Collagen Nanostructured Matrices with Cardiomyocytes as a Model for the Regeneration of Infarcted Myocardium. *Adv Funct Mater*. 2011;21(12):2291-2300. doi:10.1002/adfm.201002434

37. Kasahara H, Hayashi I. Polyglycolic acid sheet with fibrin glue potentiates the effect of a fibrin-based haemostat in cardiac surgery. *J Cardiothorac Surg*. 2014;9:121. doi:10.1186/1749-8090-9-121

38. Martins AM, Eng G, Caridade SG, Mano JF, Reis RL, Vunjak-Novakovic G. Electrically conductive chitosan/carbon scaffolds for cardiac tissue engineering. *Biomacromolecules*. 2014;15(2):635-643. doi:10.1021/bm401679q

39. McDevitt TC, Laflamme MA, Murry CE. Proliferation of cardiomyocytes derived from human embryonic stem cells is mediated via the IGF/PI 3-kinase/Akt signaling pathway. *J Mol Cell Cardiol*. 2005;39(6):865-873. doi:10.1016/j.yjmcc.2005.09.007

40. Zhu W-Z, Xie Y, Moyes KW, Gold JD, Askari B, Laflamme M a. Neuregulin/ErbB signaling regulates cardiac subtype specification in differentiating human embryonic stem cells. *Circ Res*. 2010;107(6):776-786. doi:10.1161/CIRCRESAHA.110.223917

41. Yang X, Rodriguez M, Pabon L, et al. Tri-iodo-l-thyronine promotes the maturation of human cardiomyocytes-derived from induced pluripotent stem cells. *J Mol Cell Cardiol*. 2014;72:296-304. doi:10.1016/j.yjmcc.2014.04.005

42. Parikh SS, Blackwell DJ, Gomez-Hurtado N, et al. Thyroid and Glucocorticoid Hormones Promote Functional T-Tubule Development in Human-Induced Pluripotent Stem Cell–Derived Cardiomyocytes. *Circ Res*. 2017;121(12):1323-1330. doi:10.1161/CIRCRESAHA.117.311920

43. Birket MJ, Ribeiro MC, Kosmidis G, et al. Contractile Defect Caused by Mutation in MYBPC3 Revealed under Conditions Optimized for Human PSC-Cardiomyocyte Function. *Cell Rep*. 2015;13(4):733-745. doi:10.1016/j.celrep.2015.09.025

44. Tandon N, Cannizzaro C, Chao P-HG, et al. Electrical stimulation systems for cardiac tissue engineering. *Nat Protoc*. 2009;4(2):155-173. doi:10.1038/nprot.2008.183

45. Radisic M, Park H, Shing H, et al. Functional assembly of engineered myocardium by electrical stimulation of cardiac myocytes cultured on scaffolds. *Proc Natl Acad Sci U S A*. 2004;101(52):18129-18134. doi:10.1073/pnas.0407817101

46. Chiu LLY, Iyer RK, King J-P, Radisic M. Biphasic electrical field stimulation aids in tissue engineering of multicell-type cardiac organoids. *Tissue Eng Part A*. 2011;17(11-12):1465-

1477. doi:10.1089/ten.tea.2007.0244

47. Tandon N, Marsano A, Maidhof R, Wan L, Park H, Vunjak-Novakovic G. Optimization of electrical stimulation parameters for cardiac tissue engineering. *J Tissue Eng Regen Med*. 2011;5(6):e115-25. doi:10.1002/term.377

48. Ronaldson-Bouchard K, Ma SP, Yeager K, et al. Advanced maturation of human cardiac tissue grown from pluripotent stem cells. *Nature*. 2018;556(7700):239-243. doi:10.1038/s41586-018-0016-3

49. Lindsey SE, Butcher JT, Yalcin HC. Mechanical regulation of cardiac development. *Front Physiol*. 2014;5:318. doi:10.3389/fphys.2014.00318

50. Shimko VF, Claycomb WC. Effect of mechanical loading on three-dimensional cultures of embryonic stem cell-derived cardiomyocytes. *Tissue Eng Part A*. 2008;14(1):49-58. doi:10.1089/ten.a.2007.0092

51. FINK C, ERGUN S, KRALISCH D, REMMERS U, WEIL J, ESCHENHAGEN T. Chronic stretch of engineered heart tissue induces hypertrophy and functional improvement. *FASEB J*. 2000;14(5):669-679. http://www.fasebj.org/content/14/5/669.long. Accessed May 20, 2015.

52. Ruan J-L, Tulloch NL, Saiget M, et al. Mechanical Stress Promotes Maturation of Human Myocardium from Pluripotent Stem Cell-Derived Progenitors. *Stem Cells*. April 2015. doi:10.1002/stem.2036

53. Miklas JW, Nunes SS, Sofla A, et al. Bioreactor for modulation of cardiac microtissue phenotype by combined static stretch and electrical stimulation. *Biofabrication*. 2014;6(2):024113. doi:10.1088/1758-5082/6/2/024113

54. Brown MA, Iyer RK, Radisic M. Pulsatile perfusion bioreactor for cardiac tissue

engineering. *Biotechnol Prog*. 24(4):907-920. doi:10.1002/btpr.11

55. Dvir T, Levy O, Shachar M, Granot Y, Cohen S. Activation of the ERK1/2 cascade via pulsatile interstitial fluid flow promotes cardiac tissue assembly. *Tissue Eng*. 2007;13(9):2185-2193. doi:10.1089/ten.2006.0364

56. Doevendans P. Cardiovascular phenotyping in mice. *Cardiovasc Res*. 1998;39(1):34-49. doi:10.1016/S0008-6363(98)00073-X

57. Nag AC. Study of non-muscle cells of the adult mammalian heart: a fine structural analysis and distribution. *Cytobios*. 1980;28(109):41-61. http://www.ncbi.nlm.nih.gov/pubmed/7428441. Accessed May 20, 2015.

58. Tiburcy M, Hudson JE, Balfanz P, et al. Defined Engineered Human Myocardium with Advanced Maturation for Applications in Heart Failure Modelling and Repair. *Circulation*. 2017. http://circ.ahajournals.org/content/early/2017/02/03/CIRCULATIONAHA.116.024145. Accessed July 17, 2017.

59. Kreutziger KL, Muskheli V, Johnson P, Braun K, Wight TN, Murry CE. Developing Vasculature and Stroma in Engineered Human Myocardium. *Tissue Eng Part A*. 2011;17(9-10):1219. doi:10.1089/TEN.TEA.2010.0557

60. Serrao GW, Turnbull IC, Ancukiewicz D, et al. Myocyte-Depleted Engineered Cardiac Tissues Support Therapeutic Potential of Mesenchymal Stem Cells. *Tissue Eng Part A*. 2012;18(13-14):1322. doi:10.1089/TEN.TEA.2011.0278

61. Sekine H, Shimizu T, Hobo K, et al. Endothelial Cell Coculture Within Tissue-Engineered Cardiomyocyte Sheets Enhances Neovascularization and Improves Cardiac Function of Ischemic Hearts. *Circulation*. 2008;118(14_suppl_1):S145-S152.

doi:10.1161/CIRCULATIONAHA.107.757286

62. Wendel JS, Ye L, Tao R, et al. Functional Effects of a Tissue-Engineered Cardiac Patch From Human Induced Pluripotent Stem Cell-Derived Cardiomyocytes in a Rat Infarct Model. *Stem Cells Transl Med*. 2015;4(11):1324-1332. doi:10.5966/sctm.2015-0044

63. Chen G, Qi Y, Niu L, et al. Application of the cell sheet technique in tissue engineering. *Biomed reports*. 2015;3(6):749-757. doi:10.3892/br.2015.522

64. Farzaneh M, Rahimi F, Alishahi M, Khoshnam SE. Paracrine Mechanisms Involved in Mesenchymal Stem Cell Differentiation into Cardiomyocytes. *Curr Stem Cell Res Ther*. 2019;14(1):9-13. doi:10.2174/1574888X13666180821160421

65. Caspi O, Lesman A, Basevitch Y, et al. Tissue Engineering of Vascularized Cardiac Muscle From Human Embryonic Stem Cells. *Circ Res*. 2007;100(2):263-272. doi:10.1161/01.RES.0000257776.05673.ff

66. Berthiaume A-A, Hartmann DA, Majesky MW, Bhat NR, Shih AY. Pericyte Structural Remodeling in Cerebrovascular Health and Homeostasis. *Front Aging Neurosci*. 2018;10:210. doi:10.3389/fnagi.2018.00210

67. Tracy LE, Minasian RA, Caterson EJ. Extracellular Matrix and Dermal Fibroblast Function in the Healing Wound. *Adv wound care*. 2016;5(3):119-136. doi:10.1089/wound.2014.0561

68. Nussinovitch U, Shinnawi R, Gepstein L. Modulation of cardiac tissue electrophysiological properties with light-sensitive proteins. *Cardiovasc Res*. 2014;102(1):176-187. doi:10.1093/cvr/cvu037

69. Parrag IC, Zandstra PW, Woodhouse KA. Fiber alignment and coculture with fibroblasts improves the differentiated phenotype of murine embryonic stem cell-derived

cardiomyocytes for cardiac tissue engineering. *Biotechnol Bioeng*. 2012;109(3):813-822. doi:10.1002/bit.23353

70. Radisic M, Park H, Martens TP, et al. Pre-treatment of synthetic elastomeric scaffolds by cardiac fibroblasts improves engineered heart tissue. *J Biomed Mater Res A*. 2008;86(3):713-724. doi:10.1002/jbm.a.31578

71. Ottaviano FG, Yee KO. Communication Signals Between Cardiac Fibroblasts and Cardiac Myocytes. *J Cardiovasc Pharmacol*. 2011;57(5):513-521. doi:10.1097/FJC.0b013e31821209ee

72. Falls D. Neuregulins: functions, forms, and signaling strategies. *Exp Cell Res*. 2003;284(1):14-30. doi:10.1016/S0014-4827(02)00102-7

73. Holmes WE, Sliwkowski MX, Akita RW, et al. Identification of heregulin, a specific activator of p185erbB2. *Science*. 1992;256(5060):1205-1210. http://www.ncbi.nlm.nih.gov/pubmed/1350381. Accessed December 14, 2014.

74. Peles E, Bacus SS, Koski RA, et al. Isolation of the NeuHER-2 stimulatory ligand: A 44 kd glycoprotein that induces differentiation of mammary tumor cells. *Cell*. 1992;69(1):205-216. doi:10.1016/0092-8674(92)90131-U

75. Wen D, Peles E, Cupples R, et al. Neu differentiation factor: a transmembrane glycoprotein containing an EGF domain and an immunoglobulin homology unit. *Cell*. 1992;69(3):559-572. http://www.ncbi.nlm.nih.gov/pubmed/1349853. Accessed December 14, 2014.

76. Goodearl AD, Davis JB, Mistry K, et al. Purification of multiple forms of glial growth factor. *J Biol Chem*. 1993;268(24):18095-18102. http://www.ncbi.nlm.nih.gov/pubmed/8394360. Accessed December 14, 2014.

77. Marchionni MA, Goodearl AD, Chen MS, et al. Glial growth factors are alternatively spliced erbB2 ligands expressed in the nervous system. *Nature*. 1993;362(6418):312-318. doi:10.1038/362312a0

78. Gassmann M, Casagranda F, Orioli D, et al. Aberrant neural and cardiac development in mice lacking the ErbB4 neuregulin receptor. *Nature*. 1995;378(6555):390-394. doi:10.1038/378390a0

79. Lee KF, Simon H, Chen H, Bates B, Hung MC, Hauser C. Requirement for neuregulin receptor erbB2 in neural and cardiac development. *Nature*. 1995;378(6555):394-398. doi:10.1038/378394a0

80. Meyer D, Birchmeier C. Multiple essential functions of neuregulin in development. *Nature*. 1995;378(6555):386-390. doi:10.1038/378386a0

81. Mei L, Nave K-A. Neuregulin-ERBB signaling in the nervous system and neuropsychiatric diseases. *Neuron*. 2014;83(1):27-49. doi:10.1016/j.neuron.2014.06.007

82. Vasti C, Hertig CM. Neuregulin-1/erbB activities with focus on the susceptibility of the heart to anthracyclines. *World J Cardiol*. 2014;6(7):653-662. doi:10.4330/wjc.v6.i7.653

83. Wadugu B, Kühn B. The role of neuregulin/ErbB2/ErbB4 signaling in the heart with special focus on effects on cardiomyocyte proliferation. *Am J Physiol Heart Circ Physiol*. 2012;302(11):H2139-47. doi:10.1152/ajpheart.00063.2012

84. Kumar R, Yarmand-Bagheri R. The role of HER2 in angiogenesis. *Semin Oncol*. 2001;28(5 Suppl 16):27-32. http://www.ncbi.nlm.nih.gov/pubmed/11706393. Accessed December 9, 2014.

85. Jiang Z, Zhou M. Neuregulin signaling and heart failure. *Curr Heart Fail Rep*. 2010;7(1):42-47. doi:10.1007/s11897-010-0003-y

86. Buonanno A, Fischbach GD. Neuregulin and ErbB receptor signaling pathways in the nervous system. *Curr Opin Neurobiol*. 2001;11(3):287-296. http://www.ncbi.nlm.nih.gov/pubmed/11399426. Accessed November 4, 2014.

87. Yokozeki T, Wakatsuki S, Hatsuzawa K, Black RA, Wada I, Sehara-Fujisawa A. Meltrin beta (ADAM19) mediates ectodomain shedding of Neuregulin beta1 in the Golgi apparatus: fluorescence correlation spectroscopic observation of the dynamics of ectodomain shedding in living cells. *Genes Cells*. 2007;12(3):329-343. doi:10.1111/j.1365-2443.2007.01060.x

88. Hu X, Hicks CW, He W, et al. Bace1 modulates myelination in the central and peripheral nervous system. *Nat Neurosci*. 2006;9(12):1520-1525. doi:10.1038/nn1797

89. Montero JC, Yuste L, Díaz-Rodríguez E, Esparís-Ogando A, Pandiella A. Differential shedding of transmembrane neuregulin isoforms by the tumor necrosis factor-alpha-converting enzyme. *Mol Cell Neurosci*. 2000;16(5):631-648. doi:10.1006/mcne.2000.0896

90. Odiete O, Hill MF, Sawyer DB. Neuregulin in cardiovascular development and disease. *Circ Res*. 2012;111(10):1376-1385. doi:10.1161/CIRCRESAHA.112.267286

91. Taylor AR, Taylor SB, Koenig JI. The involvement of Type II Neuregulin-1 in rat visuospatial learning and memory. *Neurosci Lett*. 2012;531(2):131-135. doi:10.1016/j.neulet.2012.10.018

92. Corfas G, Roy K, Buxbaum JD. Neuregulin 1-erbB signaling and the molecular/cellular basis of schizophrenia. *Nat Neurosci*. 2004;7(6):575-580. doi:10.1038/nn1258

93. Yarden Y, Sliwkowski MX. Untangling the ErbB signalling network. *Nat Rev Mol Cell Biol*. 2001;2(2):127-137. doi:10.1038/35052073

94. Jones JT, Akita RW, Sliwkowski MX. Binding specificities and affinities of egf domains for

ErbB receptors. *FEBS Lett*. 1999;447(2-3):227-231. http://www.ncbi.nlm.nih.gov/pubmed/10214951. Accessed November 4, 2014.

95. Huertas-Vazquez A, Teodorescu C, Reinier K, et al. A common missense variant in the neuregulin 1 gene is associated with both schizophrenia and sudden cardiac death. *Heart Rhythm*. 2013;10(7):994-998. doi:10.1016/j.hrthm.2013.03.020

96. McBride KL, Zender GA, Fitzgerald-Butt SM, et al. Association of common variants in ERBB4 with congenital left ventricular outflow tract obstruction defects. *Birth Defects Res A Clin Mol Teratol*. 2011;91(3):162-168. doi:10.1002/bdra.20764

97. Sudol M. Neuregulin 1-activated ERBB4 as a “dedicated” receptor for the Hippo-YAP pathway. *Sci Signal*. 2014;7(355):pe29. doi:10.1126/scisignal.aaa2710

98. Reischauer S, Arnaout R, Ramadass R, Stainier DYR. Actin Binding GFP Allows 4D In Vivo Imaging of Myofilament Dynamics in the Zebrafish Heart and the Identification of Erbb2 Signaling as a Remodeling Factor of Myofibril Architecture. *Circ Res*. 2014;115(10):845-856. doi:10.1161/CIRCRESAHA.115.304356

99. Hertig CM, Kubalak SW, Wang Y, Chien KR. Synergistic Roles of Neuregulin-1 and Insulin-like Growth Factor-I in Activation of the Phosphatidylinositol 3-Kinase Pathway and Cardiac Chamber Morphogenesis. *J Biol Chem*. 1999;274(52):37362-37369. http://www.jbc.org/content/274/52/37362.long. Accessed April 21, 2014.

100. Baliga RR, Pimental DR, Zhao Y-Y, et al. NRG-1-induced cardiomyocyte hypertrophy. Role of PI-3-kinase, p70S6K, and MEK-MAPK-RSK. *Am J Physiol Hear Circ Physiol*. 1999;277(5):H2026-2037. http://ajpheart.physiology.org/content/277/5/H2026?ijkey=ac29aa766d882cb6409596cd41a202d9ab131262&keytype2=tf_ipsecsha. Accessed November 24, 2014.

101. Rentschler S, Zander J, Meyers K, et al. Neuregulin-1 promotes formation of the murine cardiac conduction system. *Proc Natl Acad Sci U S A*. 2002;99(16):10464-10469. doi:10.1073/pnas.162301699

102. Wang Z, Xu G, Wu Y, et al. Neuregulin-1 enhances differentiation of cardiomyocytes from embryonic stem cells. *Med Biol Eng Comput*. 2009;47(1):41-48. doi:10.1007/s11517-008-0383-2

103. Chen M, Bi L-L, Wang Z-Q, Zhao F, Gan X-D, Wang Y-G. Time-dependent regulation of neuregulin-1β/ErbB/ERK pathways in cardiac differentiation of mouse embryonic stem cells. *Mol Cell Biochem*. 2013;380(1-2):67-72. doi:10.1007/s11010-013-1658-y

104. Patel R, Kos L. Endothelin-1 and Neuregulin-1 convert embryonic cardiomyocytes into cells of the conduction system in the mouse. *Dev Dyn*. 2005;233(1):20-28. doi:10.1002/dvdy.20284

105. Sun M, Yan X, Bian Y, Caggiano AO, Morgan JP. Improving murine embryonic stem cell differentiation into cardiomyocytes with neuregulin-1: differential expression of microRNA. *Am J Physiol Cell Physiol*. 2011;301(1):C21-30. doi:10.1152/ajpcell.00141.2010

106. Hao J, Galindo CL, Tran T-L, Sawyer DB. Neuregulin-1β induces embryonic stem cell cardiomyogenesis via ErbB3/ErbB2 receptors. *Biochem J*. 2014;458(2):335-341. doi:10.1042/BJ20130818

107. Zhao YY, Sawyer DR, Baliga RR, et al. Neuregulins promote survival and growth of cardiac myocytes. Persistence of ErbB2 and ErbB4 expression in neonatal and adult ventricular myocytes. *J Biol Chem*. 1998;273(17):10261-10269. http://www.ncbi.nlm.nih.gov/pubmed/9553078. Accessed November 5, 2014.

108. Montaigne D, Hurt C, Neviere R. Mitochondria death/survival signaling pathways in

cardiotoxicity induced by anthracyclines and anticancer-targeted therapies. *Biochem Res Int*. 2012;2012:951539. doi:10.1155/2012/951539

109. Minotti G, Menna P, Salvatorelli E, Cairo G, Gianni L. Anthracyclines: molecular advances and pharmacologic developments in antitumor activity and cardiotoxicity. *Pharmacol Rev*. 2004;56(2):185-229. doi:10.1124/pr.56.2.6

110. Vejpongsa P, Yeh ETH. Prevention of Anthracycline-Induced Cardiotoxicity. *J Am Coll Cardiol*. 2014;64(9):938-945. doi:10.1016/j.jacc.2014.06.1167

111. Horie T, Ono K, Nishi H, et al. Acute doxorubicin cardiotoxicity is associated with miR-146a-induced inhibition of the neuregulin-ErbB pathway. *Cardiovasc Res*. 2010;87(4):656-664. doi:10.1093/cvr/cvq148

112. Sawyer DB. Modulation of Anthracycline-Induced Myofibrillar Disarray in Rat Ventricular Myocytes by Neuregulin-1beta and Anti-erbB2: Potential Mechanism for Trastuzumab-Induced Cardiotoxicity. *Circulation*. 2002;105(13):1551-1554. doi:10.1161/01.CIR.0000013839.41224.1C

113. Giraud M-N, Flück M, Zuppinger C, Suter TM. Expressional reprogramming of survival pathways in rat cardiocytes by neuregulin-1beta. *J Appl Physiol*. 2005;99(1):313-322. doi:10.1152/japplphysiol.00609.2004

114. Guo Yong-fang WX. NRG-1 attenuates mitochondrial dysfunction in a rat model of heart failure. http://www.cmj.org/ch/reader/view_abstract.aspx?volume=125&issue=5&start_page=807. Accessed November 4, 2014.

115. Crone SA, Zhao Y-Y, Fan L, et al. ErbB2 is essential in the prevention of dilated cardiomyopathy. *Nat Med*. 2002;8(5):459-465. doi:10.1038/nm0502-459

116. Pentassuglia L, Sawyer DB. ErbB/integrin signaling interactions in regulation of myocardial cell-cell and cell-matrix interactions. *Biochim Biophys Acta*. 2013;1833(4):909-916. doi:10.1016/j.bbamcr.2012.12.007

117. Kuramochi Y, Guo X, Sawyer DB. Neuregulin activates erbB2-dependent src/FAK signaling and cytoskeletal remodeling in isolated adult rat cardiac myocytes. *J Mol Cell Cardiol*. 2006;41(2):228-235. doi:10.1016/j.yjmcc.2006.04.007

118. Cote GM, Miller TA, Lebrasseur NK, Kuramochi Y, Sawyer DB. Neuregulin-1alpha and beta isoform expression in cardiac microvascular endothelial cells and function in cardiac myocytes in vitro. *Exp Cell Res*. 2005;311(1):135-146. doi:10.1016/j.yexcr.2005.08.017

119. Cantó C, Pich S, Paz JC, et al. Neuregulins increase mitochondrial oxidative capacity and insulin sensitivity in skeletal muscle cells. *Diabetes*. 2007;56(9):2185-2193. doi:10.2337/db06-1726

120. Goldshmit Y, Erlich S, Pinkas-Kramarski R. Neuregulin rescues PC12-ErbB4 cells from cell death induced by H(2)O(2). Regulation of reactive oxygen species levels by phosphatidylinositol 3-kinase. *J Biol Chem*. 2001;276(49):46379-46385. doi:10.1074/jbc.M105637200

121. Patel N, Barrientos A, Landgraf R. The growth factor receptor ERBB2 regulates mitochondrial activity on a signaling time scale. *J Biol Chem*. 2013;288(49):35253-35265. doi:10.1074/jbc.M113.478271

122. Waring CD, Vicinanza C, Papalamprou A, et al. The adult heart responds to increased workload with physiologic hypertrophy, cardiac stem cell activation, and new myocyte formation. *Eur Heart J*. 2012;35(39):2722-2731. doi:10.1093/eurheartj/ehs338

123. Naqvi N, Li M, Calvert JW, et al. A proliferative burst during preadolescence establishes

the final cardiomyocyte number. *Cell*. 2014;157(4):795-807. doi:10.1016/j.cell.2014.03.035

124. Lemmens K, Doggen K, De Keulenaer GW. Activation of the neuregulin/ErbB system during physiological ventricular remodeling in pregnancy. *Am J Physiol Heart Circ Physiol*. 2011;300(3):H931-42. doi:10.1152/ajpheart.00385.2010

125. Okoshi K, Nakayama M, Yan X, et al. Neuregulins regulate cardiac parasympathetic activity: muscarinic modulation of beta-adrenergic activity in myocytes from mice with neuregulin-1 gene deletion. *Circulation*. 2004;110(6):713-717. doi:10.1161/01.CIR.0000138109.32748.80

126. Lemmens K, Fransen P, Sys SU, Brutsaert DL, De Keulenaer GW. Neuregulin-1 induces a negative inotropic effect in cardiac muscle: role of nitric oxide synthase. *Circulation*. 2004;109(3):324-326. doi:10.1161/01.CIR.0000114521.88547.5E

127. Kuramochi Y, Lim CC, Guo X, Colucci WS, Liao R, Sawyer DB. Myocyte contractile activity modulates norepinephrine cytotoxicity and survival effects of neuregulin-1beta. *Am J Physiol Cell Physiol*. 2004;286(2):C222-9. doi:10.1152/ajpcell.00312.2003

128. Noireaud J, Andriantsitohaina R. Recent insights in the paracrine modulation of cardiomyocyte contractility by cardiac endothelial cells. *Biomed Res Int*. 2014;2014:923805. doi:10.1155/2014/923805

129. Hedhli N, Russell KS. Cytostatic drugs, neuregulin activation of erbB receptors, and angiogenesis. *Curr Hypertens Rep*. 2010;12(6):411-417. doi:10.1007/s11906-010-0148-9

130. Kuramochi Y, Cote GM, Guo X, et al. Cardiac endothelial cells regulate reactive oxygen species-induced cardiomyocyte apoptosis through neuregulin-1beta/erbB4 signaling. *J Biol Chem*. 2004;279(49):51141-51147. doi:10.1074/jbc.M408662200

131. Lemmens K, Segers VFM, Demolder M, De Keulenaer GW. Role of neuregulin-1/ErbB2 signaling in endothelium-cardiomyocyte cross-talk. *J Biol Chem*. 2006;281(28):19469-19477. doi:10.1074/jbc.M600399200

132. Kalinowski A, Plowes NJR, Huang Q, Berdejo-Izquierdo C, Russell RR, Russell KS. Metalloproteinase-dependent cleavage of neuregulin and autocrine stimulation of vascular endothelial cells. *FASEB J*. 2010;24(7):2567-2575. doi:10.1096/fj.08-129072

133. Iivanainen E, Paatero I, Heikkinen S-M, et al. Intra- and extracellular signaling by endothelial neuregulin-1. *Exp Cell Res*. 2007;313(13):2896-2909. doi:10.1016/j.yexcr.2007.03.042

134. Szmit S, Jank M, Maciejewski H, et al. Relationship between clinical data and gene expression in the HER2/ErbB2-dependent signaling pathway in patients with acute heart failure. *J Appl Genet*. 2013;54(4):447-453. doi:10.1007/s13353-013-0164-y

135. Fang S-J, Wu X-S, Han Z-H, et al. Neuregulin-1 preconditioning protects the heart against ischemia/reperfusion injury through a PI3K/Akt-dependent mechanism. *Chin Med J (Engl)*. 2010;123(24):3597-3604. http://www.ncbi.nlm.nih.gov/pubmed/22166638. Accessed December 3, 2014.

136. Hedhli N, Huang Q, Kalinowski A, et al. Endothelium-derived neuregulin protects the heart against ischemic injury. *Circulation*. 2011;123(20):2254-2262. doi:10.1161/CIRCULATIONAHA.110.991125

137. Xiao J, Li B, Zheng Z, et al. Therapeutic effects of neuregulin-1 gene transduction in rats with myocardial infarction. *Coron Artery Dis*. 2012;23(7):460-468. doi:10.1097/MCA.0b013e32835877da

138. Formiga FR, Pelacho B, Garbayo E, et al. Controlled delivery of fibroblast growth factor-1

and neuregulin-1 from biodegradable microparticles promotes cardiac repair in a rat myocardial infarction model through activation of endogenous regeneration. *J Control Release*. 2014;173:132-139. doi:10.1016/j.jconrel.2013.10.034

139. Bersell K, Arab S, Haring B, Kühn B. Neuregulin1/ErbB4 signaling induces cardiomyocyte proliferation and repair of heart injury. *Cell*. 2009;138(2):257-270. doi:10.1016/j.cell.2009.04.060

140. Gu X, Liu X, Xu D, et al. Cardiac functional improvement in rats with myocardial infarction by up-regulating cardiac myosin light chain kinase with neuregulin. *Cardiovasc Res*. 2010;88(2):334-343. doi:10.1093/cvr/cvq223

141. Galindo CL, Kasasbeh E, Murphy A, et al. Anti-remodeling and anti-fibrotic effects of the neuregulin-1β glial growth factor 2 in a large animal model of heart failure. *J Am Heart Assoc*. 2014;3(5):e000773. doi:10.1161/JAHA.113.000773

142. Hill MF, Patel A V, Murphy A, et al. Intravenous glial growth factor 2 (GGF2) isoform of neuregulin-1β improves left ventricular function, gene and protein expression in rats after myocardial infarction. *PLoS One*. 2013;8(2):e55741. doi:10.1371/journal.pone.0055741

143. Liu X, Gu X, Li Z, et al. Neuregulin-1/erbB-activation improves cardiac function and survival in models of ischemic, dilated, and viral cardiomyopathy. *J Am Coll Cardiol*. 2006;48(7):1438-1447. doi:10.1016/j.jacc.2006.05.057

144. Ky B, Kimmel SE, Safa RN, et al. Neuregulin-1 beta is associated with disease severity and adverse outcomes in chronic heart failure. *Circulation*. 2009;120(4):310-317. doi:10.1161/CIRCULATIONAHA.109.856310

145. Rohrbach S, Niemann B, Silber R-E, Holtz J. Neuregulin receptors erbB2 and erbB4 in failing human myocardium -- depressed expression and attenuated activation. *Basic Res*

Cardiol. 2005;100(3):240-249. doi:10.1007/s00395-005-0514-4

146. Uray IP, Connelly JH, Thomázy V, et al. Left ventricular unloading alters receptor tyrosine kinase expression in the failing human heart. *J Hear Lung Transplant*. 2002;21(7):771-782. doi:10.1016/S1053-2498(02)00390-X

147. Rohrbach S, Yan X, Weinberg EO, et al. Neuregulin in Cardiac Hypertrophy in Rats With Aortic Stenosis : Differential Expression of erbB2 and erbB4 Receptors. *Circulation*. 1999;100(4):407-412. doi:10.1161/01.CIR.100.4.407

148. Li B, Zheng Z, Wei Y, et al. Therapeutic effects of neuregulin-1 in diabetic cardiomyopathy rats. *Cardiovasc Diabetol*. 2011;10:69. doi:10.1186/1475-2840-10-69

149. Gao R. Study of Efficacy on Cardiac Remodeling of Recombinant Human Neuregulin-1 in Stable Chronic Systolic Heart Failure Patients. 2012.

150. Gao R. Study of Efficacy on NT-proBNP of Recombinant Human Neuregulin-1 in Chronic Heart Failure Patients.

151. Gao R. Clinical Trial to Evaluate the Efficacy and Safety of Recombinant Human Neuregulin-1 for Subcutaneous Administration in Patients With Chronic Systolic Heart Failure.

152. Mendes-Ferreira P, De Keulenaer GW, Leite-Moreira AF, Brás-Silva C. Therapeutic potential of neuregulin-1 in cardiovascular disease. *Drug Discov Today*. 2013;18(17-18):836-842. doi:10.1016/j.drudis.2013.01.010

153. Gao R, Zhang J, Cheng L, et al. A Phase II, randomized, double-blind, multicenter, based on standard therapy, placebo-controlled study of the efficacy and safety of recombinant human neuregulin-1 in patients with chronic heart failure. *J Am Coll Cardiol*. 2010;55(18):1907-1914. doi:10.1016/j.jacc.2009.12.044

154. Jabbour A, Hayward CS, Keogh AM, et al. Parenteral administration of recombinant human neuregulin-1 to patients with stable chronic heart failure produces favourable acute and chronic haemodynamic responses. *Eur J Heart Fail*. 2011;13(1):83-92. doi:10.1093/eurjhf/hfq152

155. Laflamme MA, Murry CE. Heart regeneration. *Nature*. 2011;473(7347):326-335. doi:10.1038/nature10147

156. Home - ClinicalTrials.gov. https://clinicaltrials.gov/. Accessed February 26, 2015.

157. WHO | The top 10 causes of death. http://www.who.int/mediacentre/factsheets/fs310/en/. Accessed January 19, 2015.

158. Pasumarthi KBS. Cardiomyocyte Cell Cycle Regulation. *Circ Res*. 2002;90(10):1044-1054. doi:10.1161/01.RES.0000020201.44772.67

159. Lian X, Zhang J, Azarin SM, et al. Directed cardiomyocyte differentiation from human pluripotent stem cells by modulating Wnt/β-catenin signaling under fully defined conditions. *Nat Protoc*. 2013;8(1):162-175. doi:10.1038/nprot.2012.150

160. Chong JJH, Yang X, Don CW, et al. Human embryonic-stem-cell-derived cardiomyocytes regenerate non-human primate hearts. *Nature*. 2014;510(7504):273-277. doi:10.1038/nature13233

161. Riegler J, Tiburcy M, Ebert A, et al. Human Engineered Heart Muscles Engraft and Survive Long Term in a Rodent Myocardial Infarction Model. *Circ Res*. 2015;117(8):720-730. doi:10.1161/CIRCRESAHA.115.306985

162. Bass GT, Ryall KA, Katikapalli A, et al. Automated image analysis identifies signaling pathways regulating distinct signatures of cardiac myocyte hypertrophy. *J Mol Cell Cardiol*. 2012;52(5):923-930. doi:10.1016/j.yjmcc.2011.11.009

163. Rodriguez ML, Graham BT, Pabon LM, Han SJ, Murry CE, Sniadecki NJ. Measuring the contractile forces of human induced pluripotent stem cell-derived cardiomyocytes with arrays of microposts. *J Biomech Eng*. 2014;136(5):051005. doi:10.1115/1.4027145

164. Lundy SD, Zhu W-Z, Regnier M, Laflamme MA. Structural and functional maturation of cardiomyocytes derived from human pluripotent stem cells. *Stem Cells Dev*. 2013;22(14):1991-2002. doi:10.1089/scd.2012.0490

165. Hazeltine LB, Simmons CS, Salick MR, et al. Effects of substrate mechanics on contractility of cardiomyocytes generated from human pluripotent stem cells. *Int J Cell Biol*. 2012;2012:508294. doi:10.1155/2012/508294

166. Bryan AK, Hecht VC, Shen W, Payer K, Grover WH, Manalis SR. Measuring single cell mass, volume, and density with dual suspended microchannel resonators. *Lab Chip*. 2014;14(3):569-576. doi:10.1039/c3lc51022k

167. Phillips KG, Velasco CR, Li J, et al. Optical quantification of cellular mass, volume, and density of circulating tumor cells identified in an ovarian cancer patient. *Front Oncol*. 2012;2:72. doi:10.3389/fonc.2012.00072

168. Coelho-Filho OR, Shah R V, Mitchell R, et al. Quantification of cardiomyocyte hypertrophy by cardiac magnetic resonance: implications for early cardiac remodeling. *Circulation*. 2013;128(11):1225-1233. doi:10.1161/CIRCULATIONAHA.112.000438

169. Carpenter AE, Jones TR, Lamprecht MR, et al. CellProfiler: image analysis software for identifying and quantifying cell phenotypes. *Genome Biol*. 2006;7(10):R100. doi:10.1186/gb-2006-7-10-r100

170. Zhang W, Anger T, Su J, et al. Selective loss of fine tuning of Gq/11 signaling by RGS2 protein exacerbates cardiomyocyte hypertrophy. *J Biol Chem*. 2006;281(9):5811-5820.

doi:10.1074/jbc.M507871200

171. Schneider CA, Rasband WS, Eliceiri KW. NIH Image to ImageJ: 25 years of image analysis. *Nat Methods*. 2012;9(7):671-675. doi:10.1038/nmeth.2089

172. Xia Y, Rajapurohitam V, Cook MA, Karmazyn M. Inhibition of phenylephrine induced hypertrophy in rat neonatal cardiomyocytes by the mitochondrial KATP channel opener diazoxide. *J Mol Cell Cardiol*. 2004;37(5):1063-1067. doi:10.1016/j.yjmcc.2004.07.002

173. Dambrot C, Braam SR, Tertoolen LGJ, Birket M, Atsma DE, Mummery CL. Serum supplemented culture medium masks hypertrophic phenotypes in human pluripotent stem cell derived cardiomyocytes. *J Cell Mol Med*. 2014;18(8):1509-1518. doi:10.1111/jcmm.12356

174. Földes G, Mioulane M, Wright JS, et al. Modulation of human embryonic stem cell-derived cardiomyocyte growth: a testbed for studying human cardiac hypertrophy? *J Mol Cell Cardiol*. 2011;50(2):367-376. doi:10.1016/j.yjmcc.2010.10.029

175. Engelmann GL, Vitullo JC, Gerrity RG. Morphometric analysis of cardiac hypertrophy during development, maturation, and senescence in spontaneously hypertensive rats. *Circ Res*. 1987;60(4):487-494. http://www.ncbi.nlm.nih.gov/pubmed/2954715. Accessed February 15, 2016.

176. Bergmann O, Zdunek S, Alkass K, Druid H, Bernard S, Frisén J. Identification of cardiomyocyte nuclei and assessment of ploidy for the analysis of cell turnover. *Exp Cell Res*. 2011;317(2):188-194. doi:10.1016/j.yexcr.2010.08.017

177. Tanaka A, Yuasa S, Mearini G, et al. Endothelin-1 induces myofibrillar disarray and contractile vector variability in hypertrophic cardiomyopathy-induced pluripotent stem cell-derived cardiomyocytes. *J Am Heart Assoc*. 2014;3(6):e001263.

doi:10.1161/JAHA.114.001263

178. Földes G, Matsa E, Kriston-Vizi J, et al. Aberrant α-adrenergic hypertrophic response in cardiomyocytes from human induced pluripotent cells. *Stem cell reports*. 2014;3(5):905-914. doi:10.1016/j.stemcr.2014.09.002

179. Kreipke R, Wang Y, Miklas JW, Mathieu J, Ruohola-Baker H. Metabolic Remodeling in early development and cardiomyocyte maturation. *Semin Cell Dev Biol*. February 2016. doi:10.1016/j.semcdb.2016.02.004

180. Thornburg K, Jonker S, O'Tierney P, et al. Regulation of the cardiomyocyte population in the developing heart. *Prog Biophys Mol Biol*. 2011;106(1):289-299. doi:10.1016/j.pbiomolbio.2010.11.010

181. Mollova M, Bersell K, Walsh S, et al. Cardiomyocyte proliferation contributes to heart growth in young humans. *Proc Natl Acad Sci U S A*. 2013;110(4):1446-1451. doi:10.1073/pnas.1214608110

182. Taylor JM, Rovin JD, Parsons JT. A role for focal adhesion kinase in phenylephrine-induced hypertrophy of rat ventricular cardiomyocytes. *J Biol Chem*. 2000;275(25):19250-19257. doi:10.1074/jbc.M909099199

183. Raeker MÖ, Shavit JA, Dowling JJ, Michele DE, Russell MW. Membrane-myofibril cross-talk in myofibrillogenesis and in muscular dystrophy pathogenesis: lessons from the zebrafish. *Front Physiol*. 2014;5:14. doi:10.3389/fphys.2014.00014

184. Siddiqui RA, Shaikh SR, Kovacs R, Stillwell W, Zaloga G. Inhibition of phenylephrine-induced cardiac hypertrophy by docosahexaenoic acid. *J Cell Biochem*. 2004;92(6):1141-1159. doi:10.1002/jcb.20135

185. Kaushik G, Spenlehauer A, Sessions AO, et al. Vinculin network-mediated cytoskeletal

remodeling regulates contractile function in the aging heart. *Sci Transl Med*. 2015;7(292):292ra99. doi:10.1126/scitranslmed.aaa5843

186. Laustsen PG, Russell SJ, Cui L, et al. Essential role of insulin and insulin-like growth factor 1 receptor signaling in cardiac development and function. *Mol Cell Biol*. 2007;27(5):1649-1664. doi:10.1128/MCB.01110-06

187. McMullen JR, Shioi T, Huang W-Y, et al. The insulin-like growth factor 1 receptor induces physiological heart growth via the phosphoinositide 3-kinase(p110alpha) pathway. *J Biol Chem*. 2004;279(6):4782-4793. doi:10.1074/jbc.M310405200

188. Palpant NJ, Hofsteen P, Pabon L, Reinecke H, Murry CE. Cardiac Development in Zebrafish and Human Embryonic Stem Cells Is Inhibited by Exposure to Tobacco Cigarettes and E-Cigarettes. Dettman RW, ed. *PLoS One*. 2015;10(5):e0126259. doi:10.1371/journal.pone.0126259

189. Zhu W-Z, Van Biber B, Laflamme MA. *Human Pluripotent Stem Cells*. Vol 767. (Schwartz PH, Wesselschmidt RL, eds.). Totowa, NJ: Humana Press; 2011. doi:10.1007/978-1-61779-201-4

190. Xu C, Police S, Hassanipour M, et al. Efficient generation and cryopreservation of cardiomyocytes derived from human embryonic stem cells. *Regen Med*. 2011;6(1):53-66. doi:10.2217/rme.10.91

191. Clement S, Stouffs M, Bettiol E, et al. Expression and function of -smooth muscle actin during embryonic-stem-cell-derived cardiomyocyte differentiation. *J Cell Sci*. 2007;120(2):229-238. doi:10.1242/jcs.03340

192. Munarin F, Kaiser NJ, Kim TY, Choi B-R, Coulombe KLK. Laser-Etched Designs for Molding Hydrogel-Based Engineered Tissues. *Tissue Eng Part C Methods*.

2017;23(5):311-321. doi:10.1089/ten.TEC.2017.0068

193. Fukazawa R. Neuregulin-1 protects ventricular myocytes from anthracycline-induced apoptosis via erbB4-dependent activation of PI3-kinase/Akt. *J Mol Cell Cardiol*. 2003;35(12):1473-1479. doi:10.1016/j.yjmcc.2003.09.012

194. Regnier M, Rivera AJ, Wang C-K, Bates MA, Chase PB, Gordon AM. Thin filament near-neighbour regulatory unit interactions affect rabbit skeletal muscle steady-state force-Ca(2+) relations. *J Physiol*. 2002;540(Pt 2):485-497. http://www.pubmedcentral.nih.gov/articlerender.fcgi?artid=2290239&tool=pmcentrez&rendertype=abstract. Accessed April 24, 2015.

195. Livak KJ, Schmittgen TD. Analysis of relative gene expression data using real-time quantitative PCR and the 2(-Delta Delta C(T)) Method. *Methods*. 2001;25(4):402-408. doi:10.1006/meth.2001.1262

196. Shiels HA, White E. The Frank-Starling mechanism in vertebrate cardiac myocytes. *J Exp Biol*. 2008;211(Pt 13):2005-2013. doi:10.1242/jeb.003145

197. Makarenko I. Passive Stiffness Changes Caused by Upregulation of Compliant Titin Isoforms in Human Dilated Cardiomyopathy Hearts. *Circ Res*. 2004;95(7):708-716. doi:10.1161/01.RES.0000143901.37063.2f

198. Ruan J-L, Tulloch NL, Razumova M V., et al. Mechanical Stress Conditioning and Electrical Stimulation Promote Contractility and Force Maturation of Induced Pluripotent Stem Cell-Derived Human Cardiac TissueClinical Perspective. *Circulation*. 2016;134(20):1557-1567. doi:10.1161/CIRCULATIONAHA.114.014998

199. Hasenfuss G, Reinecke H, Studer R, et al. Relation between myocardial function and expression of sarcoplasmic reticulum Ca(2+)-ATPase in failing and nonfailing human

myocardium. *Circ Res*. 1994;75(3):434-442. http://www.ncbi.nlm.nih.gov/pubmed/8062417. Accessed April 19, 2015.

200. Dolnikov K, Shilkrut M, Zeevi-Levin N, et al. Functional properties of human embryonic stem cell-derived cardiomyocytes: intracellular Ca2+ handling and the role of sarcoplasmic reticulum in the contraction. *Stem Cells*. 2006;24(2):236-245. doi:10.1634/stemcells.2005-0036

201. Bielawski KS, Leonard A, Bhandari S, Murry CE, Sniadecki NJ. Real-Time Force and Frequency Analysis of Engineered Human Heart Tissue Derived from Induced Pluripotent Stem Cells Using Magnetic Sensing. *Tissue Eng Part C Methods*. September 2016. doi:10.1089/ten.TEC.2016.0257

202. Godier-Furnémont AFG, Tiburcy M, Wagner E, et al. Physiologic force-frequency response in engineered heart muscle by electromechanical stimulation. *Biomaterials*. 2015;60:82-91. doi:10.1016/j.biomaterials.2015.03.055

203. Brito-Martins M, Harding SE, Ali NN. β 1 - and β 2 -adrenoceptor responses in cardiomyocytes derived from human embryonic stem cells: comparison with failing and non-failing adult human heart. *Br J Pharmacol*. 2008;153(4):751-759. doi:10.1038/sj.bjp.0707619

204. Sergeeva IA, Christoffels VM. Regulation of expression of atrial and brain natriuretic peptide, biomarkers for heart development and disease. *Biochim Biophys Acta*. 2013;1832(12):2403-2413. doi:10.1016/j.bbadis.2013.07.003

205. Koss KL, Kranias EG. Phospholamban: A Prominent Regulator of Myocardial Contractility. *Circ Res*. 1996;79(6):1059-1063. doi:10.1161/01.RES.79.6.1059

206. Stieber J, Herrmann S, Feil S, et al. The hyperpolarization-activated channel HCN4 is

required for the generation of pacemaker action potentials in the embryonic heart. *Proc Natl Acad Sci U S A*. 2003;100(25):15235-15240. doi:10.1073/pnas.2434235100

207. Guo Y, Zhang X, Liu Y, Duan H, Jie B, Wu X. Neuregulin-1 attenuates mitochondrial dysfunction in a rat model of heart failure. *Chin Med J (Engl)*. 2012;125(5):807-814. http://www.ncbi.nlm.nih.gov/pubmed/22490579. Accessed November 25, 2014.

208. Vander Heiden MG, Cantley LC, Thompson CB. Understanding the Warburg effect: the metabolic requirements of cell proliferation. *Science*. 2009;324(5930):1029-1033. doi:10.1126/science.1160809

209. Ito H, Hiroe M, Hirata Y, et al. Insulin-like growth factor-I induces hypertrophy with enhanced expression of muscle specific genes in cultured rat cardiomyocytes. *Circulation*. 1993;87(5):1715-1721. http://www.ncbi.nlm.nih.gov/pubmed/7683979. Accessed December 22, 2016.

210. Baliga RR, Pimental DR, Zhao YY, et al. NRG-1-induced cardiomyocyte hypertrophy. Role of PI-3-kinase, p70(S6K), and MEK-MAPK-RSK. *Am J Physiol*. 1999;277(5 Pt 2):H2026-37. http://www.ncbi.nlm.nih.gov/pubmed/10564160. Accessed December 22, 2016.

211. Zhang D, Shadrin IY, Lam J, Xian H-Q, Snodgrass HR, Bursac N. Tissue-engineered cardiac patch for advanced functional maturation of human ESC-derived cardiomyocytes. *Biomaterials*. 2013;34(23):5813-5820. doi:10.1016/j.biomaterials.2013.04.026

212. Ibrahim M, Gorelik J, Yacoub MH, Terracciano CM. The structure and function of cardiac t-tubules in health and disease. *Proc Biol Sci*. 2011;278(1719):2714-2723. doi:10.1098/rspb.2011.0624

213. Abdul Kadir SHS, Ali NN, Mioulane M, et al. Embryonic stem cell-derived cardiomyocytes

as a model to study fetal arrhythmia related to maternal disease. *J Cell Mol Med*. 2009;13(9B):3730-3741. doi:10.1111/j.1582-4934.2009.00741.x

214. Freytes DO, O'Neill JD, Duan-Arnold Y, Wrona EA, Vunjak-Novakovic G. Natural cardiac extracellular matrix hydrogels for cultivation of human stem cell-derived cardiomyocytes. *Methods Mol Biol*. 2014;1181:69-81. doi:10.1007/978-1-4939-1047-2_7

215. Williams C, Budina E, Stoppel WL, et al. Cardiac extracellular matrix-fibrin hybrid scaffolds with tunable properties for cardiovascular tissue engineering. *Acta Biomater*. 2015;14:84-95. doi:10.1016/j.actbio.2014.11.035

216. Bergmann O, Bhardwaj RD, Bernard S, et al. Evidence for cardiomyocyte renewal in humans. *Science*. 2009;324(5923):98-102. doi:10.1126/science.1164680

217. Risebro CA, Smart N, Dupays L, Breckenridge R, Mohun TJ, Riley PR. Hand1 regulates cardiomyocyte proliferation versus differentiation in the developing heart. *Development*. 2006;133(22):4595-4606. doi:10.1242/dev.02625

218. Dai D-F, Danoviz ME, Wiczer B, Laflamme MA, Tian R. Mitochondrial Maturation in Human Pluripotent Stem Cell Derived Cardiomyocytes. *Stem Cells Int*. 2017;2017:1-10. doi:10.1155/2017/5153625

219. Cameron VA, Ellmers LJ. Minireview: natriuretic peptides during development of the fetal heart and circulation. *Endocrinology*. 2003;144(6):2191-2194. doi:10.1210/en.2003-0127

220. Rupert CE, Coulombe KL. The roles of neuregulin-1 in cardiac development, homeostasis, and disease. *Biomark Insights*. 2015;10(Suppl 1):1-9. doi:10.4137/BMI.S20061

221. Falcão LM, Pinto F, Ravara L, van Zwieten PA. BNP and ANP as diagnostic and predictive markers in heart failure with left ventricular systolic dysfunction. *J Renin*

Angiotensin Aldosterone Syst. 2004;5(3):121-129. doi:10.3317/jraas.2004.028

222. Pioner JM, Racca AW, Klaiman JM, et al. Isolation and Mechanical Measurements of Myofibrils from Human Induced Pluripotent Stem Cell-Derived Cardiomyocytes. *Stem cell reports*. 2016;6(6):885-896. doi:10.1016/j.stemcr.2016.04.006

223. Hakkinen KM, Harunaga JS, Doyle AD, Yamada KM. Direct comparisons of the morphology, migration, cell adhesions, and actin cytoskeleton of fibroblasts in four different three-dimensional extracellular matrices. *Tissue Eng Part A*. 2011;17(5-6):713-724. doi:10.1089/ten.TEA.2010.0273

224. Herold KE, Vossoughi J, Bentley WE, eds. *26th Southern Biomedical Engineering Conference SBEC 2010, April 30 - May 2, 2010, College Park, Maryland, USA*. Vol 32. Berlin, Heidelberg: Springer Berlin Heidelberg; 2010. doi:10.1007/978-3-642-14998-6

225. Akins RE, Rockwood D, Robinson KG, Sandusky D, Rabolt J, Pizarro C. Three-dimensional culture alters primary cardiac cell phenotype. *Tissue Eng Part A*. 2010;16(2):629-641. doi:10.1089/ten.tea.2009.0458

226. Rupert CE, Chang HH, Coulombe KLK. Hypertrophy Changes 3D Shape of hiPSC-Cardiomyocytes: Implications for Cellular Maturation in Regenerative Medicine. *Cell Mol Bioeng*. 2016;10(1):1-9. doi:10.1007/s12195-016-0462-7

227. Verkerk AO, Veerman CC, Zegers JG, Mengarelli I, Bezzina CR, Wilders R. Patch-Clamp Recording from Human Induced Pluripotent Stem Cell-Derived Cardiomyocytes: Improving Action Potential Characteristics through Dynamic Clamp. *Int J Mol Sci*. 2017;18(9). doi:10.3390/ijms18091873

228. Veerman CC, Kosmidis G, Mummery CL, Casini S, Verkerk AO, Bellin M. Immaturity of Human Stem-Cell-Derived Cardiomyocytes in Culture: Fatal Flaw or Soluble Problem?

Stem Cells Dev. 2015;24(9):1035-1052. doi:10.1089/scd.2014.0533

229. Liu J, Laksman Z, Backx PH. The electrophysiological development of cardiomyocytes. *Adv Drug Deliv Rev*. 2016;96:253-273. doi:10.1016/j.addr.2015.12.023

230. Liu Y-W, Chen B, Yang X, et al. Human embryonic stem cell-derived cardiomyocytes restore function in infarcted hearts of non-human primates. *Nat Biotechnol*. 2018;36(7):597-605. doi:10.1038/nbt.4162

231. Gerbin KA, Yang X, Murry CE, Coulombe KLK. Enhanced Electrical Integration of Engineered Human Myocardium via Intramyocardial versus Epicardial Delivery in Infarcted Rat Hearts. Backx PH, ed. *PLoS One*. 2015;10(7):e0131446. doi:10.1371/journal.pone.0131446

232. Jackman CP, Ganapathi AM, Asfour H, et al. Engineered cardiac tissue patch maintains structural and electrical properties after epicardial implantation. *Biomaterials*. 2018;159:48. doi:10.1016/J.BIOMATERIALS.2018.01.002

233. Zhou P, Pu WT. Recounting Cardiac Cellular Composition. *Circ Res*. 2016;118(3):368-370. doi:10.1161/CIRCRESAHA.116.308139

234. Anversa P, Loud A V, Giacomelli F, Wiener J. Absolute morphometric study of myocardial hypertrophy in experimental hypertension. II. Ultrastructure of myocytes and interstitium. *Lab Invest*. 1978;38(5):597-609. http://www.ncbi.nlm.nih.gov/pubmed/147963. Accessed March 29, 2019.

235. Bergmann O, Zdunek S, Felker A, et al. Dynamics of Cell Generation and Turnover in the Human Heart. *Cell*. 2015;161(7):1566-1575. doi:10.1016/j.cell.2015.05.026

236. Tallquist MD, Molkentin JD. Redefining the identity of cardiac fibroblasts. *Nat Rev Cardiol*. 2017;14(8):484-491. doi:10.1038/nrcardio.2017.57

237. Eghbali M, Blumenfeld OO, Seifter S, et al. Localization of types I, III and IV collagen mRNAs in rat heart cells by in situ hybridization. *J Mol Cell Cardiol*. 1989;21(1):103-113. http://www.ncbi.nlm.nih.gov/pubmed/2716064. Accessed April 16, 2019.

238. Bashey RI, Donnelly M, Insinga F, Jimenez SA. Growth properties and biochemical characterization of collagens synthesized by adult rat heart fibroblasts in culture. *J Mol Cell Cardiol*. 1992;24(7):691-700. http://www.ncbi.nlm.nih.gov/pubmed/1404409. Accessed April 16, 2019.

239. Ivey MJ, Tallquist MD. Defining the Cardiac Fibroblast. *Circ J*. 2016;80(11):2269-2276. doi:10.1253/circj.CJ-16-1003

240. Miragoli M, Gaudesius G, Rohr S. Electrotonic Modulation of Cardiac Impulse Conduction by Myofibroblasts. *Circ Res*. 2006;98(6):801-810. doi:10.1161/01.RES.0000214537.44195.a3

241. Rook MB, van Ginneken AC, de Jonge B, el Aoumari A, Gros D, Jongsma HJ. Differences in gap junction channels between cardiac myocytes, fibroblasts, and heterologous pairs. *Am J Physiol*. 1992;263(5 Pt 1):C959-77. http://www.ncbi.nlm.nih.gov/pubmed/1279981. Accessed October 23, 2017.

242. Rubart M, Tao W, Lu X-L, et al. Electrical coupling between ventricular myocytes and myofibroblasts in the infarcted mouse heart. *Cardiovasc Res*. 2018;114(3):389-400. doi:10.1093/cvr/cvx163

243. Quinn TA, Camelliti P, Rog-Zielinska EA, et al. Electrotonic coupling of excitable and nonexcitable cells in the heart revealed by optogenetics. *Proc Natl Acad Sci U S A*. 2016;113(51):14852-14857. doi:10.1073/pnas.1611184114

244. Shah MK, Garcia-Pak IH, Darling EM. Influence of Inherent Mechanophenotype on

Competitive Cellular Adherence. *Ann Biomed Eng*. 2017;45(8):2036-2047. doi:10.1007/s10439-017-1841-5

245. Rupert CE, Coulombe KLK. IGF1 and NRG1 Enhance Proliferation, Metabolic Maturity, and the Force-Frequency Response in hESC-Derived Engineered Cardiac Tissues. *Stem Cells Int*. 2017;2017:7648409. doi:10.1155/2017/7648409

246. Kim TY, Kunitomo Y, Pfeiffer Z, et al. Complex excitation dynamics underlie polymorphic ventricular tachycardia in a transgenic rabbit model of long QT syndrome type 1. *Hear Rhythm*. 2015;12(1):220-228. doi:10.1016/j.hrthm.2014.10.003

247. Sousa AM, Liu T, Guevara O, et al. Smooth muscle alpha-actin expression and myofibroblast differentiation by TGFbeta are dependent upon MK2. *J Cell Biochem*. 2007;100(6):1581-1592. doi:10.1002/jcb.21154

248. Rook MB, Jongsma HJ, de Jonge B. Single channel currents of homo- and heterologous gap junctions between cardiac fibroblasts and myocytes. *Pflugers Arch*. 1989;414(1):95-98. http://www.ncbi.nlm.nih.gov/pubmed/2471143. Accessed October 23, 2017.

249. Doble BW, Kardami E. Basic fibroblast growth factor stimulates connexin-43 expression and intercellular communication of cardiac fibroblasts. *Mol Cell Biochem*. 1995;143(1):81-87. http://www.ncbi.nlm.nih.gov/pubmed/7776963. Accessed October 23, 2017.

250. Asazuma-Nakamura Y, Dai P, Harada Y, Jiang Y, Hamaoka K, Takamatsu T. Cx43 contributes to TGF-β signaling to regulate differentiation of cardiac fibroblasts into myofibroblasts. *Exp Cell Res*. 2009;315(7):1190-1199. doi:10.1016/j.yexcr.2008.12.021

251. Mason JW, Ramseth DJ, Chanter DO, Moon TE, Goodman DB, Mendzelevski B. Electrocardiographic reference ranges derived from 79,743 ambulatory subjects. *J Electrocardiol*. 2007;40(3):228-234. doi:10.1016/j.jelectrocard.2006.09.003

252. Armoundas AA, Rosenbaum DS, Ruskin JN, Garan H, Cohen RJ. Prognostic significance of electrical alternans versus signal averaged electrocardiography in predicting the outcome of electrophysiological testing and arrhythmia-free survival. *Heart*. 1998;80(3):251-256. doi:10.1136/hrt.80.3.251

253. Huang X, Yang N, Fiore VF, et al. Matrix stiffness-induced myofibroblast differentiation is mediated by intrinsic mechanotransduction. *Am J Respir Cell Mol Biol*. 2012;47(3):340-348. doi:10.1165/rcmb.2012-0050OC

254. Kollmannsberger P, Bidan CM, Dunlop JWC, Fratzl P, Vogel V. Tensile forces drive a reversible fibroblast-to-myofibroblast transition during tissue growth in engineered clefts. *Sci Adv*. 2018;4(1):eaao4881. doi:10.1126/sciadv.aao4881

255. Evans RA, Tian Y. C, Steadman R, Phillips AO. TGF-β1-mediated fibroblast–myofibroblast terminal differentiation—the role of smad proteins. *Exp Cell Res*. 2003;282(2):90-100. doi:10.1016/S0014-4827(02)00015-0

256. Desai VD, Hsia HC, Schwarzbauer JE. Reversible modulation of myofibroblast differentiation in adipose-derived mesenchymal stem cells. *PLoS One*. 2014;9(1):e86865. doi:10.1371/journal.pone.0086865

257. Zhou Y, Richards AM, Wang P. Characterization and Standardization of Cultured Cardiac Fibroblasts for *Ex Vivo* Models of Heart Fibrosis and Heart Ischemia. *Tissue Eng Part C Methods*. 2017;23(7):422-433. doi:10.1089/ten.tec.2017.0169

258. Anversa P, Olivetti G, Melissari M, Loud A V. Stereological measurement of cellular and subcellular hypertrophy and hyperplasia in the papillary muscle of adult rat. *J Mol Cell Cardiol*. 1980;12(8):781-795. http://www.ncbi.nlm.nih.gov/pubmed/6448301. Accessed March 22, 2019.

259. Rinn JL, Bondre C, Gladstone HB, Brown PO, Chang HY. Anatomic Demarcation by Positional Variation in Fibroblast Gene Expression Programs. *PLoS Genet*. 2006;2(7):e119. doi:10.1371/journal.pgen.0020119

260. Fahrenbach JP, Mejia-Alvarez R, Banach K. The relevance of non-excitable cells for cardiac pacemaker function. *J Physiol*. 2007;585(Pt 2):565-578. doi:10.1113/jphysiol.2007.144121

261. Vozenin MC, Lefaix JL, Ridi R, Biard DS, Daburon F, Martin M. The myofibroblast markers α-SM actin and β-actin are differentially expressed in 2 and 3-D culture models of fibrotic and normal skin. *Cytotechnology*. 1998;26(1):29-38. doi:10.1023/A:1007992824966

262. Shinde A V, Humeres C, Frangogiannis NG. The role of α-smooth muscle actin in fibroblast-mediated matrix contraction and remodeling. *Biochim Biophys acta Mol basis Dis*. 2017;1863(1):298-309. doi:10.1016/j.bbadis.2016.11.006

263. Granato G, Ruocco MR, Iaccarino A, et al. Generation and analysis of spheroids from human primary skin myofibroblasts: an experimental system to study myofibroblasts deactivation. *Cell Death Discov*. 2017;3:17038. doi:10.1038/cddiscovery.2017.38

264. Surawicz B, Fisch C. Cardiac alternans: diverse mechanisms and clinical manifestations. *J Am Coll Cardiol*. 1992;20(2):483-499. http://www.ncbi.nlm.nih.gov/pubmed/1634690. Accessed March 27, 2019.

265. Vasquez C, Benamer N, Morley GE. The Cardiac Fibroblast: Functional and Electrophysiological Considerations in Healthy and Diseased Hearts. *J Cardiovasc Pharmacol*. 2011;57(4):380-388. doi:10.1097/FJC.0b013e31820cda19

266. Yue L, Xie J, Nattel S. Molecular determinants of cardiac fibroblast electrical function and

therapeutic implications for atrial fibrillation. *Cardiovasc Res*. 2011;89(4):744-753. doi:10.1093/cvr/cvq329

267. Pellman J, Zhang J, Sheikh F. Myocyte-fibroblast communication in cardiac fibrosis and arrhythmias: Mechanisms and model systems. *J Mol Cell Cardiol*. 2016;94:22-31. doi:10.1016/j.yjmcc.2016.03.005

268. Zhang Y, Kanter EM, Yamada KA. Remodeling of cardiac fibroblasts following myocardial infarction results in increased gap junction intercellular communication. *Cardiovasc Pathol*. 2010;19(6):e233-40. doi:10.1016/j.carpath.2009.12.002

269. Xie Y, Garfinkel A, Weiss JN, Qu Z. Cardiac alternans induced by fibroblast-myocyte coupling: mechanistic insights from computational models. *Am J Physiol Circ Physiol*. 2009;297(2):H775-H784. doi:10.1152/ajpheart.00341.2009

270. Narsinh KH, Sun N, Sanchez-Freire V, et al. Single cell transcriptional profiling reveals heterogeneity of human induced pluripotent stem cells. *J Clin Invest*. 2011;121(3):1217-1221. doi:10.1172/JCI44635

271. Nguyen QH, Lukowski SW, Chiu HS, et al. Single-cell RNA-seq of human induced pluripotent stem cells reveals cellular heterogeneity and cell state transitions between subpopulations. *Genome Res*. 2018;28(7):1053-1066. doi:10.1101/gr.223925.117

272. Karagiannis P, Eto K. Ten years of induced pluripotency: from basic mechanisms to therapeutic applications. *Development*. 2016;143(12):2039-2043. doi:10.1242/dev.138172

273. Burridge PW, Thompson S, Millrod MA, et al. A universal system for highly efficient cardiac differentiation of human induced pluripotent stem cells that eliminates interline variability. *PLoS One*. 2011;6(4):e18293. doi:10.1371/journal.pone.0018293

274. Huebsch N, Loskill P, Mandegar MA, et al. Automated Video-Based Analysis of Contractility and Calcium Flux in Human-Induced Pluripotent Stem Cell-Derived Cardiomyocytes Cultured over Different Spatial Scales. *Tissue Eng Part C Methods*. 2015;21(5):467-479. doi:10.1089/ten.TEC.2014.0283

275. Kaiser NJ, Kant RJ, Minor AJ, Coulombe KLK. Optimizing Blended Collagen-Fibrin Hydrogels for Cardiac Tissue Engineering with Human iPSC-derived Cardiomyocytes. *ACS Biomater Sci Eng*. 2019;5(2):887-899. doi:10.1021/acsbiomaterials.8b01112

276. D'Antonio-Chronowska A, Donovan MKR, Benaglio P, et al. Human iPSC gene signatures and X chromosome dosage impact response to WNT inhibition and cardiac differentiation fate. *bioRxiv*. May 2019:644633. doi:10.1101/644633

277. Guhr A, Kobold S, Seltmann S, Seiler Wulczyn AEM, Kurtz A, Löser P. Recent Trends in Research with Human Pluripotent Stem Cells: Impact of Research and Use of Cell Lines in Experimental Research and Clinical Trials. *Stem cell reports*. 2018;11(2):485-496. doi:10.1016/j.stemcr.2018.06.012

278. Williams C, Quinn KP, Georgakoudi I, Black LD, III. Young developmental age cardiac extracellular matrix promotes the expansion of neonatal cardiomyocytes in vitro. *Acta Biomater*. 2014;10(1):194-204. doi:10.1016/j.actbio.2013.08.037

279. Kaiser NJ, Coulombe KLK. Physiologically inspired cardiac scaffolds for tailored in vivo function and heart regeneration. *Biomed Mater*. 2015;10(3):034003. doi:10.1088/1748-6041/10/3/034003

280. Hsiao C-W, Bai M-Y, Chang Y, et al. Electrical coupling of isolated cardiomyocyte clusters grown on aligned conductive nanofibrous meshes for their synchronized beating. *Biomaterials*. 2013;34(4):1063-1072. doi:10.1016/j.biomaterials.2012.10.065

281. Spearman BS, Hodge AJ, Porter JL, et al. Conductive interpenetrating networks of polypyrrole and polycaprolactone encourage electrophysiological development of cardiac cells. *Acta Biomater*. 2015;28:109-120. doi:10.1016/j.actbio.2015.09.025

282. Wang W, Tan B, Chen J, et al. An injectable conductive hydrogel encapsulating plasmid DNA-eNOs and ADSCs for treating myocardial infarction. *Biomaterials*. 2018;160:69-81. doi:10.1016/j.biomaterials.2018.01.021

283. Dong R, Zhao X, Guo B, Ma PX. Self-Healing Conductive Injectable Hydrogels with Antibacterial Activity as Cell Delivery Carrier for Cardiac Cell Therapy. *ACS Appl Mater Interfaces*. 2016;8(27):17138-17150. doi:10.1021/acsami.6b04911

284. Feiner R, Engel L, Fleischer S, et al. Engineered hybrid cardiac patches with multifunctional electronics for online monitoring and regulation of tissue function. *Nat Mater*. 2016;15(6):679-685. doi:10.1038/nmat4590

285. Zimmermann W-H, Schneiderbanger K, Schubert P, et al. Tissue Engineering of a Differentiated Cardiac Muscle Construct. *Circ Res*. 2002;90(2):223-230. doi:10.1161/hh0202.103644

286. III LDB, Meyers JD, Weinbaum JS, Shvelidze YA, Tranquillo RT. Cell-Induced Alignment Augments Twitch Force in Fibrin Gel–Based Engineered Myocardium via Gap Junction Modification. October 2009. http://online.liebertpub.com.revproxy.brown.edu/doi/full/10.1089/ten.tea.2008.0502. Accessed November 12, 2013.

287. Leary E, Rhee C, Wilks BT, Morgan JR. Quantitative Live-Cell Confocal Imaging of 3D Spheroids in a High-Throughput Format. *SLAS Technol Transl Life Sci Innov*. 2018;23(3):231-242. doi:10.1177/2472630318756058

288. Russell S, Wojtkowiak J, Neilson A, Gillies RJ. Metabolic Profiling of healthy and cancerous tissues in 2D and 3D. *Sci Rep*. 2017;7(1):15285. doi:10.1038/s41598-017-15325-5

289. Nunes SS, Miklas JW, Liu J, et al. Biowire: a platform for maturation of human pluripotent stem cell-derived cardiomyocytes. *Nat Methods*. 2013;10(8):781-787. doi:10.1038/nmeth.2524

290. Taegtmeyer H, Sen S, Vela D. Return to the fetal gene program: a suggested metabolic link to gene expression in the heart. *Ann N Y Acad Sci*. 2010;1188:191-198. doi:10.1111/j.1749-6632.2009.05100.x

291. McCright B, Dang JM, Hursh DA, et al. Synopsis of the Food and Drug Administration–National Institute of Standards and Technology Co-Sponsored " *In Vitro* Analyses of Cell/Scaffold Products" Workshop. *Tissue Eng Part A*. 2009;15(3):455-460. doi:10.1089/ten.tea.2008.0558